Université de Lille, Faculté des Sciences et Technologies

École Doctorale des Sciences de la Matière, du Rayonnement et de l'Environnement

Thèse de Doctorat

En vue de l'obtention du grade de

Docteur de l'Université de Lille

Discipline:

Optique, Lasers, Physico-Chimie et Atmosphère

Thèse en cotutelle avec l'Université ITMO (Saint-Pétersbourg, Russie)

par

Yulia Ashina

Raman transduction and unconventional membrane compositions for polymeric sensors

Soutenance le 1 Octobre 2018

Rapporteurs:	
Dr. Manel del VALLE	Professeur, Universitat Autònoma de Barcelona
Dr. Jean-François BARDEAU	Directeur de recherche, Institut des Molecules et Materiaux du Mans
Examinateurs:	
Dr. Vasily BABAIN	Expert, ThreeArc Mining Ltd., Saint-Pétersbourg
Dr. Ludovic DUPONCHEL	Professeur, Université de Lille
Directeurs de Thèse:	
Dr. Dmitry KIRSANOV	Professeur, Université ITMO, Saint-Pétersbourg
Dr. Cyril RUCKEBUSCH	Professeur, Université de Lille
Invité	
Myriam Moreau	Ingénieur, CNRS, Université de Lille

Preface

The present document, resulting of four years of research, would not have been possible without the support of many persons.

First of all, I would like I would like to express my gratitude to the supervisors, Dr. Cyril Ruckebusch and Dr. Dmitry Kirsanov, for their guidance, encouragement and the incredible motivational capabilities during these years.

I also want to thank the jury members for their participation to my thesis committee: Dr. Jean-François Bardeau for the insightful and challenging comments, Dr. Manel del Valle for viewing at my results from different angles, Dr. Vasily Babain and Dr. Ludovic Duponchel for clarifying unexpected findings and outlining the unusual prospects for further research, Myriam Moreau for offering plenty of assistance with Raman spectroscopy.

I consider myself very lucky to share the office with amazing people, both in Russia and France, and I am very grateful to my colleagues for being an infinite source of inspiration and support during hard times.

I gladly acknowledge the ITMO University (Saint-Petersburg, Russia) that gave me the opportunity to be enrolled in the double-degree program.

Last but not the least I would like to thank my boyfriend, mom, dad and my sisters for the unconditional support and sense of humour that helped me to keep balance.

Yulia Ashina

Abstract

In recent years, the number of studies devoted to the development of simple and inexpensive chemical sensors has significantly increased. The development of new approaches is mainly aimed at novel sensor signal transduction schemes and designing sensors with programmable properties.

This thesis presents three new approaches to the analytical signal transduction in the polymeric membranes of potentiometric sensors. The first part of the study describes a novel technique for indirect metal cations detection with micro-Raman spectroscopy. The evolution of the Raman spectrum of the polymeric membrane, upon contact with the sample solution, is used as the analytical signal. Multivariate calibration methods were used to provide a quantitative estimation of the metal content in the aqueous solutions from the measured Raman spectra.

The second part of the thesis reports on studying the feasibility of ionophore-free sensor array with membranes based on various ion-exchangers and plasticizers only. The sensor performance in the analysis of Ca^{2+}-Mg^{2+} mixtures was evaluated through a combination of multisensor approach and multivariate calibration and was compared to traditional ionophore-based selective sensors.

The final part of the thesis is aimed at programmable modification of the sensor sensitivity patterns using the membranes containing several ionophores. Three ionophores, which were previously used for the determination of the lanthanide cations, were chosen for the membrane preparation. The performance of the corresponding multi-ionophore array was tested in the analysis of Ln^{3+} mixtures and compared to conventional mono-ionophore sensors.

Keywords: potentiometric sensors, PVC-plasticized membranes, multisensory systems, Raman spectroscopy, multivariate calibration

Résumé

Au cours des dernières années, le nombre de travaux scientifiques qui portent sur le développement de capteurs chimiques simples et moins chers a été significativement augmenté. Les études dans ce domaine sont principalement orientées vers la recherche de nouveaux schémas de transduction du signal du capteur et vers le développement de capteurs dont les propriétés peuvent être programmées.

Trois approches originales pour la transduction du signal des membranes polymères des capteurs potentiométriques sont présentées dans la thèse. La première partie de l'étude est consacrée à la description d'une nouvelle technique pour la détection indirecte de cations métalliques au moyen de la spectrométrie micro-Raman. Le spectre Raman est mesuré à la surface de la membrane polymère au contact avec la solution échantillon. Ce spectre est converti en information analytique quantitative par le biais de méthodes d'étalonnage multivariée. Dans la deuxième partie, nous étudions la faisabilité de capteurs ne contenant pas d'ionophore, les membranes n'étant alors composées que des différents échangeurs d'ions et plastifiants. La performance de ces capteurs pour l'analyse quantitative de mélanges binaires de Ca^{2+}-Mg^{2+} est évaluée en combinant une approche originale basée sur des capteurs multiples. Les résultats sont comparés à ceux obtenus avec des capteurs à base d'ionophores traditionnels. Enfin, la modification à façon des schémas de sensibilité des capteurs utilisant des membranes contenant plusieurs ionophores est présentée dans la dernière partie de la thèse. Trois ionophores (utilisés auparavant pour la détermination de cations des lanthanides) ont été choisis pour la préparation de la membrane. Les performances du réseau de capteurs ainsi créé sont testées sur l'analyse de mélanges de Ln^{3+} et les résultats sont comparés à ceux des capteurs mono-ionophores conventionnels.

Mots-clés: capteurs potentiométriques, membranes PVC plastifiées, systèmes multicapteurs, spectroscopie Raman, calibration multivariée

Table of contents

List of abbreviations

AsLS	Asymmetric Least Squares
CARS	Coherent anti-Stokes Raman spectroscopy
CCD	Charged coupled device
CTA	Cellulose triacetate
DOP	bis(2-ethylhexyl) phthalate (“dioctyl phthalate”)
DOS	bis-(2-ethylhexyl) sebacate (“dioctyl sebacate”)
EIS	Electrochemical Impedance Spectroscopy
EMF	Electromotive Force
ET	Electronic tongue
FNDPE	2-fluoro-2'-nitrodiphenyl ether
IR	Infrared
ISE	Ion-Selective Electrode
ISFET	Ion-Selective Field Effect Transistors
IUPAC	International Union of Pure and Applied Chemistry
KTTFPB	Potassium 3,5-bis(trifluoromethyl)phenyl] borate
KTClPB	Potassium tetrakis(4-chlorophenyl)borate
LOD	Limit of Detection
MSC	Multiplicative Scatter Correction
NPOE	2-nitrophenyl octyl ether
PCA	Principal Component Analysis
PDAM	N^2,N^2,N^9,N^9-tetrabutyl-1,10-phenanthroline-2,9-dicarboxamide
PMMA	Poly (methyl methacrylate)
PLS	Partial Least Squares
PU	Polyurethane
PVC	Poly (vinyl chloride)
REE	Rare-earth elements
RMSE	Root-Mean-Square Error
RSS	Residual sum of squares
SERS	Surface-Enhanced Raman spectroscopy

TEHP	tris(ethylhexyl) phosphate
TSS	Total Sum of Squares
VIP	Variable Importance in Projection

Introduction

According to the modern definition, a chemical sensor is a compact device that transforms chemical information into useful analytical signal [1]. With the development of chemical sensing, these devices became smaller, simpler and more widely available [2]. One can think of a traditional pH sensor converting the hydrogen ion activity in solution into electrical potential measured with an mV-meter. Chemical sensors normally have both recognition and transduction functions combined within one device. The recognition function is related to the chemical or physical changes of the sensing element, and its changes are proportional to the analyte concentration in the investigated object. Interaction of an analyte with recognition centers may consist of either a chemical reaction (e.g. affinity recognition in biosensors) or a physical sorption on a recognition site. The transduction function assumes the transformation of these changes into measurable values. The nature of a sensor output then defines the classification of chemical sensors into physical and chemical sensors. Chemical transduction consists of the quantification of changes in the chemical composition of the sensing element. If the analytical signal is not derived from the analyte itself but it is the product of an interaction with a secondary molecule, then the transduction is called indirect, or also labeled transduction. Physical transduction in its turn is derived from varying the physical properties and, therefore, physical transduction is usually label-free.

Electrochemical sensors are the largest and the oldest type of chemical sensors. Due to their simple and robust instrumentation, and relatively easy

production, electrochemical sensors are widely applied in different areas of industry and research. By now, it is the most widespread platform for routine analyses in clinical chemistry [3]. Progress in this area is mainly associated with the application of new chemical materials and optimization of sensor construction. Potentiometric membrane sensors are among the most popular research objects in the field, not only due to their simplicity and robustness, but also due to the variety of possibilities that exist for the modification of their sensing properties.

One of the main challenges of sensor applications is the analysis of real objects. High content of various interfering components is the most common reason of inadequate sensor selectivity towards the target analyte. Also, the influence of the sample matrix on the sensor performance is hardly predictable as it is sample-dependent. For example, limitations of the analysis would be drastically different for Mg^{2+} determination in seawater [4, 5], food products [6] and biological liquids [7]. For instance, in blood electrolytes determination, the sensor surface will be continuously altered due to the adsorption of blood plasma/serum proteins, resulting in a poor reproducibility of the analysis.

Although novel sensors appear regularly, their application is strictly specified by the objects of analysis [8, 9]. This extensive way of problem-solving requires a significant time and money investment, and the development of selective sensors for each type of sample is hardly possible. Regarding electrochemical sensors, one of the most successful ways to address this issue is the multisensor approach [10]. Instead of using one selective sensor, several cross-sensitive sensors are used simultaneously. Sensors of the array should be selected in relation to the type of object analyzed in order to compensate for interferences and sample matrix effects [11]. The multisensor approach is indispensable in cases where integral parameters are required instead of the information on the exact sample composition. For example, the concentration of individual toxicants in a given environmental sample may be below the threshold limit value, but the sample would still be classified as “toxic” in terms of bioassay evaluation. The assessment of such “integral toxicity” can be performed with

multisensor system as far as it is calibrated against the reference response (i.e. the one of the chosen bioassay), without *a priori* knowledge on the sample composition [12].

Modern studies on sensor arrays are aiming at the development of a sensor array that can be easily adapted to an unpredictable environment. This task includes simplification of the measurement procedure, sensor construction [13] or data processing without losing the sensor performance [14]. More recently, attention has focused on multi-transduction platforms (e.g. opto-potentiometric [15] when both optical and electrochemical signals are registered simultaneously for one particular sensor), providing complementary information on a sample composition using the same polymeric membrane. It was shown that this approach can significantly improve sensor performance [16].

This thesis research is dedicated to the development of new approaches for the transduction of analytical signals in potentiometric sensor membranes. In Chapter 1 the main aspects of electrochemical sensors and related techniques are given. At first, the different types of electrochemical sensors are discussed in general. The main focus is on potentiometric sensors, namely ion-selective membrane electrodes (ISE). Their working principle, construction, types of membranes and components are reviewed. In the end of the Chapter 1, the objectives of this study are described. The three following chapters then give the detailed description of the results of this study. Chapter 2 describes a new methodology for Raman signal transduction from potentiometric sensor membranes. This methodology is directed towards the above-mentioned multi-transduction approach, e.g. the possibility of getting optical information from the membrane of an electrochemical sensor. The changes in the Raman spectrum of the membrane upon binding of the analyte by the ionophore are used as analytical signal. The first part is devoted to Raman spectroscopy with a focus on the micro-Raman technique. In addition, the basics of multivariate data analysis are given in this chapter. This includes the principal component analysis (PCA) and partial least squares regression (PLS). The feasibility of the approach is performed with Cd^{2+} cations binding with phenanthroline diamide ligand immobilized in a polymeric sensor

membrane and the study includes the optimization of the membrane composition (e.g. ligand concentration, polymer type, etc.). In the following chapters, two new modifications of the multisensor approach are described. Chapter 3 presents the application of ionophore-free sensors based on a polymer, plasticizer and a lipophilic additive only. The sensor membranes based on the combination of different plasticizers and lipophilic additives are used within a multisensor approach for ion mixtures analysis. Chapters 4 discusses the design and implementation of multi-ionophore polymeric sensor membranes. Several kinds of sensors containing 2 or 3 ligands within one membrane were united into the array and tested for the analysis of multicomponent solutions of lanthanide cations, demonstrating mutual interference in mixtures. Chapter 5 contains the summary of the main research findings and conclusions.

CHAPTER 1. Potentiometric sensors

1.1. Electrochemical sensors

The response of electrochemical sensors is in general governed by the processes of electronic and/or ionic transfer. There are different types of electrochemical sensors depending on the way the analytical signal is obtained. These types are amperometric (voltammetric), conductometric, impedimetric and potentiometric sensors. In amperometry, the potential of an electrochemical cell is measured while the current flowing through the cell is varied. By contrast, for voltammetry, a subclass of amperometry, the current is measured as a function of the potential variation. Voltammetric sensing is very popular for construction of biosensors, with mainly enzymatic applications, for the specific determination of biomolecules [17-19]. Voltammetry can also be applied for qualitative analysis, because the voltammetric peak current values are associated with the potential of Red/Ox half-reaction, making the recognition of different ions and functional groups of organic molecules possible. The most popular technique – cyclic voltammetry – is based on inverting the direction of the applied potential once the half-reaction point has been reached, so that the oxidized species get reduced and vice versa. Cyclic voltammetry can be used for the investigation of Red/Ox processes, e.g. reversibility, reaction speed, etc. [20]. Voltammetry is also extensively applied to study various fermentative reactions. One of the most popular devices are enzymatic biosensors which are used for the determination of glucose, and is based on glucose oxidase [21]. This kind of measurement can be performed not only in laboratory conditions but also on test strips and even as a component of implantable devices. This way, blood analysis became commercially available and simple enough for daily household use by untrained customers [22].

Another parameter of the electrochemical cell that can give essential information about the analyzed substance is conductivity. Conductometric sensors rely on the measurement of the conductivity of electrolyte solutions, which is a function of

the total ion concentration with respect to individual constants k_i' for each of the components:

$$k = F\sum k_i' c_i \qquad \text{(Eq.1)}$$

where c_i is the concentration of individual ions, F is the Faraday constant. The constant k_i' is determined by the ion mobility, ion activity coefficients and the dissociation degree of the electrolyte. Since the difference between mobility values is quite small for most of the ions (except for H_3O^+ and OH^-), classical conductometric sensors are only suitable for the determination of the total ion concentration (e.g. salinity of seawater), and not for the distinction between the concentrations of individual species [1]. However, a few types of selective layer-based conductometric devices have opened new fields of application. For example, there are many types of gas sensors based on the measurement of the conductivity variation of a sensitive layer due to the absorption of the volatile compounds [23].

Electrochemical impedance spectroscopy (EIS) can be employed for the analysis of liquids [2]. The impedance of the electrochemical cell is evaluated under the application of a voltage of varying frequency. Electrochemical impedance (Z) is a complex multiparametric value that depends on double layer capacitance, electrolyte resistance, charge transfer resistance, Warburg impedance and some other parameters in complex systems. In practice, the equivalent electrical circuit considering all the contributions should be used for calculations. Considering the phase shift value φ and the Euler equation, the following expression is obtained, translating the dependence of electrochemical impedance on frequency:

$$Z(\omega) = Z_0 e^{i\varphi} = Z_0(\cos\varphi + i\sin\varphi) \qquad \text{(Eq.2)}$$

The results of EIS measurements can be displayed by plotting |Z| as a function of the phase shift (Bode plot), or Re(Z) – the real part – as a function of Im(Z) – the imaginary part (Nyquist plot). One of the features of impedance spectroscopy is that the signal amplitude depends on the area of the working surface. The conductivity of the layer can also be influenced by selective interactions of analyte species with the

binding agents immobilized on the sensor surface. As one of the recent trends in EIS, these two features found an application for biosensing with interdigitated electrodes [24, 25].

In this thesis we will deal with potentiometric sensors. Their analytical signal is registered under zero-current conditions (without the current flowing through the electrochemical cell). The simplicity of potentiometric measurements together with the tendency to miniaturization brought up the concept of ion-selective electrodes (ISE). Starting from the glass membrane electrode that was originally used as ion-selective pH sensor [26], ISE became one of the most popular analytical instruments. Their analytical signal is the electromotive force (EMF) across the cell. It should be noted that unlike for voltammetric and conductometric sensors, the analytical signal for potentiometric systems does not depend on the surface area of the electrode. Techniques based on ISE have numerous applications (see 1.2.6) due to fast and inexpensive manufacturing procedures, low response times, wide working concentration ranges and the relatively low limit of detection. The detailed description of some fundamental aspects and the working principle of ISE, their analytical characteristics, and modern applications are given in the following sections.

1.2. Construction of ion-selective electrodes (ISE)

Potentiometric measurements are typically performed in an electrochemical cell, made of two half-cells – a reference electrode and an ISE itself. The EMF of such cell is equal to the potential difference between two half-cells, according to Eq.3:

$$EMF = E_{ref.el.} - E_{ISE} \qquad \text{(Eq.3)}$$

where $E_{ref.el.}$ and E_{ISE} are the potential values of the reference electrode and ion-selective electrode, respectively.

The potential of the system is determined by the E_{ISE} only if all other contributions are kept constant during the measurements. For this reason the reference electrode should be mechanically and chemically stable. The potential of the

reference electrode should be reproducible in time and at a given temperature, is reversible and sample-independent. Silver/silver chloride electrodes are the most widely applied reference electrode for electrochemical measurements (Fig. 1.1). This is a second-type electrode, based on two equilibrium reactions: a redox equilibrium at the Ag^0/Ag^+ interface, and a $AgCl/Ag^+$ solubility equilibrium. Due to the low water solubility of AgCl, the concentration of Ag^+ ($[Ag^+]$) is considered to be constant in the inner KCl solution, whatever the sample is.

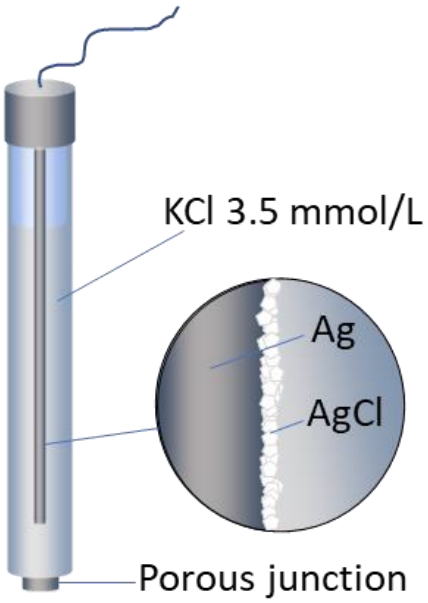

Figure 1.1. Silver/silver chloride reference electrode construction.

1.2.1. Solid membrane ISE

The history of ISE started with solid-state sensing membranes. The first type of solid membrane for ISE sensors were the glass membranes. These membranes, developed by Haber and Klemensiewicz in 1909 [27], are made of silicate glass doped with metal oxides, in order to provide for Frenkel-type defects in the glass lattice. These defects are acting like binding sites for H^+. In general, glass membrane electrodes demonstrate excellent selectivity to H^+ over a wide working range. As a consequence, these electrodes became the most widely employed chemical sensors. At high pH,

monovalent metal cations can interfere with the response, as [M^+] becomes comparable with [H^+] (alkaline error). This issue, however, can be fixed by doping the glass with e.g. Li^+ ions. The development of glass membrane electrodes was followed by many others based on different membrane materials, such as chalcogenide glasses, polycrystalline metal sulphides etc. [23, 28]. One of the most remarkable examples of solid state ISE is monocrystalline LaF_3 doped with Eu^{3+}. This sensor is extremely selective to F^-, with a detection limit as small as 10^{-10} mol/L [29].

The ISEs with solid state membranes are robust and convenient tools widely applied in routine laboratory practice. However, the number of analytes that can be detected with these sensors is quite limited. For example, in case of polycrystalline membranes, only simple inorganic anions (e.g. halides) and cations (copper, cadmium, lead) are usually detected. Moreover, the selectivity patterns of these sensors cannot be tailored to some particular analytical tasks as they are depending on the fundamental properties of the membrane materials – e.g. solubility of corresponding sulphides. Moreover, the difficulty of designing crystalline materials, selective for particular ions of interest, hinders their further development. Thus, many studies are devoted to the search of alternative materials for ISE membranes that could allow for selectivity tuning with a wide range of practical applications [30]. The use of organic ligands as ion binding sites became the most prominent strategy for the ISE technique development.

1.2.2. Liquid membrane ISE

In the 1970's, liquid membrane ISEs with sensing components dissolved in organic solvent were developed [31]. In these membranes the sample-dependent changes in the EMF of the cell were generated by charge separation at the membrane/sample interface, once the analyte is extracted into the liquid membrane and complexed by an incorporated ligand. The main disadvantage of these membranes was that it requires handling liquid phases, which is not very convenient for routine laboratory use. Lately, the sensor configuration was optimized and relatively

big volumes of liquid organic matrices were transformed into thin liquid layers dwelling in thin pores of a special filter membrane. The most popular type of liquid membrane ISE was based on organophosphorus compounds (see e.g. reference [32]) (Fig. 1.2). Then the approach underwent further improvements [33] and liquid membranes of ISE were transformed in plasticized polymeric membranes [34],[35], which should be considered more as organic gels rather than liquids in the traditional sense. Nowadays this type of ISE membranes is the most widely spread one (see Fig. 1.3).

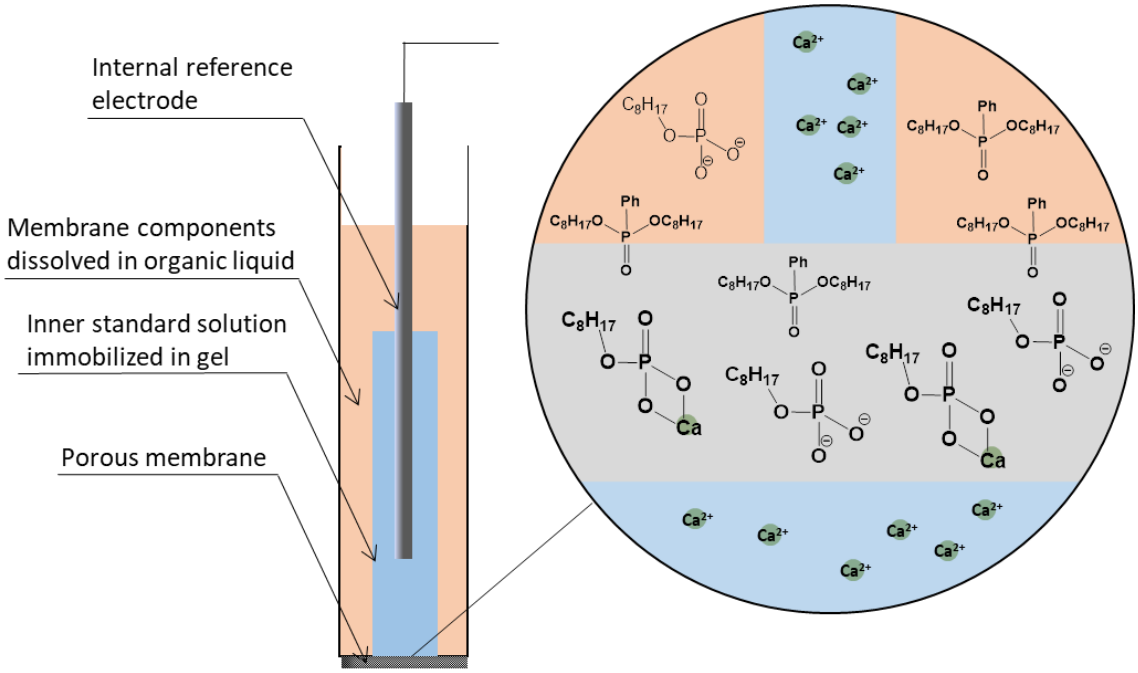

Figure 1.2. Liquid membrane ISE construction illustrated with the example from [32]. Here, 2-ethylhexyl phosphoric acid is used as an ion exchanger and di(octyl) phenyl phosphonate acts as a solvent.

1.2.3. Polymeric membrane ISE

Plasticized polymeric ISE membranes are composed of organic solvent-plasticizers and polymers. The plasticizer is the media to dissolve active organic ligands and ion-exchangers. The polymer acts as an inert matrix to impart the desirable mechanical properties to the membrane. The mechanical and chemical stability of polymeric matrices, as well as their flexibility to experimental conditions, resulted in the dominance of ISE in some application fields, such as clinical determination of sodium, potassium, calcium and magnesium [36]. Thus, the main functional parts of these ISEs are more compact and easier to handle than those with liquid membranes discussed above. Nevertheless, as for liquid membranes, plasticized polymeric ISE membranes require the inner reference electrode to be immersed into the internal solution that acts as a liquid junction. The typical construction of the polymeric ISE is described in the Fig. 1.3. The membrane is in equilibrium with the liquid internal reference solution that basically contains low concentrations of the analyzed ion. Changes in the concentration of the analyzed ion in the membrane, caused by its migration from the sample solution, result in changes in the EMF value.

The constituents of a conventional ISE membrane, along with the polymeric matrix, are the lipophilic additive and the complexing agent (ionophore). More detailed information on the function, properties and typical examples of each membrane component will be given in the following subsections.

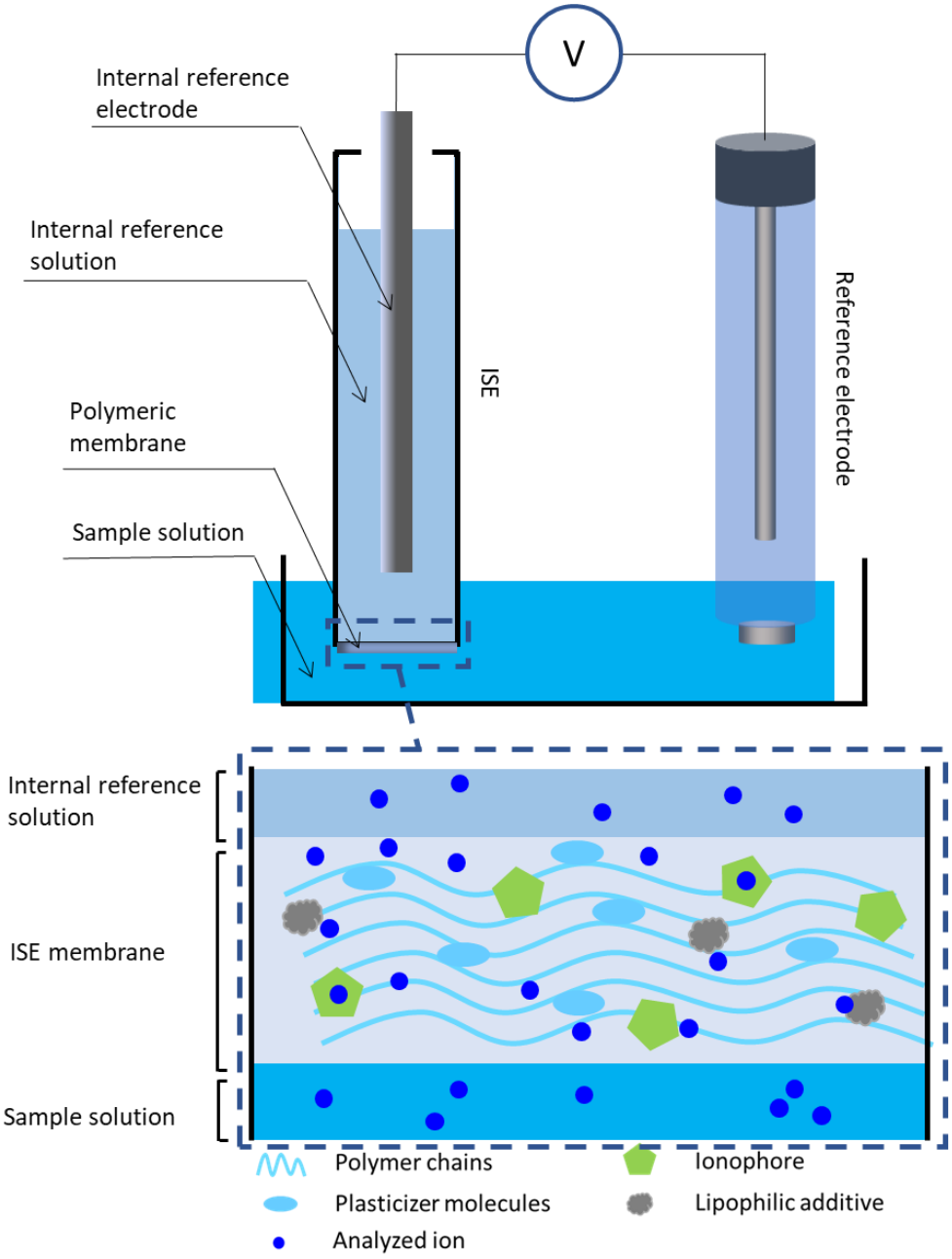

Figure 1.3. The electrochemical cell for ISE measurements.

Polymeric matrix

The polymers considered as membrane matrices now include acrylates, cellulose triacetate (CTA) [37], polyurethanes (PU) [27, 38], silicon rubbers [39], polysiloxanes [40] or polystyrenes [41]. By now, among the huge variety of available

polymers, the most common is high-molecular weight poly (vinyl chloride)(PVC) [42]. This is due to its low price, its chemical inertness and stability.

While for liquid membrane ISEs, the permeability of components of interest does not represent a problem, this issue is the key for the design of polymeric membranes. To obtain sufficient ion mobility in the membrane phase, the polymer should have a glass transition temperature (T_g) below ambient temperature. In case of PVC membrane (T_g=80 ^oC), it is essential to use plasticizers to decrease the T_g. Moreover, an additional advantage is that the plasticizer acts as a solvent for all the other components of the membrane. A wide range of compounds utilized in PVC processing industry was adopted as plasticizers for the adjustment of membrane mechanical properties. The structure of these compounds, their functional groups and, consequently, their physico-chemical properties may differ drastically. The majority of plasticizers are the molecules containing long alkyl chains, providing sufficient lipophilicity and polar or polarizable functional groups (e.g. phenyl, nitro- or carbonyl). This allows enhancing the interactions of the plasticizer with both hydrocarbon and polar groups of the polymer (C-Cl for PVC) and thus provides a minimal plasticizer leaching into a sample solution. The most common plasticizers for polymeric sensor membranes are: 2-nitrophenyl octyl ether, 2-fluoro-2'-nitrodiphenyl ether, bis-(2-ethylhexyl) sebacate, bis(2-ethylhexyl) phthalate.

One of the most essential requirements for ISE membranes is homogeneity of their chemical composition. All the components of the membrane should have a sufficient lipophilicity to prevent their leaching from the membrane into the sample, thus avoiding decomposition of the membrane [43]. The exact lipophilicity can be estimated by structural increments for each of membrane components with methods of Quantitative Structure-Activity Relationship [44]. However, a simple relation can be established by comparison of the dielectric constant values (ε), but the drastic difference of this value with respect to that one of the plasticized polymeric membrane should be taken into account. For instance, for PVC plasticized by NPOE (1:2 wt %), ε is 14, while for the pure NPOE, ε is 21 [45]. It is also important to point out that the

terms “lipophilicity” and “hydrophobicity” do not mean the same – for example most of the fluorocarbons are hydrophobic but not lipophilic [23, 28]. Also, PVC-plasticized membranes may lose their mechanical properties within approximately 6 months, due to the gradual leakage of plasticizer and other components into the aqueous solution in contact with the membrane.

Lipophilic additive

In order to obtain stable analytical signals, ISE membranes should exhibit good ion exchanging properties. For this purpose, they contain an ionic additive which consists of a lipophilic ion-exchanging site (also called lipophilic ionic additive) and a counter-ion that can be easily substituted with the analyzed ion. The counter-ion should be relatively hydrophilic to allow fast ion exchange at the membrane surface. The typical lipophilic cation-exchangers are tetraphenyl borate derivatives [46] (Fig. 1.4 a). The alkyl substituted quaternary ammonium salts are examples of typical anion-exchanging lipophilic additives [47-49] (Fig. 1.4 b).

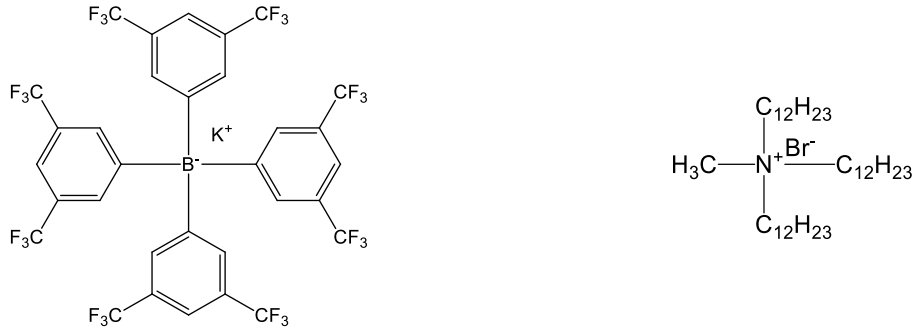

Figure 1.4. a – Potassium tetrakis[3,5-bis(trifluoromethyl)phenyl] borate (KTTFPB); b – tridodecylmethylammonium bromide (TDMABr).

The presence of a lipophilic additive lowers the electrical resistance of the membrane and facilitates ion transfer. This additive also acts as a counter-ion for the analyzed ionic species, and thus it compensates the charge excess in a membrane and prevents co-extraction of the interfering counter-ions from the sample solution.

Ionophore

The main functional part of ISE membrane is the ionophore (ion-carrier). It is responsible for the selectivity of the plasticized polymeric ISE and is capable of reversible selective complexation with the target ion. Ionophores can be either neutral or charged molecules. The presence of ionophore molecules promotes permselective mass transfer across a phase boundary (see 1.2.4.) [50]. This lowers the energy required for transferring the ion of interest into the membrane. This turns into an increased selectivity compared to that of ion-exchanger-based ISE. One of the first substances that was used as an ionophore was an antibiotic, named valinomycin [51] (Fig. 1.5), which selectively binds potassium cations, discriminating sodium as its common interference. Valinomycin-based ISE is still a very common instrument in clinical analysis.

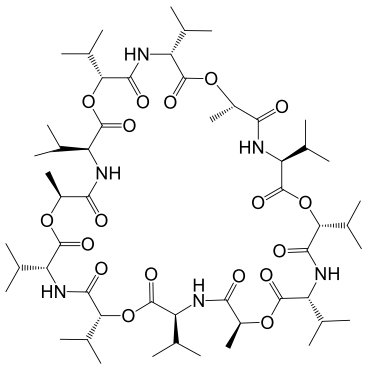

Figure 1.5. The chemical structure of valinomycin, a widely employed potassium-selective ionophore.

The strategy to design an ionophore consists in creating a molecule having a required binding capability towards the analyzed species, but, also important, a sufficient affinity to the membrane matrix (e.g. solubility in the plasticizer). The latter requires a suitable lipophilicity, usually provided by the presence of long alkyl substituents or other hydrocarbon subunits. Advances in ionophore design resulted in the availability of a big range of organic compounds [52, 53] such as amides [54], polyethers, peptides, crown ethers [55], thiourea derivatives [56, 57], etc. The mechanism of formation of the complex between target ion and ionophore can be of

various natures, such as e.g. donor-acceptor interaction, hydrogen bonding or inclusion.

The design of ligands relies on the concepts of Pearson acid-base, chelate effect, ligand conformation stability and other principles of ligand chemistry. The ligand selectivity can be influenced by incorporation of donor groups acting as binding sites. Depending on the number of binding sites involved into the formation of the complex, ligands are divided into mono- and polydentate. Ionophores for metal cations are mainly polydentate ligands, typically containing neutral oxygen or nitrogen donor groups [58-60]. The high affinity of these ligands to metal cations is driven by their lower energy of complex formation, compared to that of monodentate ligands (chelate effect, from greek *"chela"* - claw). The chelate effect is driven by the entropic contribution to complex stabilization which plays a bigger role for the preorganized polydentate ligands compared to monodentate ones. When the chelate ring size of the ligand molecule and the size of metal cation match well, it results in an enhanced selectivity of the complexation, which is typical for ligands with rigid structures (e.g. [61]). Introducing the different donor groups and substituents in the rigid backbone of the ligand may also affect the size-based selectivity of complexation [62]. For example, using diamide of dipicolinic acid A (Fig. 1.6) as an ionophore provides a two times higher sensitivity to Lu^{3+} cations compared to diamide B [63]. This effect can be explained by delocalization of the electron density from the phenyl substituent to the amide group in diamide A. This leads to the strengthening of a ligand-ion complex (so-called "effect of anomalous aryl strengthening" [64]).

The concentration of the analyte in the membrane phase is restricted by the lipophilic additive concentration. The ligand concentration should be sufficiently higher than the one of the lipophilic additive.

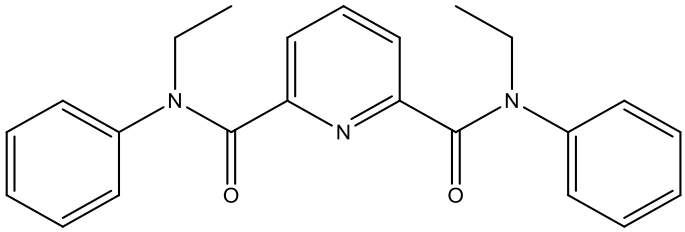

N, N'-Diethyl-N, N'-di-p-tolyl diamide of dipicolinic acid **(A)**

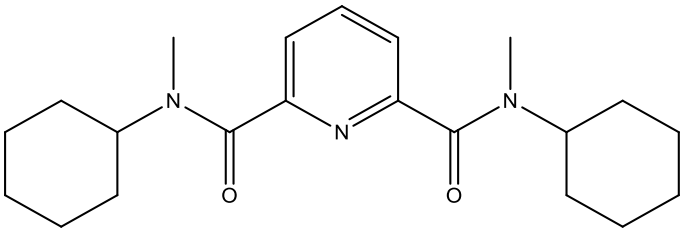

N,N'-Dimethyl-N,N'-dicyclohexyl diamide of dipicolinic acid **(B)**

Figure 1.6. Dipicoline diamide ligands with different substituents.

1.2.4. Phase boundary potential model

The analytical signal of ISE sensors is determined solely by the membrane potential. According to Bakker et al. [65], it is a function of the phase boundary potential across the membrane. Initially, the membrane potential is the sum of the interface potentials and the diffusion potential, as in Eq. 4.

$$E_{membrane} = const + E_{diff} + E_{P.B.(membrane/sample)} + E^{*}_{P.B.(membrane/inner\ solution)} \qquad \text{(Eq.4)}$$

where $E_{membrane}$ is the membrane potential, E_{diff} is the diffusion potential and $E_{P.B.}$ and $E^{*}_{P.B}$ are the phase boundary potential across the membrane at the membrane/sample and membrane/inner solution interface, respectively. If there is no concentration gradient across the membrane, the diffusion potential E_{diff} can be omitted. The potential at the membrane/inner solution interface $E^{*}_{P.B.}$ can be considered constant and is sample-independent if the membrane is quite thick. These two assumptions bring up the following expression for membrane potential $E_{membrane}$ (Eq. 5):

$$E_{membrane} = const + E_{P.B.} \quad \text{(Eq.5)}$$

where $E_{P.B.}$ is the phase boundary potential at the membrane/sample interface. The physical meaning of $E_{P.B.}$ is the difference of potential arising from the separation of charges across the electrolyte and membrane interface. The thermodynamical definition of the chemical potential is described by Eq. 6,

$$\tilde{\mu}_{aq} - \tilde{\mu}_{org} = \left(\mu^0_{aq} + RT\ln a_{i\ (aq)} + zF\varphi_{aq}\right) - \left(\mu^0_{org} + RT\ln a_{i\ (org)} + zF\varphi_{org}\right) =$$
$$= \mu^0_{aq} - \mu^0_{org} + RT\ln\frac{a_{i\ (aq)}}{a_{i(org)}} + zF(\varphi_{aq} - \varphi_{org}) \quad \text{(Eq.6)}$$

where $\tilde{\mu}$ is the electrochemical potential, μ^o is a chemical potential under standard conditions, z is an ion charge, a_i is the activity of the ion, R is the universal gas constant, T is the absolute temperature and F is the Faraday constant. “(org)” or “(aq)” indices denote the organic or aqueous phases, respectively. The phase boundary potential at the membrane/sample interface can be expressed through the difference of electrochemical potentials (Eq.7):

$$E_{P.B.} = \Delta\varphi = (\varphi_{aq} - \varphi_{org}) = \frac{\mu^0_{aq} - \mu^0_{org}}{zF} + \frac{RT}{zF}\ln\frac{a_{i\ (aq)}}{a_{i\ (org)}} \quad \text{(Eq.7)}$$

Once the membrane/sample solution equilibrium is reached, the activity of the target ion in the membrane phase $a_{i\ org}$ is expected to be constant. This way, the phase boundary potential, and, therefore, the membrane potential, both depend linearly on the analyte activity $a_{i\ aq}$ in the sample solution. Merging all the sample-independent contributions into E^0 value results in the expression for the potential of electrochemical cell (Eq.8), also known as Nernst equation, which describes the main principle of potentiometric measurements, i.e. linear dependence of the EMF on the logarithmic ion activity:

$$E = E^0 + \frac{RT}{zF}\ln a_{i\ (aq)} \quad \text{(Eq.8)}$$

1.2.5. Analytical characteristics of ISEs

The main characteristics of the sensor performance are well-established and are similar to those used for other analytical methods. Analytical characteristics of ISEs can be found in the reports of International Union of Pure and Applied Chemistry (IUPAC) [50, 66]. They are briefly recapped below.

- The response time is determined as the time required for EMF/time slope to become equal to a limiting value selected on the basis of the experimental conditions and/or requirements concerning the accuracy. As a figure of merit for sensors the time taken to reach 95 % of the response value ($t_{0.95}$) can be used.
- Stability stands for the ability of the sensor to maintain its performance for a certain period of time. Stability can be assessed with a drift value (e.g. variation of the analytical signal in a solution of constant composition and temperature).
- Repeatability can be described as the variability of the signal within a series of measurements performed under the same conditions by a given operator within a short period of time.
- Sensitivity of the ISE is expressed as a slope of the calibration curve of an ISE toward a given ion.
- Lower limit of detection (LOD, detection limit) is a concentration for which, under the specified conditions, the cell EMF, E, deviates from the average EMF in region I by a multiple of the standard error of a single measurement of the EMF in this region I The upper LOD is also observed for the ISE and denotes the analyte concentration, corresponding to the limiting high activity response and in practice is denoted as a plateau on the response curve. The graphical representation of the LOD values is shown in the Fig. 1.7.
- Selectivity is the ability of an ion-selective electrode to distinguish a particular ion from the others in a mixture, without generating false-positive or false-negative signals. Selectivity is determined by the value of potentiometric selectivity coefficient (k_{ij}).

According to the Nernst equation (Eq. 8), the ISE response curve can be represented as a dependent of the EMF of the electrochemical cell on the logarithm of activity of the analyzed ion (lga_i). The typical calibration curve is represented in Fig. 1.7.

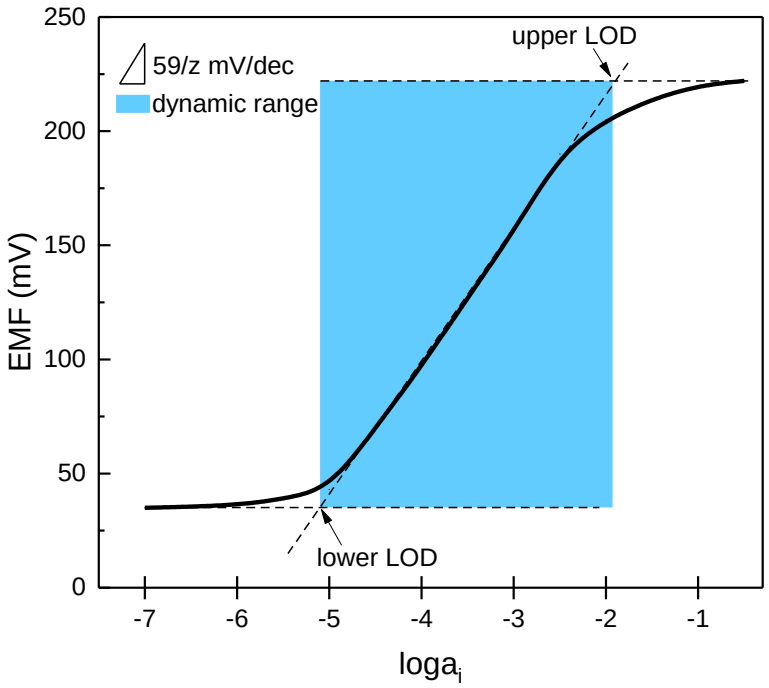

Figure 1.7. Graphical representation of the LOD values in the ISE calibration curve.

The sensitivity of ISEs can be determined graphically as the slope of the linear part of the calibration curve. Under standard conditions and switching to decimal logarithm, the Nernst equation (Eq. 8) turns into Eq. 9,

$$E = E^0 + \frac{0.059}{z} lga_{i\,(aq)} \qquad \text{(Eq.9)}$$

The “ideal” sensitivity of ISE, expressed in mV/dec (unit of a logarithm of analyzed ion activity), is equal to 59/*z* mV/dec (25º C), (z is the charge of the analyzed ion). As follows from the phase boundary potential model, reversibility of the complexation of ionic species by the ionophore is required. If this condition is not met, non-Nernstian values can be observed for sensitivity. The reason of this may also be

related to a presence of interfering ionic species with charge values lower than the one of the target ion (e.g. formation of $M(OH)^+$ in polyvalent metal salt solutions). For this reason, all the secondary processes like hydrolysis should be suppressed, and potentiometric measurements should be performed under controlled pH in order to get reliable results. It should be noted that the sensitivity value can be determined for the concentration range between lower and upper LOD in the so-called dynamic range (denoted in blue in Fig.1.7).

The limit of detection (LOD, detection limit) for ISEs, considering the logarithmic nature of the response, is defined by IUPAC as the intersection of the extrapolated linear part of the calibration plot and the “final low concentration level segments” for lower LOD, and the “limiting high activity response” for upper LOD [50]. Both lower and upper LOD values may be observed experimentally and determined graphically from the calibration curve [67]. LODs of classical polymeric membrane ISEs are around 10^{-6} M. Several methods can be employed to decrease the lower LOD value, e.g. super-Nernstian sensitivity values can find their application in trace-level analysis [68]. The equilibrium shift leading to super-Nernstian response can be generated intentionally by creating a concentration polarization at the membrane interface with applying the current pulse (so-called pulstrodes [69]), or by using acidic ionophores [70]. Another way to decrease the LOD is bufferization of the ISE inner solution. The use of an ion buffer (e.g. EDTA) maintains the constant concentration of the primary ion in the inner solution, so its leaching toward the sample does not occur. This prevents biasing the analyzed ion activity at the corresponding membrane surface as it is not influenced by the inner solution anymore [71]. The upper LOD is related mainly to the influence of interfering counter-ions. At high concentration of an analyte in a sample solution, the concentration of the ionophore-analyte complex in the membrane significantly increases. As the membrane gets enriched with excessive charge, brought in by the complexed ions, it tends to possess ion-exchanging properties for the counter-ions, promoting their co-extraction into the membrane phase. This phenomenon, also known as Donnan exclusion failure [50], is the primary factor framing the upper LOD of ISEs. This may have significant influence on the sensor

performance when one has strong complexation of highly lipophilic target ions by an ionophore [72].

The main contribution of interfering ions to the response is related to the ISE membrane permselectivity. Thus, one should have information about selectivity of the ISE prior to the analysis of real samples. Selectivity is driven mainly by ionophore-analyte complex stability. In case of the presence of two interfering ions A^{n+} and B^{n+} in the solution at a time, for an ordinary ISE, two complex formation processes occur in the membrane media based on the neutral ionophore (I):

$$\begin{aligned} A^{n+} + I &\xrightarrow{k_A} AI^{n+} \\ B^{n+} + I &\xrightarrow{k_B} BI^{n+} \end{aligned} \qquad \text{(Eq.10)}$$

If the stoichiometry is the same for AI^+ and BI^+, the selectivity of the ISE would depend on the ratio of the two complex formation constants, K_a and K_b. Within the dynamic range for both target and interfering ions determination, the influence of the interfering ions was described by Nikolsky and Eisenmann [26, 73], later expressed as the semi-empirical Nikolsky-Eisenmann equation (Eq. 11):

$$E = E^0 + \frac{RT}{z_p F} \ln\left(a_p^{mix} + \sum_i K_{pi} \cdot a_i^{mix^{z_p/z_i}} \right), \qquad \text{(Eq.11)}$$

where a_p^{mix} and a_i^{mix} are the primary and interfering ion activities in their mixture, respectively, K_{pi} is a potentiometric selectivity coefficient and z_i is the charge of the analyzed ion. The Nikolsky selectivity coefficient is the most widely applied measure of selectivity. It is supposed to be independent of the experimental conditions and thus, it is the main value to be reported for the characterization of selectivity. IUPAC suggests two procedures for the determination of this selectivity coefficient in practice: the separate solution method and the fixed interference method [67]. In the separate solution method, the lg*a* vs E relations of an ISE for the primary (P) and interfering (I) ions are obtained independently. Then, the activities that correspond to the same EMF are used to determine the K_{pi} value. From the Nernst equation (Eq. 8) and Nikolsky-

Eisenmann equation (Eq. 11), the activity a_p in a single-component solution can be expressed as (Eq.12):

$$a_p = a_p^{mix} + K_{pi} \cdot a_i^{mix^{z_p/z_i}}, \quad \text{(Eq.12)}$$

In the limiting case where the primary and interfering ion activities induce the same EMF, the approximation of $a_p^{mix} = 0$ can be taken. Therefore, $a_p^{mix} = a_p$, and the K_{pi} will be equal to the following ratio (Eq. 13):

$$K_{pi} = \left(\frac{a_p}{a_i^{z_p/z_i}} \right) \quad \text{(Eq.13)}$$

As E^0 values for both calibrations (on *P* and *I*, respectively), are considered as constant, the resulting selectivity coefficient can be calculated according to the equation:

$$\log K_{pi} = \frac{z_p F\left(E_i - E_p\right)}{2.303RT} + \log\left(\frac{a_p}{a_i^{z_p/z_i}} \right), \quad \text{(Eq.14)}$$

If the target and interfering ions have the same charge value, the second part in the right term is equal to zero. Thus, an estimation of selectivity can be done by comparison of the EMF values for both ions at the same concentration (Fig. 1.8.).

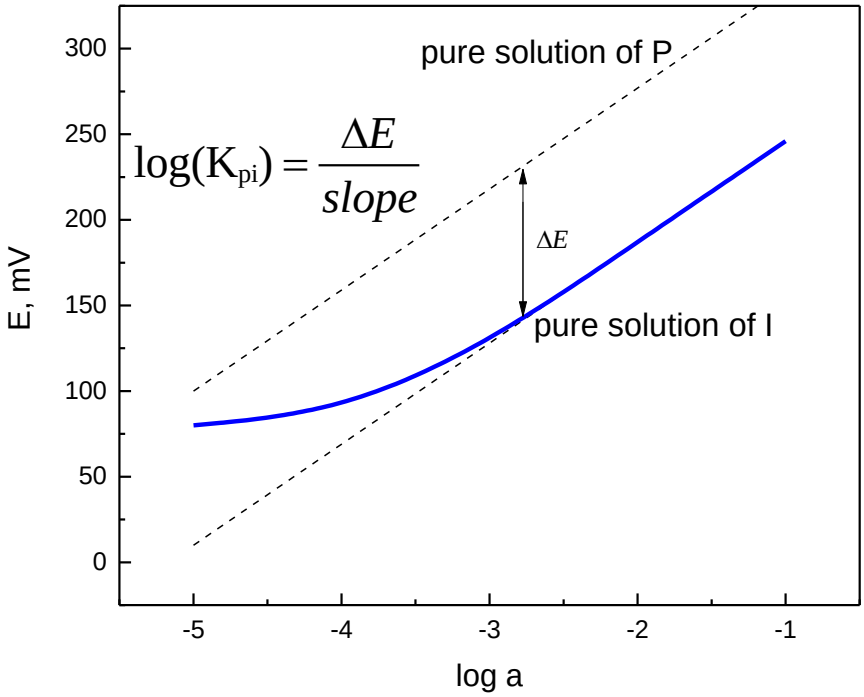

Figure 1.8. Graphical determination of the selectivity coefficient by the separate solutions method.

The fixed interference method consists of the evaluation of the sensor sensitivity in the presence of a fixed concentration of the interfering ion [74]. The selectivity coefficient is then calculated according to the same approximation as for (Eq.12) (Fig. 1.9.) and a_P is determined from the intersection of the two linear parts of the calibration curve that correspond to the lower LOD for P and a_i background value (Eq.15):

$$\lg K_{pi} = \lg\left(\frac{a_p}{a_i^{z_p/z_i}}\right) \qquad \text{(Eq.15)}$$

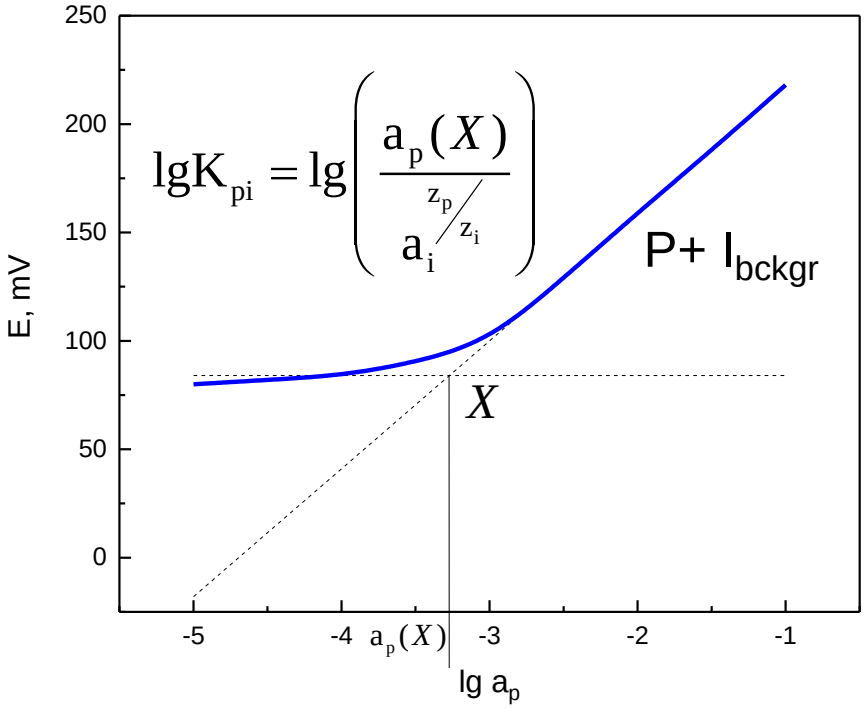

Figure 1.9. Graphical determination of the selectivity coefficient by the fixed interference method.

Both the separate solution method and fixed interference method are based on the assumptions that the interfering ion only substitutes the target one at the ionic site, and that no “mixed ion response” is observed. Also, an equilibrium at the phase boundary is presumed. In case of deviations from a Nernstian response, it is recommended to use the matched potential method [75] instead. Unlike the two previous methods, the matched potential method is not bound by the limitations of the theoretical model. Within this method, a calibration for the target ion *i* is carried out by sequentially adding portions of Δ*i* to the reference solution, containing known concentrations of *i*. Then the interfering ions *j* are added to an identical starting solution until the same potential change is observed [75]. As a figure of merit, the selectivity factor, $k_{i,j}$ is used. $k_{i,j}$ represents the ratio of Δi/Δj, that cause the same potential difference for both of the calibrations. The main disadvantage of the matched potential method is the dependence of $k_{i,j}$ on prescribed concentrations of the primary and

interfering ions, and thus reported values should be provided together with experimental conditions.

1.2.6. Applications of ISEs and recent developments

Clinical analysis is the main application domain for ISEs, mainly for the determination of electrolytes in biological liquids. Valinomycin-based ISEs have up to now been employed for the determination of K^+ in blood. Other common application fields are soil analysis, plant analysis, quality control for food production, wastewater treatment or environmental monitoring [76-78]. The ease of operation, along with its reversibility and insusceptibility to the turbidity and color of the sample, allow ISEs to be used for online monitoring of technological processes [79]. Flow-injection systems were also successfully employed together with potentiometric detection for different analytical tasks [80]. The durability and long-term stability of polymeric membranes make ISE applicable even under extreme experimental conditions, such as in the analysis of soluble ionic species in Martian soils [81, 82] .

The development of modern analytical methods is typically associated with the question of miniaturization [83]. Within the last 40 years, ISE membranes of 0.1–1 mm dimensions came into general use [84]. In some applications, even the sensors with the diameter in the order of 100 nm were reported [85]. Modern clinical analysis requires analyte volumes in the microliter scale. However, the analysis of microvolumes requires significant modifications of the technique. For instance, instead of the conventional reference electrode, another membrane ISE, highly selective to some ion of the background, can be used, as it is easier to miniaturize. Also, the concentration of the background ion should be kept constant in order to provide stable potential readings of the reference ISE [86, 87].

In the last decades, the construction of ion-selective field effect transistors (ISFET) revealed the possibility of reducing the scale of analytical instruments down to the micrometer size. One of the modifications of this technique consists of the

deposition of an ISE membrane on the transistor gate. For routine analysis, the durability of the system becomes especially important. Therefore, the range of possible membrane matrices significantly narrows, since, for example, a PVC matrix has a poor adhesion to the solid support of the ISFET [88], making this method very sensitive to the ambient conditions. A strategy for choosing the membrane composition should take into account the solubility of the components, adhesiveness of the polymeric matrix to the ISFET surface and membrane resistance, all at the same time. Recent studies are focused on ISFET geometry optimization [89, 90] using photopolymerized acrylic or polyurethane matrices [91]. Miniaturization of ISEs opened up the possibilities to integrate several technologies in one device, such as microfluidic platform [92].

An important problem in clinical analyses is the poor biocompatibility of ISE membranes that get in contact with biological liquids. For the majority of the membranes, an inflammatory effect on living tissues may be observed or the membrane may lose its functionality because of protein adsorption. Plasticizer leaching, inherent to PVC-plasticized membranes should be avoided, and for this reason, the membrane composition should be adjusted to the type of the biological object under analysis. This way, the requirement of haemocompatibility for medical applications brought cellulose triacetate and polyurethane into use for biocompatible membrane matrices [93]. For example, polyurethane-based membranes are widely applied for implantable devices [94].

A popular research direction is the development of disposable sensors for clinical analysis. A wide range of wearable electrochemical biosensors for online monitoring of electrophysiological parameters is available. For example, the concentration of glucose in saliva is found to be correlated with the blood glucose level, and saliva analysis can be used for indirect non-invasive monitoring of the glucose level in blood, lowering the requirements to biocompatibility [95]. By now, many types of compact devices have been constructed by immobilization of the sensing

compounds into various polymers [96, 97], on textile support [98], paper support [99] and even in a form of tattoo-based sensors [100].

Another perspective for modern ISE is switching from traditional plasticized PVC membranes to plasticizer-free ones. This approach aims to eliminate the main problems of the plasticized PVC, i.e. plasticizer leaching and polymeric matrix degradation. The requirements the polymer should follow are in this case the same as those for the conventional membrane matrices: low T_g and resistance of the polymer and high solubility of the active sensing components in the membrane phase. In this area, remarkable results were demonstrated with various acrylate co-polymers by the group of Heng and Hall [101, 102]. They investigated the influence of the monomer content on the T_g and the influence of the molecular weight on the properties of the acrylate co-polymers. They could come up with sensor membranes that do not require the use of any plasticizer (or only at the low level of 10%). It was shown that copolymers containing more than 80% wt of n-butyl acrylate yield membranes with T_g below −20° C and allow obviating the need of the plasticizer.

1.2.7. Multisensor systems

Conventional ISEs often exhibit a high sensitivity towards several species at a time. There is very little chance for absolute selective complexation of one particular type of ions. This property is called cross-sensitivity. Moreover, the analytical objects under study often contain neutral species that can influence the sensor response towards ionic species. When analyzing multicomponent samples with ISE, the response function cannot be modelled with satisfactory precision using the traditional Nikolsky-Eisenmann equation. The problem of poor selectivity of a single sensor can be potentially solved with the use of multisensor approach. It consists of merging several sensors into an array and processing the response of this array by means of multivariate data analysis tools. This way, the data – the electrochemical signal – represent a kind of “fingerprint” of the analyzed multicomponent solution. This fingerprint can be processed further with various chemometric tools in order to derive

qualitative and quantitative information about the sample. Another important idea behind the development of multisensor approaches can be formulated as follows. While most of the complex quality parameters of a sample are not correlated with the content of a single chemical compound, a robust and reliable correlation with such parameters can still be found when multiple chemical compounds (groups of compounds) are being considered simultaneously. The elucidation of the detailed qualitative and/or quantitative composition of the sample may consume a lot of time and efforts and may still not produce the desired result. The multisensor arrays use the integral characteristics of the sample (e.g. its identity, such as belonging to a particular class of other samples, its taste attributes, toxicity (safety) or potential harmfulness of the sample for biota) as the output data instead of the information on the content or presence of a particular compound. The relative simplicity of the approach boosted numerous applications of sensor arrays in the food industry [103], manufacturing processes control [104], etc. When multisensor systems are aimed at evaluation of taste and quality parameters of food products, beverages and pharmaceuticals, the methodology is called “electronic tongue” (ET), and it has been a field under constant development since the mid 90’s [11, 105-108].

The traditional way of assessing the quality of food products is organoleptic and it is performed by descriptive sensory panels. It is well-known that taste is not directly correlated with the chemical structure of the constituents, but it is based on five basic taste features: sweet (taste of sucrose), sour (flavor associated with citric acid), salty (taste associated with sodium chloride), bitter (taste elicited by caffeine). The fifth one, umami, represents “taste intensity”. Umami receptors can be stimulated by, for example, glutamic acid. The resulting taste of the product is not just a superposition of these parameters, and, for example, the bitter taste of certain substances can be sometimes masked by the presence of sucrose. The sensitivity of the receptors differs in a wide range from person to person and depends on external factors, such as temperature, health condition etc. These circumstances complicate the objective perception of taste even within a well-trained sensory panel, so the results of routine determination are often biased. The evaluation of the taste of pharmaceutical has even

more difficulties due to the ethical implications associated with a sensory panel test of the substances that may have various health effects.

The concept of “electronic tongue” (ET) consists of the evaluation of taste descriptors through mathematical models relating the response of a sensor array with target sample quality parameters (e.g. taste descriptors). The cross-sensitive sensor array intends to mimic the global selectivity concept, which assumes that every single sensor is not required to have specific interactions with the analyte [109], but should have a response towards several components of the sample simultaneously. The analysis of real samples by means of multisensor system is preceded by a “training” step where a set of samples with known characteristics (e.g. available from traditional sensory panel) is analyzed [110-113] and a regression model relating sensor responses with these parameters is constructed. Once the calibration is done, the mathematical model can be employed further to predict the target parameters in new samples based on the response of the multisensor system. ET may act as a complementary instrument to sensory panels in order to minimize their work load in routine analysis. In case of pharmaceutical samples using the ET is aimed to substitute human sensory panels completely. At the moment, there are numerous applications of ET described in the literature for the analysis of food products, beverages and pharmaceuticals [106, 112, 114, 115].

In spite of the name “electronic tongue”, the concept of cross-sensitive sensor arrays has found many applications far beyond the taste evaluation task. The multisensor approach allows for an elegant handling of complex analytical problems, like e.g. circumventing selectivity limitations of individual sensors. As a nice example of such advantage, one can consider the work in references [63, 116] addressing the quantitative analysis of individual lanthanides in their mixtures in aqueous solutions. Being neighbors in the periodic system of elements, lanthanides have similar electronic structure and thus very similar chemical properties. The determination of one particular lanthanide in the presence of others is a challenge for certain industrial applications (like e.g. analysis of spent nuclear fuel) which is hardly addressable by

using a conventional potentiometric sensor with one ionophore. It was shown that sensor arrays based on potentiometric membrane electrodes containing various ligands adopted from liquid extraction can effectively resolve lanthanide mixtures providing information on individual metal contents.

Another interesting application field for multisensor systems is the analysis of complex media where individual sensors fail due to the large number of interfering species. A very representative example [117] is the quantification of metal content in sea water, where a multisensor system allows simultaneous determination of Cu^{2+}, Zn^{2+}, Cd^{2+} and Pb^{2+} in mixed buffered solutions at nanomolar level. Another example is the monitoring of industrial fermentation processes where numerous factors (presence of microbial population, specialized conditions, large number of interferents) hinder the application of individual selective sensors. This task can also be successfully accomplished with various sensor arrays, e.g. potentiometric sensor array can be used for automated on-line control of a fermentation process in a flow-through mode [118].

Within the last decade, a number of authors have considered the integration of sensor arrays into miniaturized devices to supply the needs of clinical analysis. For example, in the study in reference [119], flow injection was complemented by a multisensor approach in a “lab-on-a-chip” device. Also, the concept of sensor arrays as an alternative to more expensive instruments remains very popular for industrial process control. For instance, it can be advantageously used for waste water analysis or fermentation monitoring [104, 120]. Their low response time and the fast recovery of the sensor membranes make sensor arrays very useful for in-line monitoring procedures [121, 122].

Finally, the majority of the environmental applications of multisensor arrays is devoted to the analysis of natural waters [123, 124]. The main challenge today consists of the development of rapid test methods using compact devices for on-site measurements [125, 126]. Integral quality parameters that cannot be directly related to the presence of a single particular chemical substance in a sample can also be

predicted from the multisensor system response, like e.g. chemical oxygen demand [127] or toxicity in terms of bioassay [128].

1.3. Statement of purpose

Potentiometric analysis with polymeric membrane ISEs is a rapidly growing research field, due to the numerous advantages of this method. Most of the studies nowadays are focused on lowering LODs, improving robustness, lifetime, and optimizing sensor performance in complex solutions.

This manuscript describes three novel approaches to the development of polymeric membrane sensors in order to extend the analytical capabilities of the method. In the first part, the possibility of Raman transduction of analytical signal for ISE membranes is studied. The second part is devoted to sensor arrays based on ionophore-free membranes and the third section is a feasibility study of a multi-ionophore sensor array.

1.3.1. Raman transduction for ISE membranes

Raman spectroscopy can be employed for the analysis of aqueous solutions and for the determination of ionic species. There are numerous applications of this technique reported, ranging from the exploration of chemical reactions (e.g. disproportionation, hydration) to the monitoring of the content of ionic species [129-131]. Obviously, some of the ions, e.g. monoatomic metal cations, have no vibrational modes and cannot be quantified with Raman directly. This issue can be circumvented using an indirect quantification procedure where the spectral signature of a reagent upon the interaction with the ion is registered [132],[133]. This approach, however, requires an additional step of preparation/titration of the sample solution. A possible way to simplify the analytical procedure is the micro-Raman investigation of a reagent immobilized in a solid matrix. The composition of a typical polymer plasticized ISE membrane not only allows traditional electrochemical transduction but also enables the readout of spectroscopic information.

In this thesis, we propose a novel technique for the ion quantification at the ISE polymeric membrane surface using micro-Raman spectroscopy. The idea behind Raman transduction is that the Raman spectrum of the ligand (ionophore) at the ISE surface will evolve upon the formation of a complex with the target analyte. This evolution could then be correlated with the analyte concentration. The advantage of micro-Raman is the possibility of analyzing micro volumes of liquid samples – something unusual for conventional ISEs. Taking into account all the benefits of polymeric potentiometric sensors, this combination of ISE membranes with micro-Raman for the analysis of microliter sample could potentially be a very promising analytical approach.

1.3.2. Ionophore-free sensors

The main components of polymeric membranes are a polymer, a plasticizer, a lipophilic additive and an ionophore. Ionophores have always been developed to reach the highest possible selectivity [52]. The design of a new ligand, or its selection for the particular analytical task, requires significant time and efforts. Moreover, the characteristics of ionophores can hardly be predicted beforehand with theoretical calculations since they depend on a number of complex factors such as the composition of the membrane matrix and the stoichiometry of the ionophore-ion complex. The sensitivity and selectivity parameters of an ionophore and its behavior in the presence of interfering ionic background (or organic compounds, etc.) can only be analyzed in real-world conditions [53]. For this reason, apart from the synthesis itself, ionophore development includes the full cycle of fabrication of the ISE and the examination of the sensor performance.

One of the possible answers to this challenge is a multisensor approach. An array of cross-sensitive sensors combined with multivariate calibration tools may, under certain conditions, compensate for the insufficient selectivity and interferences typical of individual sensors. It makes possible to get reasonable analytical information about multicomponent analytes [106, 134]. Cross-sensitivity effects can also provide

better selectivity and a lower LOD than individual selective sensors [135, 136]. Ultimately, this approach suggests that ionophore-free sensors can provide a way for selective ion determination. Traditionally, ionophore-free sensors were used for the determination of the complex formation constants [137] or the investigation of lipophilic additives performance [46, 48, 138]. However, ionophore-free sensors may act in the sensor arrays as part of these systems, facilitating the cation or anion content analysis [114, 139-141].

In the absence of an ionophore in the membrane, the sensor selectivity is much more affected by the lipophilic additive and plasticizer. The contribution of plasticizers to the membrane selectivity is complex and not fully understood yet. A well-known influencing factor is the plasticizer polarity, usually described in terms of the influence of the medium with a certain dielectric constant value. Besides, some of the neutral donor groups in a plasticizer molecule may act as complex formation centers and thus compete with the ionophore [43]. The combination of plasticizer and lipophilic additive provides an individual response pattern for each membrane composition. However, these effects are usually masked in traditional ISEs by the overwhelming power of the ionophore.

The idea of this part of the study is to explore whether or not it is possible to attain potentiometric selectivity without using an ionophore in sensor membranes. In this case, selectivity is governed by target ion hydrophobicity/lipophilicity, ion-exchanger and solvent-plasticizer. A multisensor approach allows for the simultaneous application of sensors with different membrane compositions. This gives a good chance to reach a certain selectivity, even without special ligands, by means of a simple analytical procedure. Ca^{2+}-Mg^{2+} solutions were selected as a case study to check the viability of the proposed approach, as the Mg^{2+} cation exhibits a strong interference by Ca^{2+} while being analyzed in mixtures [142]. The performance of the ionophore-free sensor array with varying cation-exchanger and plasticizer was explored in the determination of individual ion concentrations in mixed aqueous solutions containing both Ca^{2+} and Mg^{2+} cations.

1.3.3. Multi-ionophore ISE membranes

Due to the similarity of the operating principle of liquid extraction and ISEs, the extracting agents were extensively used for liquid ion-exchanging membranes [143]. The essential process in these two analytical methods is the formation a complex between an ion and an ionophore/extracting agent. This similarity led to the fact that some extracting agents are employed as ionophores for polymeric plasticized ISEs [63, 144, 145]. This adoption of ligands from liquid extraction for sensor construction allows skipping the laborious procedure of choosing and designing an appropriate ionophore. The performance of the extraction criterion – the distribution ratio (D) – is equal to the ratio of the analyte concentration in each of the immiscible phases: organic (C_{org}) and aqueous (C_{aq}) (Eq.16).

$$D = \frac{C_{org}}{C_{aq}} \qquad \text{(Eq.16)}$$

The efficiency of the extraction process, as well as the ISE response, strongly depends on the stability of the ligand-ion complex. That is why the distribution ratios are often in a good agreement with selectivity series of the corresponding ISEs [144]. Nevertheless, one should not make it a rule, since additional factors, such as ionic mobility in the membrane media, should be considered for ISE selectivity.

The combination of several extracting agents may lead to synergetic effects, i.e. a non-additive increase in the performance of the system. This type of effect was successfully employed in the field of spent nuclear reprocessing, yielding simplified but effective extraction procedures [146-148]. One can assume that similar behavior with a significant deviation from single-ionophore selectivity/sensitivity patterns can be expected for polymeric sensor membranes containing a mixture of ionophores. The idea of the third part of this study is to check this assumption and to investigate sensor membranes combining two or more ionophores in order to compare them with single-ionophore sensors. Introduction of several ionophores into sensor membranes is an interesting way to govern cross-sensitivity, which is needed for multisensor systems.

Until now, to our knowledge, no study was reported on polymeric membrane sensors with ionophore mixtures. However, a similar approach has been previously implemented in different studies, dealing with detector miniaturization for ion chromatography [149, 150], development of voltammetric sensors [151, 152], constructing a pseudo reference potentiometric sensor for mixture analysis and investigation of complex stability constants [153]. As a case study to test the suggested approach, mixtures of rare-earth elements were chosen since their chemical behavior is very similar. The selectivity issue is also very crucial for the determination of individual cations with a multisensor system.

CHAPTER 2. Feasibility study of Raman transduction for polymeric ISE membranes

One of the perspective directions in sensor technology is presented by multi-transduction platforms, i.e. combining several principles of the analytical signal transduction within one sensor membrane. This type of approach may – apart from obtaining the complementary quantitative information – contribute to a better understanding of the processes underlying the analyte detection.

In this chapter, we propose Raman transduction of the analytical signal provided by the polymeric sensor membrane, which is normally used for potentiometric sensors. The goal is to relate the evolution of the Raman spectra acquired on the membrane of polymeric sensors in contact with sample solutions containing a given ion. The feasibility study of this approach was performed using the PVC-plasticized membrane containing N^2,N^2,N^9,N^9-tetrabutyl-1,10-phenanthroline-2,9-dicarboxamide as the ionophore and Cd^{2+} as the analyte cation. The procedure includes the selection of the membrane components and spectral acquisition parameters, spectral data preprocessing and interpretation of the membrane spectral signature upon the interaction with Cd^{2+} cations. The analysis of the membrane spectra was performed after interaction with the set of samples containing Cd^{2+} in the 10^{-4} – 10^{-2} M concentration range. PLS regression was used on the acquired data to provide a quantitative estimation of the metal content in the sample.

2.1. Raman spectroscopy

In very broad terms, spectroscopy consists in the measurement of emission, absorption, fluorescence or scattering of electromagnetic radiation upon its interaction with matter. Vibrational spectroscopy considers the characteristic energy transitions which are associated with the nuclear motion of a molecule, namely vibrational or vibrational-rotational states for gases. The frequency of vibrational transitions (10^{11}–10^{14} Hz) corresponds to 20–4000 cm^{-1} range. Molecular vibrations can be related to the changes in the chemical bond length, corresponding to stretching modes (v),

bending modes (δ), and torsional modes. The main types of molecular vibrations are depicted in Fig. 2.1. A vibrational spectrum is basically a combination of all vibrational modes of the functional groups of a molecule, and thus every molecule has its unique 'fingerprint'. This fact allows a qualitative analysis of various samples using extensive spectral databases [154-156].

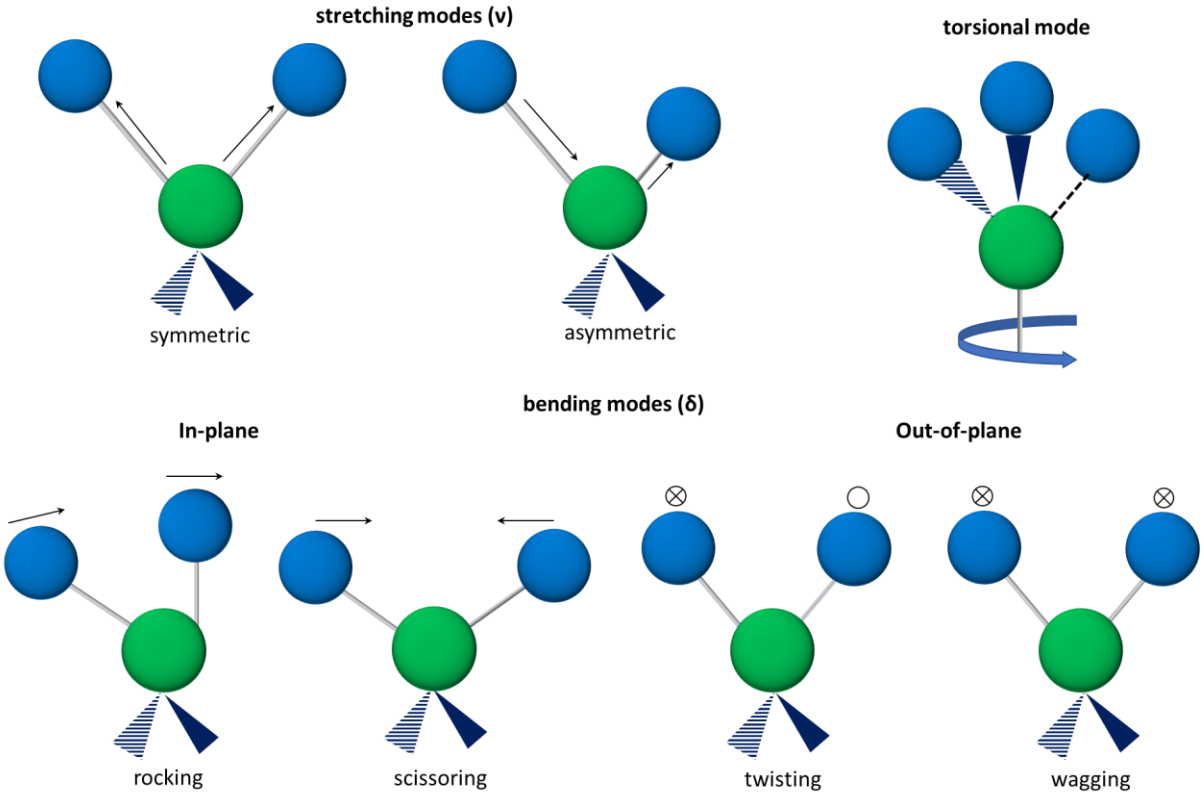

Figure 2.1. Types of fundamental vibrations exemplified with the -CH_2- group.

Infrared and Raman vibrational spectroscopy are very popular analytical methods. These techniques are widely applied for studying chemical bonding, molecule geometry, kinetics of chemical reactions, complexation, etc. [157]. Infrared spectroscopy consists of the observation of molecular vibrational transitions, caused by absorption, reflection or emission of the resonant energy by the sample. Modes that are active in the IR spectrum correspond to changes in the dipole moment of the bond. Raman scattering is complementary to IR and it is associated with inelastic scattering

of light. The Raman-active modes involve a change in the polarizability of the molecule. In this section, we will first recap the principles of Raman scattering before introducing the Raman micro-spectrometer and discussing its applications in analytical chemistry.

2.1.1. Principle of Raman scattering

The scattering of the radiation almost completely occurs without any energy change when the particle radius is less than 1/10 of the radiation wavelength (which is true for most of the molecules). This type of scattering is called elastic or Rayleigh scattering. Only a very small part of radiation scatters in an inelastic way (about 1 x 10^{-7}) and this phenomenon is called Raman scattering [158]. Depending on the vibrational energy state of the molecule, photons can either lose or acquire energy upon scattering. It is called Stokes and anti-Stokes scattering, respectively (Fig 2.2.). The Anti-Stokes scattering is weaker than its Stokes counter-part, since only a small fraction of the molecules are in the excited vibrational state. Nevertheless, in some cases, it may be also used for analytical purposes, for example, if the sample exhibits fluorescence [159]. In Raman spectroscopy the wavelength shift with respect to the monochromatic radiation of the source is studied and this energy shift provides information about the molecule structure.

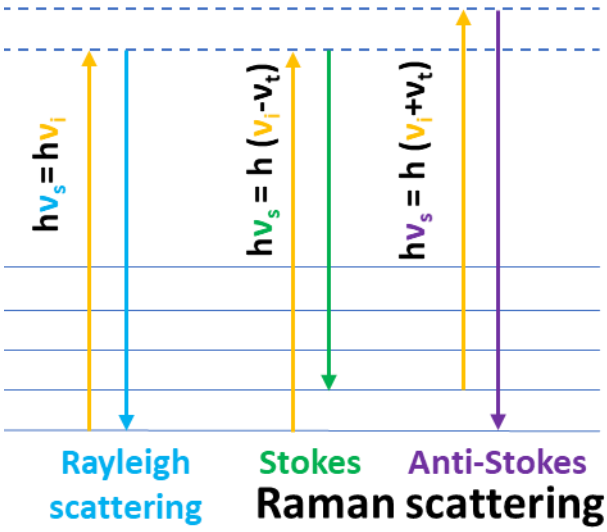

Figure 2.2. Energy diagram showing the Rayleigh and Raman scattering processes. ν_i – incident light frequency, ν_s – scattered light frequency, $h\nu_t$ – transition energy, h – Planck constant.

Unlike for IR radiation, the radiation energy in the visible range is potentially sufficient to induce deformation of an electron cloud, that is to say a deformation in the electronic density of the covalent bond. This leads to the selection rule for Raman vibrational transitions which refers to molecular polarizability change. For instance, molecules containing highly polarizable π-electrons (aromatic systems, groups with double and triple bonds) have very intense bands in Raman spectrum. Molecules possessing a center of symmetry are subjected to so-called rule of mutual exclusion, stating that, vibrational mode for the same group of atoms would be either Raman or IR active, but not both [160]. For example, ν_{8a} and ν_{8b} modes in centrosymmetric benzene at 1600 cm^{-1} are Raman active but not IR active, since displacements related to C⎓C stretching do not cause changes in the dipole moment. Introducing a substituent into the benzene ring destroys the symmetry of the aromatic system, and thus these modes become IR-active.

Since the number of inelastically scattered photons is extremely small compared to Rayleigh scattering, cross-section of a non-resonant Raman scattering is for example 10 orders of magnitude smaller than that for fluorescence [161]. For this reason, in Raman spectroscopy, radiations emitted and detected are in the visible range and the incident light should be monochromatic and frequency-stabilized to allow for reliable quantification considering the low intensity of Raman-scattered radiation. For this reason, laser sources are used for Raman spectroscopy with the excitation wavelength (λ) ranging from UV to near-infrared. The intensity of Raman scattering is proportional to λ^{-4}. Thus, all other conditions being equal, using an UV laser with λ = 325 nm is 7 times more efficient than using the green (λ = 532 nm) one. However, spectra acquisition with lasers of lower wavelength is often plagued by background fluorescence which imposes a compromise to be found for a particular task and experimental conditions.

2.1.2. Raman micro-spectroscopy

The combination of Raman spectroscopy with confocal microscopy has significantly broadened the application range of the technique. Micro-Raman simplifies sample preparation and has now taken the lead in non-destructive analysis by means of vibrational spectroscopy [162]. There are two main types of detectors used in the analytical instruments: single-channel and multi-channel. Single-channel detectors allow acquiring one frequency at a time. Nowadays, mainly multichannel charge-coupled devices (CCD detectors) are used in Raman spectrometers, allowing for simultaneous spectra acquisition at all the frequencies [159]. Typical dispersive micro-Raman set-up is represented in Fig. 2.3. The sample, which is fixed to the scan table, is irradiated by a focused laser beam. The scattered light is collected through a lens before it passes through an optical filter to remove Rayleigh scattering. It may be an edge filter (filtering out all the frequencies below a certain wavelength) or a notch-filter (transmitting Raman signals while blocking the incident laser beam). The scattered beam passes through a confocal pinhole that restricts the beam diameter. Then, a set of mirrors drives the light onto a grating that diffracts the beam into multiple rays of different frequencies. These rays are oriented towards the multichannel detector for intensity measurement. The information received by the detector is transformed into spectral information, i.e. signal intensity (counts per second, or arbitrary units) as a function of wavenumber (cm^{-1}).

The acquisition of a Raman spectrum depends on several parameters. The acquisition time consists of the exposure time multiplied by a number of accumulations (scans). Increasing the exposure time leads to higher spectral intensity as more photons are detected. However, CCD detectors have a saturation level corresponding to the maximum number of photons that can be detected at the same time. The spectral quality can also be improved by accumulating a certain number of scans. Thus, the noise level can be significantly decreased by averaging over the several

scans. Signal to Noise Ratio (SNR), regarding the signal intensity and noise level, is increased by a factor $\sqrt{n}$, with n the number of scans.

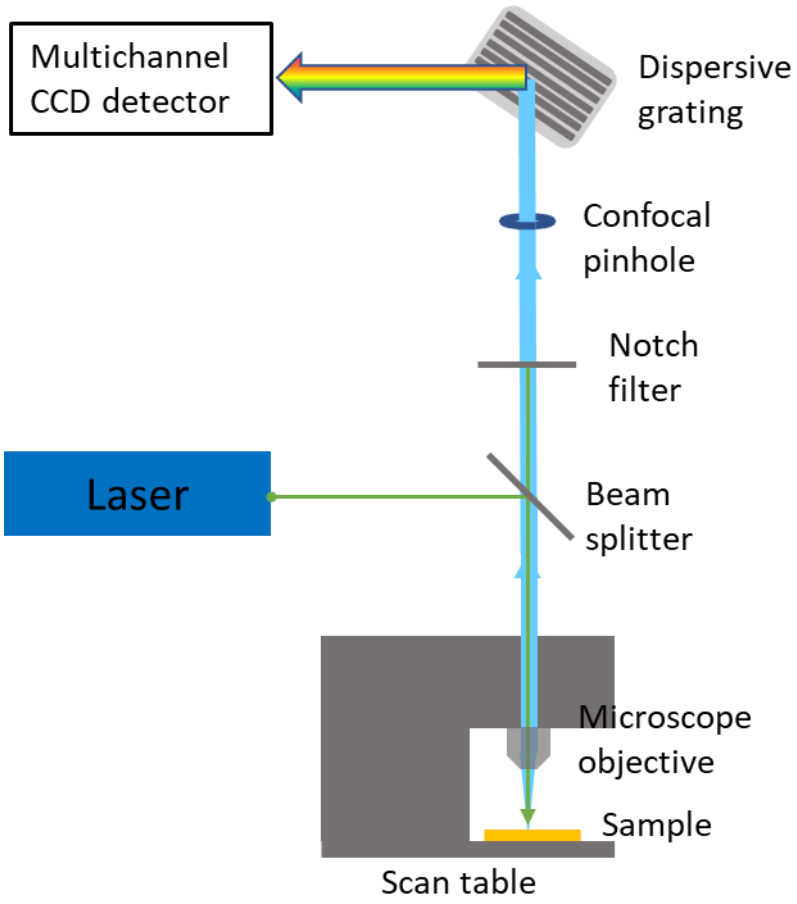

Figure 2.3. Scheme of a confocal micro-Raman set-up.

2.1.3. Applications of Raman spectroscopy

As mentioned above, IR and Raman are complementary techniques, and they can be used either alone or together in order to obtain a complete information about the sample. However, when it comes to aqueous solutions, Raman has a big advantage as it is not affected by H_2O and CO_2 that give very intense bands in IR spectrum. In addition, the relatively easy Raman spectra acquisition procedure makes this technique especially useful for the analysis of polymers, composite materials [163]

and food products [164]. The non-destructive and robust spectra acquisition allows for detection of explosives [165], identification of drugs and counterfeit medicines [166], which can be performed even through the packaging of an analyzed object [167]. Many studies were devoted to the identification of cultural heritage artefacts, including analysis of pigments, authentication, ageing and degradation [168-170]. Beyond these applications, one should mention the fiber optics instrumentation, which came to the fore in 80's, boosting the interest in spectroscopic "in field" and "*in vivo*" analysis [171-174]. The main benefits of micro-Raman are exploited in cell culture analysis [175-177]. Biological objects of different scales can be analyzed, from plant and mammal tissues [178-180] to single-cell and bacteria [181, 182]. Various imaging techniques, in combination with confocal Raman spectroscopy, yield depth-resolved biochemical information with sub-micron spatial resolution, and challenge microscopic techniques relying on fluorescent labeling. Broad possibilities of the method expanded further to *in vivo* analysis of living cells [183], forensic body fluids analysis [184, 185] and medical diagnostics [186-189].

The intensity of Raman spectral bands is proportional to the counts of the number of scattered photons. Under good reproducibility for spectra acquisition, a reference band can be chosen for the calibration. However, these assumptions can be considered only for relatively simple cases, such as analysis of monocomponent solutions. The spectral signature of multicomponent samples may contain overlapping vibrational modes of several molecules. Besides, changes in dipole moment and polarizability of a molecule are affected by their chemical environment (e.g. by solvents), meaning that the corresponding band intensities may vary for different solvents and interferents [190]. To establish the correlation between sample spectral signature and analyte concentration, multivariate calibration should be used (see e.g. [191]).

The main advances in Raman spectroscopy are towards sensitivity enhancement. The 70s marked a breakthrough in the history of the technique, as Surface-Enhanced Raman Spectroscopy (SERS) was developed [192, 193]. This

technique is based on the surface plasmon resonance phenomenon, for which the irradiation of roughened surfaces at certain frequencies causes the excitation of localized surface plasmons and, accordingly, enhancement of the electric field. Silver, gold, or copper substrates are basically used as plasmonic surfaces since their plasmonic frequencies are in the visible range. The enhancement mainly depends on the surface roughness and topography which may be achieved by mechanical or electrochemical roughening and nanolithography techniques [194, 195]. For nanostructured substrates, signal enhancement up to 10^{12} can be achieved.

One of the most impressive technological achievements is Tip-Enhanced Raman Spectroscopy (TERS), which combines the benefits of Atomic Force Microscopy and SERS at a time [196, 197]. Additionally, techniques such as coherent anti-Stokes Raman spectroscopy (CARS)[198], spatially offset Raman spectroscopy (SORS)[199] pushed the boundaries of resolution far beyond the diffraction limit.

2.2. Multivariate data analysis techniques

In general, analytical measurements are aimed at revealing the functional properties of the system and are divided into two main groups: qualitative and quantitative analysis. The qualitative task in a common case is classification, e.g. assignment of the sample to one or more groups on the basis of its (spectral) properties. Quantitative analysis consists of the determination of the concentration or any other numerical property of a sample. In the univariate case it is performed by classical calibration, for which the measured signal **x** is related with the concentration or a functional property **y**. Direct calibration can be represented by (Eq.17):

$$\mathbf{x = py + e} \qquad \text{(Eq.17)}$$

where **p** defines the coefficients for **y**, and **e** represents the error.

In practice, inverse calibration is usually performed, when the concentration **y** is defined as a function of the observation **x**, **b** is the coefficient vector for **x** and the error **f** is associated with the measurement of concentration (Eq.18):

$$y = bx + f \quad \text{(Eq.18)}$$

The majority of analytical measurements in spectroscopy, chromatography, etc. characterizes each analyzed object by a large number of variables instead of only one. Such multivariate data, and multivariate calibration, allow solving most of the problems of univariate calibration, such as when the signal of the target analyte is overlapped by some interfering species. Multivariate data can be represented in a matrix. The values of the analytical signal from *n* samples at *m* variables comprise the elements of the data matrix **X** *(n x m)*. Thus, each row corresponds to the spectrum/chromatogram/voltammogram of one particular sample (Fig. 2.3.)

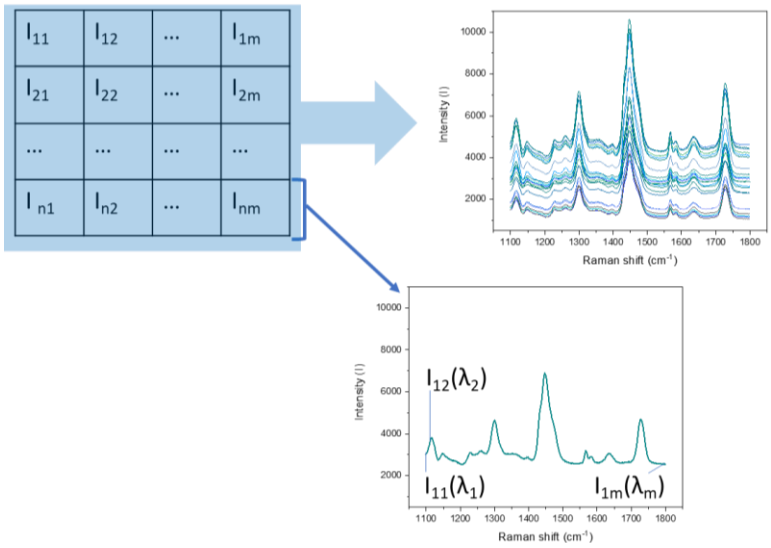

Figure 2.3. Representation of the spectral data in matrix form.

Processing the multivariate chemical data can be performed by means of various chemometric techniques. The term “chemometrics” was used for the first time in 1974 by S. Wold, by analogy with “econometrics” employed in the field of economy using multivariate statistics to derive descriptive and prognostic economical models. According to the IUPAC definition, chemometrics is “the science of relating measurements made on a chemical system or process to the state of the system via application of mathematical or statistical methods” [200] and it arose from the need to

explain the complex phenomena in chemistry. In analytical chemistry, the application of chemometric methods involves chemistry, mathematics and statistics for solving the problems of qualitative and quantitative analysis. Consequently, the goals of chemometrics include extracting the most relevant information from chemical data, appropriate representation of these multivariate data, as well as experimental design allowing yielding meaningful data.

2.2.1. Principal component analysis (PCA)

Dealing with multivariate data is often complicated by the fact that it cannot be presented visually in the 3-dimensional space without loss of useful information. However, reducing the dimensions of the initial dataset may help to understand the data structure and provide its visual representation. The basic technique employed for the visualization and exploration of multivariate data is Principal Component Analysis (PCA) [201, 202]. Principal Component Analysis aims at reducing the dimensionality of data. It is performed by calculating the new variables, principal components (PCs), which are the linear combinations of the initial variables. The PCs are basically the axes in the new latent variable (LV) space, to which the original data is projected. Considering the spectral data containing *n* samples and *m* variables (for example Raman shift), each sample can be represented as a point in *m*-dimensional space, with *m* being the number of variables of the spectra. As a result, *m* variables of the initial **X** matrix are projected into the space of *k* latent variables. For example, if the number of significant PCs is 2, each sample from the *m*-dimensional spectral dataset is projected onto 2-dimensional space (Fig. 2.4.).

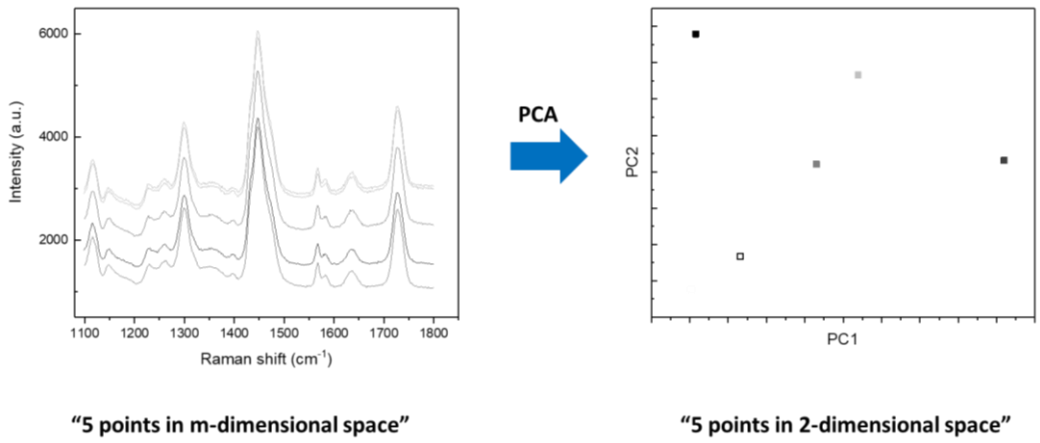

Figure 2.4.. The illustration of the projection of multidimensional spectral data into the 2-dimensional space.

The first PC is drawn in the direction corresponding to the maximal variance in the initial dataset. The second PC is drawn in the next maximal variance direction which is orthogonal to the first PC. This procedure continues until a sufficient amount of variance in the data is "explained". During PCA, the original data matrix **X** (*n* samples x *m* variables), is decomposed into the product of two new matrices: scores and loadings (Fig. 2.5.):

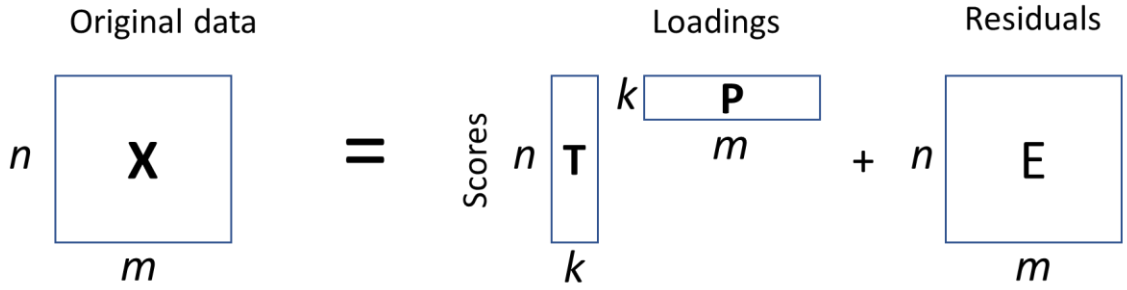

Figure 2.5. The schematic representation of data decomposition with PCA.

T (*n x k*) is the scores matrix, **P** (*k x m*) is the loadings matrix and **E** (*n x m*) is the residuals matrix. *k* is the number of PCs in decomposition. PCA decomposition of the **X** matrix can be represented as a sum of *k* sets of scores and loadings vectors:

$$\mathbf{X} = \mathbf{T}\mathbf{P}^{\mathrm{T}} + \mathbf{E} = \mathbf{t}_1\mathbf{p}_1^{\mathrm{T}} + \mathbf{t}_2\mathbf{p}_2^{\mathrm{T}} + \ldots + \mathbf{t}_k\mathbf{p}_k^{\mathrm{T}} + \mathbf{E} \qquad \text{(Eq.19)}$$

The scores **T** contain the information about the coordinates of the samples in the new LV space (Fig 2.6). In scores plots, the samples are positioned according to their similarity/dissimilarity in the original space. Although samples of the same type may form clusters in scores plots, PCA is not a classification algorithm.

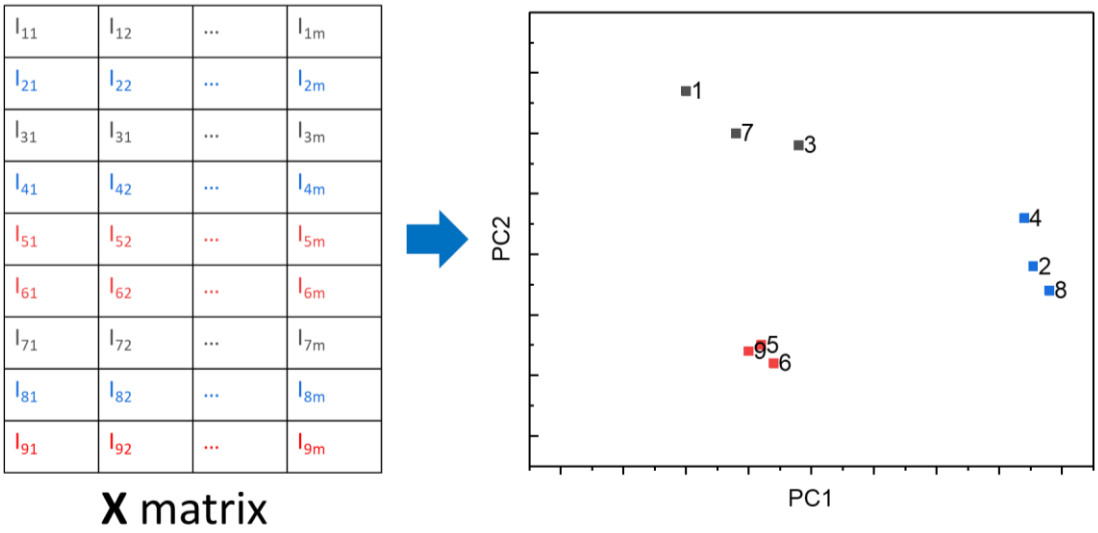

Figure 2.6. The scores plot from the PCA model built from the data matrix. The samples formed 3 clusters (grey, blue and red colors in the graph and data matrix, respectively).

The loadings matrix **P** reflects the relationship between the latent LVs and the original X-variables (namely the “weight” of each variable in the LV space). It also reveals the correlation between the initial variables and their contribution to the PCA model. The loading values for each particular PC often resemble the spectra of the pure components and can be compared to the reference spectra. As the origin of the bands within the original spectra is usually available, the examination of the “loadings spectrum” (loadings vs. wavelength) may allow for the structural interpretation of the data (Fig. 2.7).

The components can be calculated using the Nonlinear Iterative Partial Least Squares (NIPALS) algorithm [201]. In this algorithm, each component is defined by the couple of vectors **t** and **p** and is calculated one after the other. The first couple of **t** and

p vectors for the scores **T** and loadings **P** matrices are calculated using the entire **X** matrix. The details are represented in Annex 1.

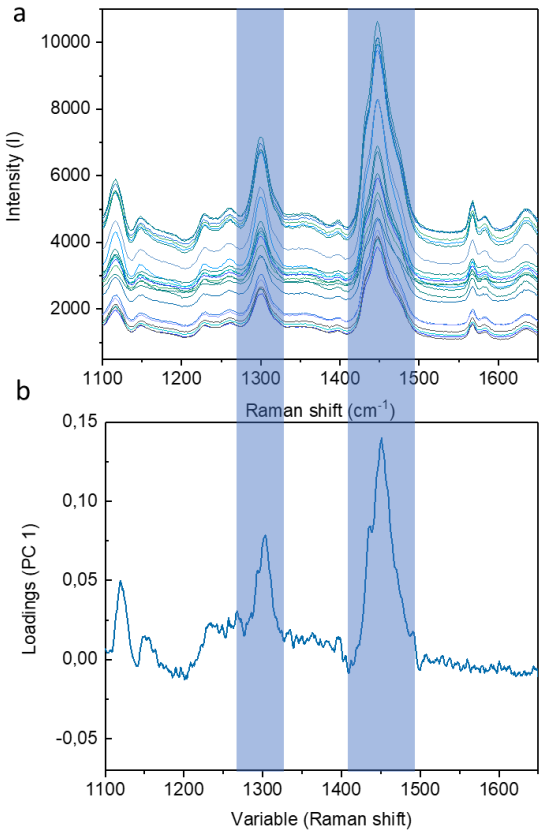

Figure 2.7. The (a) raw spectral data vs. (b) “loadings spectrum”.

As said before, the first PC explains the maximum variance of the data, the second one the second highest variance and so on. The optimal number of PCs is chosen out of the total percentage of explained X-variance (normally above 90 %, however this particular number depends strongly on the particular data processing task and may vary significantly).

The PCA itself is employed for the decomposition multivariate data in many chemical analysis fields, mainly for spectroscopic data. Besides, PCA serves as a “building block” for other chemometric techniques, such as e.g. PCR (principal component regression), SIMCA (soft independent modeling of class analogy).

2.2.2. Partial Least Squares (PLS)

Inverse calibration allows an estimation of the analyte concentration from a multivariate response. The most popular method for this purpose is Partial Least Squares (PLS) regression [203]. PLS is especially useful when there is a high collinearity in the **X**-variables and when the number of predictors largely exceeds the number of observations (e.g. for spectroscopic data). The idea of PLS consists of establishing the relation between the matrix of predictors, **X** (e.g. absorbance values) and the matrix **Y** of variables to be predicted (e.g. analyte concentration)**.** In the first step, both **X** and **Y** are projected into a new variable spaces using latent variables. Then PLS components are calculated in a way that the **X**-variance is maximally correlated with the variance in **Y**. Due to this procedure, only the **X**-variables correlated with target property in **Y** will receive significant weights for modeling.

For *n* observations and *k* latent variables, simultaneous decomposition of **X** (*m* predictors (response channels) x *n* samples) and **Y** (*n x a*, n x 1 for the single Y-variable) matrices is performed in the following way (Fig. 2.8):

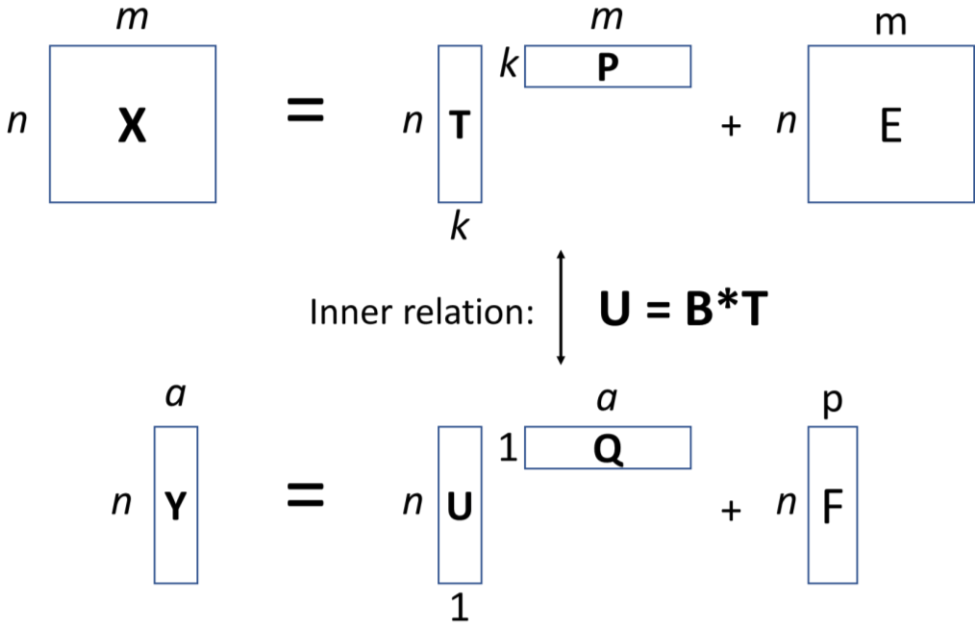

Figure 2.8. Schematic representation of the PLS regression. **T** (*n x k*) and **U** (*n x 1*) are **X**- and **Y**- scores, **P** (*k x m*) and **Q** (*1 x k*) are **X**- and **Y**-loadings, **E** (*n x m*) and **F** (*n x p*) are **X**- and **Y**-residuals, respectively.

The decomposition aims to represent the original data in the new space of *k* latent variables. Latent variables (which are technically the axes of the new space, to which **X** and **Y** values are projected) are chosen so that they provide the maximum covariance between **T** and **U**.

The PLS regression can be performed by means of various algorithms and NIPALS is the most widely used one [204]. The detailed algorithm is described in Annex 2. The implementation of PLS regression for quantitative analysis is a two-step approach. The first is the calibration step, or training. Calibration consists of model construction which is done with known values of **X** and **Y**. The obtained model should be properly validated in order to determine the optimal number of latent variables. The best option to do this is using an independent set of samples – test set, but very often cross-validation procedures are implemented. The second step is prediction. The calculated calibration model is applied for the prediction of unknown **Y** values from new **X** observations ($\mathbf{X_{new}}$) (Eq.20):

$$\hat{\mathbf{Y}} = \mathbf{X_{new}}\mathbf{B} \qquad \text{(Eq.20)}$$

The validation process is very important and normally it is at this step when the model is optimized with respect to the employed variables, potential outliers, preprocessing, etc. The main parameter to estimate the PLS model quality is the root mean square error (RMSE). RMSE has the **Y** variable units and can be calculated using the following equation:

$$\mathrm{RMSE} = \sqrt{\frac{\sum_{i=1}^{n}(y_{i,\,pred} - y_{i,ref})^2}{n}} \qquad \text{(Eq.21)}$$

where $y_{i,pred}$ – y value predicted with a model, $y_{i,ref}$ – reference *y* value (known concentration of the analyte), *n* – is the number of samples in the selected test set. The PLS model calculation is aimed to reach the lowest possible RMSE value in validation.

Another important parameter giving the information about the agreement between the explained variance of the data is correlation coefficient (R). The coefficient of determination, R^2 can be used as an additional quality criterion for the PLS model. It is function of residual sum of squares (RSS), describing the deviation of the predicted $y_{i,pred}$ values from the reference $y_{i,ref}$, and the total sum of squares (TSS) (Eq.22).

$$R^2=1-\frac{RSS}{TSS}=1-\frac{\sum_i (y_{i,\,ref}-y_{i,pred})^2}{\sum_i (y_{i,\,ref}-\bar{y})^2} \qquad \text{(Eq.22)}$$

The samples for the test set should not present in the calibration set and should be distributed continuously over the whole range of **Y**-values.

If the number of samples is small and an independent validation test set cannot be employed, cross-validation can be as mentioned above considered. In this case a part of the calibration set is left out of the model and then this part is used to assess the validation error. This step is then repeated for another combination of samples in the calibration and validation sets and the parameters are averaged all over the repetitions. The splitting of the samples into calibration and validation subsets can be made in several different ways: randomly, one by one (full cross-validation), by certain systematic segments, etc. As the same sample may be present in the validation and calibration sets for different repetitions, the results of the prediction performance assessment obtained in cross-validation are often overoptimistic. Model validation with an external test set is preferable, but it requires more samples which is not always available/economically reasonable.

Variables importance in projection (VIP) values [205, 206] can be used for the estimation of the contribution of particular variables to the model:

$$VIP_m = \sqrt{\frac{\sum_{i=1}^{k} w_{mi}^2 \cdot SSY_i \cdot M}{SSY_{total} \cdot k}} \qquad \text{(Eq.23)}$$

where *m* is the variable number, *M* is the total number of variables, w^2 stands for the squared elements of **X**-weights matrix, *i* is the PLS component number, *k* is the total number of PLS components and SSY_i is the sum of squares of explained variance for the i^{th} component. SSY_i and SSY_{total} can be calculated with regression coefficients and **X**-scores (Eq.24):

$$SSY_i = b_i^2 \mathbf{t_i^T t_i}$$
$$SSY_{total} = \mathbf{b^2 T^T T} \quad \text{(Eq.24)}$$

If the VIP_m value for m^{th} variable is bigger than 1, the variable can be considered as important. The optimal number of PLS components is normally chosen to achieve the minimum at the "RMSE vs number of components" curve. The validation results, apart from the confirmation of the model relevance, can give information about the importance of variables, interrelations between variables, experimental errors etc.

Nowadays PLS regression is a common tool in the arsenal of chemometrics and the variety of PLS applications described in literature is really huge. The data from electrochemical instruments, molecular and atomic spectrometers in various modalities and chromatographic separations with various detection types can be successfully processed with PLS. Many studies are aimed at a modification the data preprocessing and variable selection techniques in order to improve the predictive capabilities of the developed models [207, 208].

2.2.3. Data preprocessing

Multivariate calibration model requires not only optimization of the model parameters, but also data preparation prior to building a model. Data preprocessing techniques are required to eliminate various undesirable features of the data: noise, baseline shift, unequal scaling, outliers, etc.

In order to make the **X** and **Y** distributions symmetrical, the data should be centered prior to analysis. Mean-centering is performed by subtracting the column-

mean value from each variable. Both **Y**- and **X**-variables are usually mean-centered prior to building a PLS model. Standardization, also known as scaling (dividing the values of each variable by the standard deviation for this variable) may be performed as well. It gives comparable variance to all the variables thus helping to avoid artificial highlighting of the variables with a larger numerical variance, which is not always associated with the modeled phenomena. Scaling is required when **X**-variables are measured in different units. Therefore, scaling is usually not recommended in the preprocessing of spectroscopic data.

Many chemometric methods were mainly developed for spectral data treatment, and various preprocessing algorithms for baseline correction, smoothing and normalization exist for these data. Baseline curvature in the acquired spectra can be corrected, by for example the Asymmetric Least Squared algorithm (AsLS) [209, 210]. The elimination of the baseline shift effects can be also performed by taking derivatives of the acquired spectra, using the Savitzky-Golay algorithm [211].

A typical problem for spectral data is light scattering related to the nature of the sample and the experimental set-up. Such factors as morphological nonuniformity of the sample (e.g. in the spectroscopy of fibers) often lead to the data distortion and low signal-to-noise ratio. To compensate for these external non-chemical factors deteriorating the analysis precision, various spectral correction techniques were developed. Scattering correction can be performed by various preprocessing procedures. The most common ones are multiplicative scatter correction (MSC) and standard normal variates (SNV) [212]. The MSC technique is based on building a linear model (least squares regression) for the calculation of the coefficient describing the relationship between the $\mathbf{x}_i$ and a chosen reference spectrum (for example, averaged over the batch) (Eq.25).

$$\mathbf{x}_i = \mathbf{a}_i + \mathbf{b}_i\bar{\mathbf{x}} + \mathbf{e}_i \qquad \text{(Eq.25)}$$

where $\bar{\mathbf{x}}$ is the average spectrum, $\mathbf{a}_i$ the linear model parameters and $\mathbf{e}_i$ the residuals. Then all the spectra in the batch (**X** matrix) are corrected by means of these $\mathbf{b}_i$ coefficients, according to (Eq.26):

$$\mathbf{X}_i^{MSC} = \frac{\mathbf{x}_i - \mathbf{a}_i}{\mathbf{b}_i} \quad \text{(Eq.26)}$$

The SNV normalization algorithm [213] consists in centering and scaling of each spectrum by dividing it by the standard deviation in the intensity over the batch (Eq.27) :

$$\mathbf{x}_i^{SNV} = \frac{\mathbf{x}_i - \bar{X}_i}{\sigma} \quad \text{(Eq.27)}$$

where $\bar{x}_i$ is the mean value of the spectra intensity at a chosen wavelength *i*, and σ is the standard deviation of the $\boldsymbol{x}_i$ value within the batch

The selection of the best data treatment methods should be driven by the sample nature, experimental set-up and the type of the acquired data. Optimization of the preprocessing algorithm is especially important for the PLS prediction performance, as the spectral intensity may vary drastically in the case of a non-uniform sample thickness.

2.3. Experimental

The main part of investigation of complexation-induced evolution of organic ligand Raman spectral signature was performed using N^2,N^2,N^9,N^9-tetrabutyl-1,10-phenanthroline-2,9-dicarboxamide (PDAM) as a ligand. This ligand was previously shown to be capable of transition metal cations binding, and corresponding plasticized polymeric membranes yielded Nernstian sensitivity towards Cd^{2+} ions in aqueous solutions [214] (Fig. 2.9.):

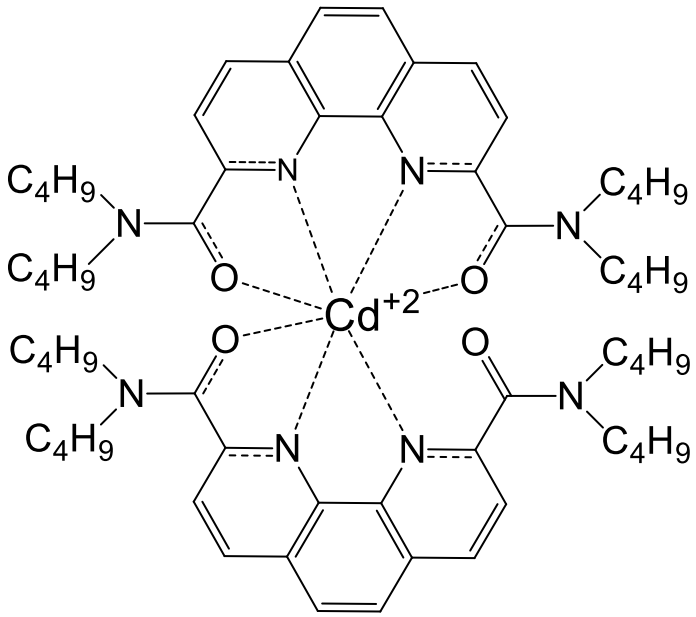

Figure 2.9. Schematic representation of the PDAM-Cd^{2+} complex (crystal structure), according to [214].

The PDAM-Cd^{2+} complex has 2:1 stoichiometry, and complexation involves 3 out of the 4 available oxygen atoms of the carbonyl groups and 4 nitrogen atoms of PDAM [214]. However, one should expect that the described stoichiometry of the complex will be sterically hindered and not necessarily remain the same in the sensor membrane phase.

2.3.1. Membrane preparation

The conventional PVC-plasticized membranes contain the high molecular weight poly(vinyl chloride) (PVC) (33 wt%), a solvent-plasticizer (66 wt%), a lipophilic additive, and an ionophore (ligand). In this study, 2-nitrophenyl octyl ether (NPOE) was used as a plasticizer. Potassium tetrakis-(4-chlorophenyl)borate (KTClPB) in a concentration 10 mmol/kg was employed as a lipophilic additive and freshly distilled tetrahydrofuran (THF) was used as a solvent for the membrane components during the synthesis.

All membranes were prepared using the standard procedure: all the weighed components were placed in a glass beaker filled with 5 mL of solvent and kept under stirring. After complete dissolution of the components, the mixture was poured into flat-bottomed Teflon beaker and left for 24h until complete evaporation of the solvent. Then, disks of 7 mm diameter were cut from the obtained film.

The membrane compositions in this study were different with respect to the polymeric matrix type, ionophore concentration and presence or absence of lipophilic additive. Three types of polymeric matrices were investigated: traditional PVC-based membranes (NPOE-1-3), the silicon rubber-based membrane (SR), and the plasticizer-free membranes prepared from acrylate copolymer (AC). Besides, three compositions containing only the polymeric matrix components (NPOE-0, SR-0 and AC-0, respectively) were employed as a reference for the estimation of the ionophore contribution to the sensor membrane spectra. The detailed membrane compositions are given in Table 2.1.

Table 2.1. Membrane composition. Mass of the components is given in wt%.

Membrane type	Polymer	Plasticizer (NPOE)	Lipophilic additive (KTCIPB)	Ligand
NPOE-0	33.5	66.5	-	-
NPOE-1	32	65	0.5	2.5 (PDAM)
NPOE-2	29	59	2	10 (PDAM)
NPOE-3	30	60	-	10 (PDAM-2)
SR-0	85	15	-	-
SR	77	13	-	10 (PDAM)
AC-0	100	-	-	-
AC	90	-	-	10 (PDAM-2)

NPOE and KTClPB were purchased from Fluka (Switzerland). THF was purchased from Merck (Germany). The ionophores PDAM and PDAM-2 were synthesized by Prof. Dmitry Dar'in (Institute of Chemistry, Saint-Petersburg State University, Russia) according to the procedure described in [22].

2.3.2. Spectra acquisition

In order to record the Raman spectrum of the surface of the membrane, a 10 µL drop of aqueous cadmium solution was placed on the membrane of 7 mm diameter and then covered with a coverslip glass (22 mm x 22 mm and thickness 0.13 mm), Menzel, Thermo Fisher Scientific). The overall scheme of the measurement set-up is given in Fig. 2.10. A fixed height of 1 mm was used to keep the optical path length constant.

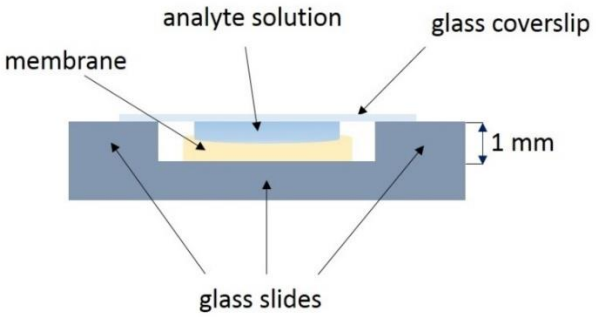

Figure 2.10. Principal scheme of the experimental set-up.

In order to standardize the measurement conditions and to avoid possible kinetic issues related to the formation of ligand-ion complexes, a fixed cut-off time of 5 min contact between the sample drop and membrane was set before spectral analysis. The membrane with the sample was irradiated with a laser beam. The laser spot diameter is equal 1.22 λ / NA, where NA is numerical aperture of the objective (0.7 μm for the 515 nm laser, with an energy of 8 mW at the sample surface). After focusing on the membrane surface, the Raman spectra were obtained using 15 accumulations (2 sec each) in the 1000 – 1700 cm^{-1} wavenumber region. The spectral range for membrane investigation was reduced in order to minimize the analysis time, while keeping all the characteristic bands of interest in the investigated range. Three spectra acquired at different points on the surface of the membrane were registered and averaged for further processing in order to decrease the effects caused by manual focusing namely the intensity variation, so that the standard deviation of spectral bands intensity values within this 3-points set did not exceed 0.5 %.

Between the measurements, sensor membranes were washed in distilled water for 2 minutes. The washing efficiency test is shown in the Fig. 2.11. It can be clearly seen that the bands of interest do not evolve over time (within 2 days).

The Raman spectra were acquired with LabRam HR visible micro-Raman spectrometer (HORIBA Jobin Yvon, France), equipped with a charge-coupled device (CCD) detector (1024×256 pixels), 600 gr/mm grating and using the 100x objective (NA = 0.9) (Olympus). A solid state laser operating at λ = 515 nm was used as an excitation source for the membrane analysis. The spectral resolution was 2 cm^{-1}.

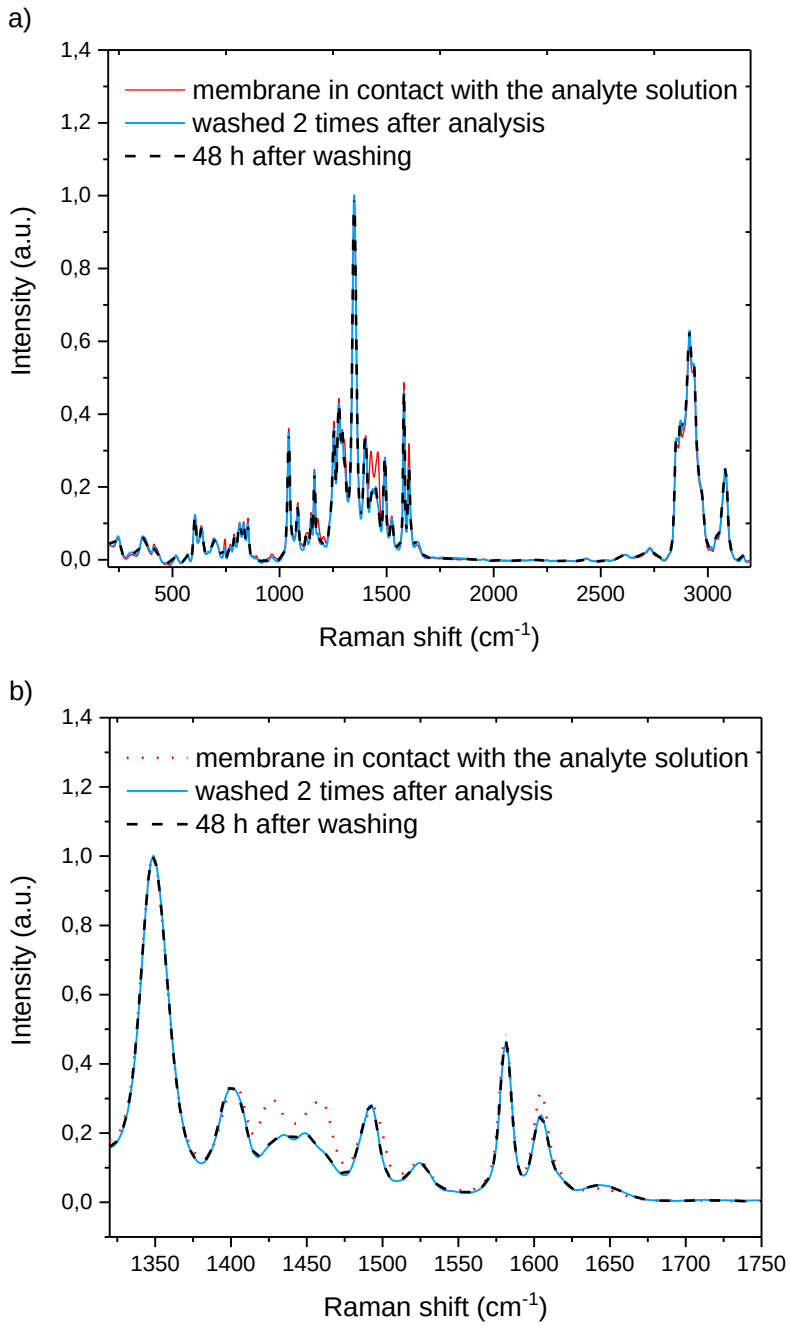

Figure 2.11. Membrane spectra acquired during the analysis (dotted red), after washing (blue) and in 48 h soaking in distilled water (dashed black): a) in the 200–3200 cm^{-1} range; b) 1300 – 1750 range

2.3.3. Raman spectra of membrane components.

Raman spectra of the pure solid ionophores were collected by the KBr pellet method (10 wt% of ligand). The laser spot size at the sample was about 1.1 μm. The spectra of ligands were obtained using 4*30 sec accumulations in the 1000 – 1700 cm^{-1} region. This particular acquisition time was chosen as it provided the biggest signal/noise value. Further increase in the acquisition time led to the saturation of the detector, while reducing the acquisition time resulted in very high noise level.

Raman spectra of the plasticizer were taken with the immersion objective (Olympus, NA = 0.9) on a 20 μL drop deposited at the concave glass slide.

In order to study the relation between the membrane spectra and metal content in the sample solution, the set of aqueous $Cd(NO_3)_2$ solutions was prepared by serial dilution of a 1 M $Cd(NO_3)_2$ (Vekton, Russia) stock solution. The studied concentration range was 10^{-5} – 10^{-2} M and all the measurements were carried out at room temperature. The calibration of the Raman spectrometer prior to measurements was performed with a silicon wafer (the band at 520 cm^{-1} in the spectrum).

2.3.4. Quantum-chemical calculations

In order to interpret more thoroughly the membrane and the ligand spectra, quantum-chemical calculations of the optimal structures followed by harmonic vibrational analysis were performed (provided by V.Koverga, University Lille 1). All the calculations reported here were conducted using density functional theory (DFT) with the Gaussian 09 program package [215]. The hybrid meta-exchange functional M06-2X from Truhlar's group [216, 217] was employed together with Pople-type split-valence triple-ζ basis set augment with polarization function 6-311G (d,p). Optimal geometry of the studied structure obtained in the gas phase was tested to be true minima by the absence of imaginary frequencies. One conformation was used for the vibrational analysis. An empirical scaling factor of 0.954 corresponding to the

employed level of theory was applied to the calculations of the harmonic frequencies [218].

2.3.5. Data analysis

The results of Raman spectral measurements were arranged into a data matrix having samples in the rows and variables (wavenumbers) in the columns. Prior to the data analysis, each spectrum was preprocessed with baseline subtraction (AsLS algorithm) [209, 210] and Savitzky-Golay smoothing (zero derivative order, 9-point window and second-order polynomial)

Since a manual focusing of the measuring system was performed for each measurement, choosing a reference band intensity and the subsequent normalization was required. Otherwise, the differences observed in the intensity of the spectral bands refereed to the polymeric matrix components can be way larger than the evolution of the relevant spectral bands within the calibration range. This means that the area of the sample under study might be different for each measurement, and thus the different amount of scattered light can result in varying spectral intensity. The reference band should have a constant relative intensity and shape in all the membrane spectra, so one of the bands assigned to the membrane matrix compounds (different for each membrane) can be chosen for normalization, similar to the normalization along the solvent bands.

Fig. 2.12 shows the effect of the normalization of 5 spectra of the membrane NPOE-2 upon the interaction with Cd^{2+}solutions. The band at 1350 cm^{-1} ($\nu(NO_2)$ mode of the membrane matrix) was chosen as a reference, as it is unaffected by Cd^{2+} presence. In the Fig. 2.12 (b) the evolution of the bands in the 1420–1480 cm^{-1} related to the interaction with Cd^{2+} can still be observed, while the intensity of the bands assigned to the membrane matrix remains constant.

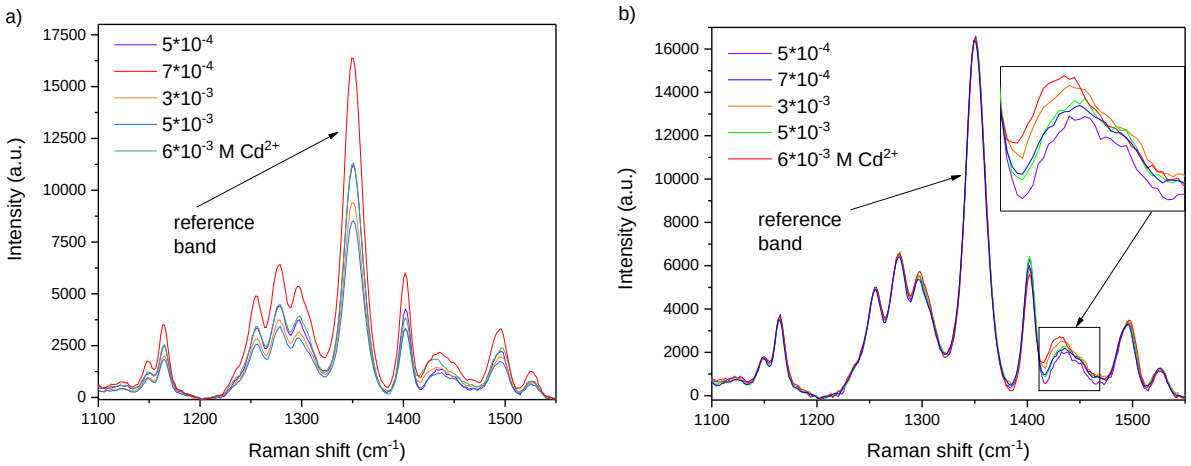

Figure 2.12. The spectra of the NPOE-2 membrane upon the interaction with 5 Cd^{2+} solutions of different concentrations. The preprocessing procedure included: a) baseline correction (AsLS algorithm); b) baseline correction (AsLS algorithm), normalization along the intensity of the reference band at 1350 cm^{-1}.

Principal component analysis (PCA) and partial least squares (PLS) regression were employed in order to establish qualitative and quantitative relationships between the Raman spectra and metal content in the sample solution. Data preprocessing and PLS modelling were done in Matlab (The MathWorks, USA).

2.4. Results and discussion

2.4.1. Membrane components spectra

In order to estimate the bands of interest appearing in the membrane spectral signature, the spectra of membrane components (ionophore (Fig. 2.13-14), plasticizer (Fig. 2.16), and a lipophilic additive (Fig. 2.17) were taken. The 1000 – 1700 cm^{-1} spectral range (the group frequency and a part of fingerprint region) was chosen for this study. The spectral range of 2850 – 3150 cm^{-1} contains overlapping bands corresponding to the C-H stretching modes from all the membrane components. As it seems impossible to estimate the contribution of each component to the membrane spectrum, this range was not used for the calibration. The bands below 1000 cm^{-1} were excluded as well due to the uncertainty in the multi-component spectra interpretation for the “fingerprint” region.

As a first step, the spectrum of PDAM in the KBr pellet was registered. The raw PDAM spectrum in the 250–3150 cm^{-1} range is shown on the Fig. 2.13.

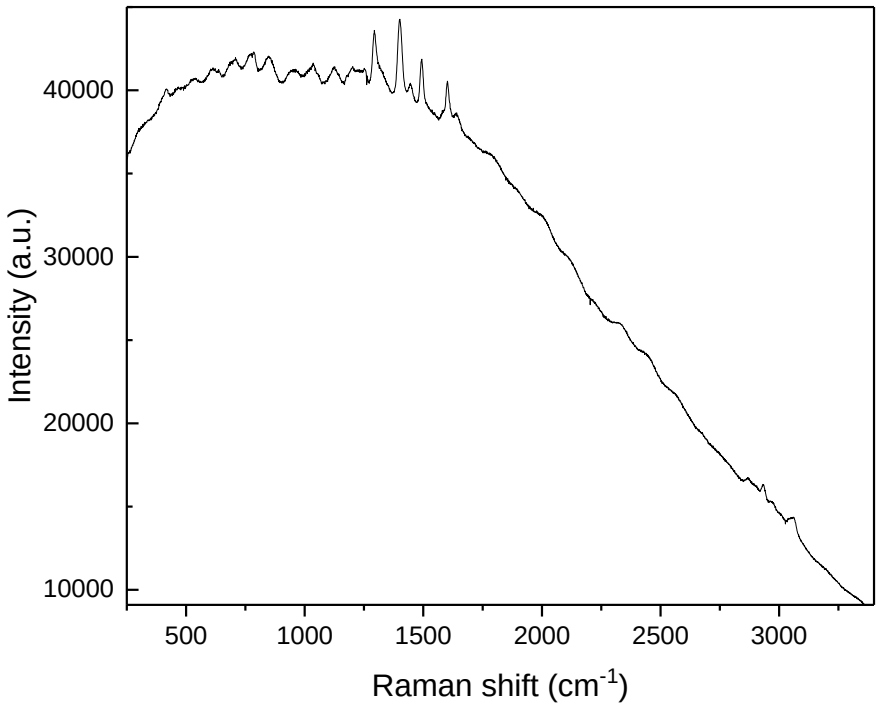

Figure 2.13. PDAM Raman spectrum (250–3150 cm^{-1}).

A high level of fluorescence can be observed. Besides, the 2750–3100 cm^{-1} region contains overlapping bands that can be attributed either to C–H of PDAM, PVC and NPOE. The interpretation of the bands in the fingerprint area (below 1100 cm^{-1}) is complicated for the same reasons. However, zoom-in in the 1000–1700 cm^{-1} range and baseline removal using AsLS algorithm [209, 210] yields the interpretable spectrum. The assignment of the PDAM vibrational modes [219-221] was performed for the interpretation of the potential changes in frequencies and the band intensity observed upon cadmium binding (Fig. 2.14).

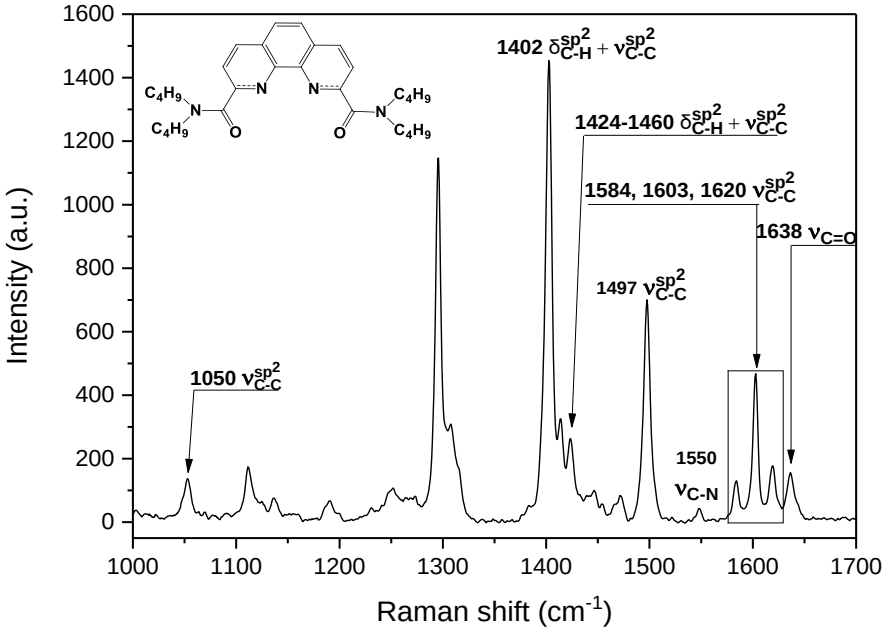

Figure 2.14. PDAM Raman spectrum (1000–1700 cm^{-1}). The preprocessing procedure included AsLS baseline removal.

The assignment was done using the information available in [219-221] and using simulated spectra obtained from quantum chemical calculations (Fig. 2.15).

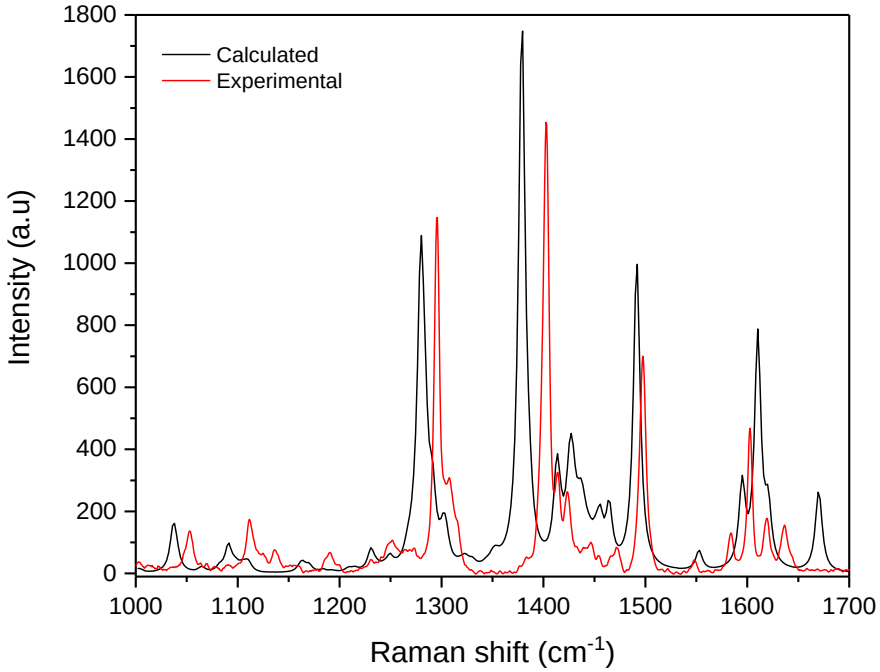

Figure 2.15. PDAM simulated Raman spectrum vs. experimental spectrum.

Spectral band shapes and relative intensities of experimental and calculated spectra are in a good agreement. However, bands in the calculated spectrum are shifted compared to the experimental, due to the obvious difference in the conditions between theoretical study (in vacuum) and experimental study (in KBr pellet).

The band position for the calculated and experimental results of the assignment are reported in Table 2.1. PDAM is a tetradentate ligand, thus oxygen atoms from amide groups (Amide I, 1638 cm^{-1}) and nitrogen atoms from the phenanthroline ring are expected to be involved in the complexation [214], giving the main contribution to the changes in the spectra [61, 222]. Additionally, changes in the C...N vibrational mode (1548 cm^{-1}) can be caused by involving the electron lone pair of the nitrogen atom into the structure of the complex. Besides, chelate formation can affect the whole phenanthroline system, similarly to 6-membered heterocycles possessing low density of polarizable electrons [223].

Table 2.1. PDAM spectrum bands assignment (v: stretching mode, δ: bending mode).

Raman shift, cm^{-1}		Assignment
Simulated	Experimental	
1037	1053	v (C-C) C_{sp}^2
1091	1111	δ (C_{sp}^2-H) in-plane
1109	1138	v (C-C) C_{sp}^2
1164	1189	v $(C\text{-}N)_{amide}$ (Amide III)
-	1231	δ (C_{sp}^2-H)
1231	1252 1274	δ $(C\text{-}H)_{twist}$ [1] for $(CH_2)_n$, n >4,
1280	1296	v $(C\text{-}H)_{symmetric}$ $(\text{-}CH_3)$
1303	1308	δ $(C\text{-}H)_{wagging}$ for $(CH_2)_n$, n >4
1379	1402	δ (C-H)+ v (C-C), C_{sp}^2[219]
1414	1414	δ (C_{sp}^2-H)
1427	1424	δ $(C\text{-}H)_{scissoring}$ + v $(C\text{--}N)_{phenanthroline}$
1436	1446	δ $(C\text{-}H)_{scissoring}$ + v (C-C), C_{sp}^2 [220]
1456	1454	v $(C\text{-}H)_{antisymmetric}$ $(\text{-}CH_3)$
1463	1473	v $(C\text{--}N)_{phenanthroline}$
1492	1497	δ (C-H)+ v (C-C), C_{sp}^2
1553	1548	v (C-C) +v $(C\text{-}N)_{phenanthroline}$
1595	1584	v (C-C), C_{sp}^2
1610	1603	v (C-C), C_{sp}^2
1620	1619	v (C-C), C_{sp}^2 [224]
1669	1638	v (C=O) (Amide I)

The raw spectrum of the plasticizer (*o*-nitrophenyl octyl ether, NPOE) is shown in the Fig. 2.16 (a). Bands in the 2800–3150 cm^{-1} range can be attributed to the C-H modes of the phenyl ring (3150 cm^{-1}) and various fragments of the octyl substituent of the aliphatic chain (2850 cm^{-1}). The assignment of the most informative bands in the 1000–1700 cm^{-1} range is shown in the Fig. 2.16 (b). The most intense band in the

spectrum is assigned to the -NO_2 group in the NPOE molecule (1350 cm^{-1}). Furthermore, the very intense bands corresponding to the phenyl ring stretching modes can be observed.

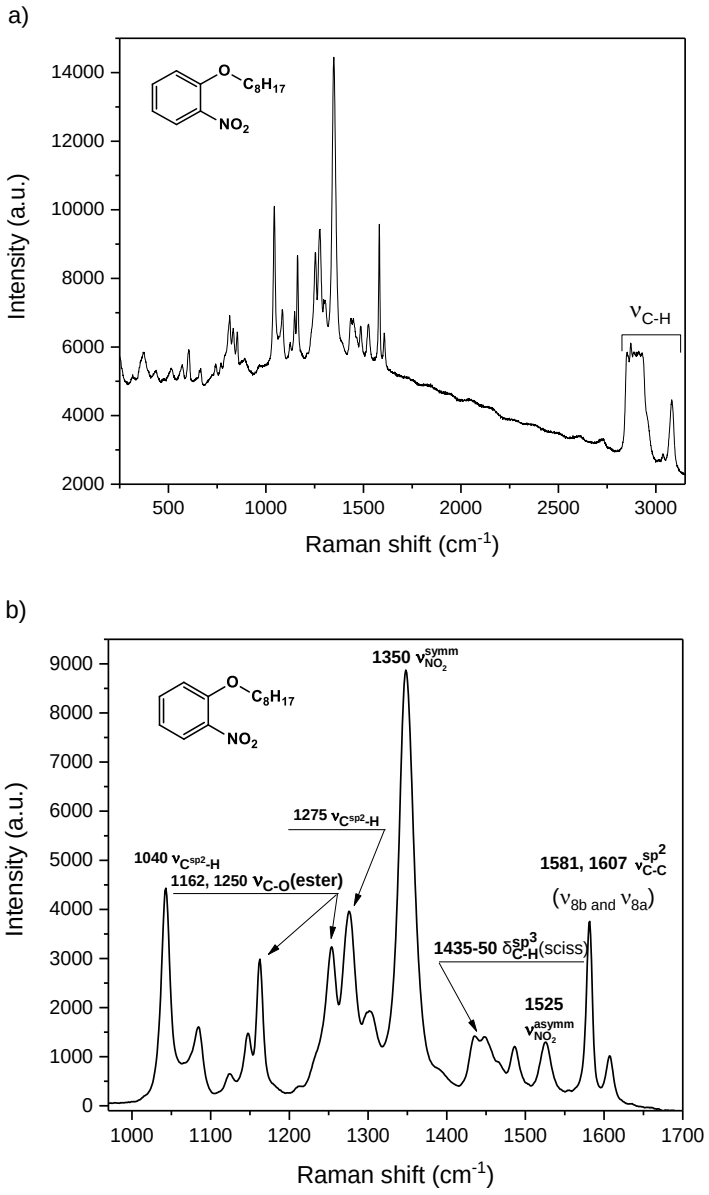

Figure 2.16. Raman spectrum of the plasticizer NPOE. (a) – raw spectrum, 250–3250 cm^{-1} range; (b) – after baseline removal using AsLS algorithm and 11-point Savitzky-Golay smoothing, 1000–1700 cm^{-1} range,.

The spectrum of the lipophilic additive KTClPB is shown in the Fig. 2.17. All bands of high intensity in this spectrum correspond to the phenyl ring stretching modes [225], except for the band at 728 cm^{-1}, which can be attributed to ν_{C-B} mode.

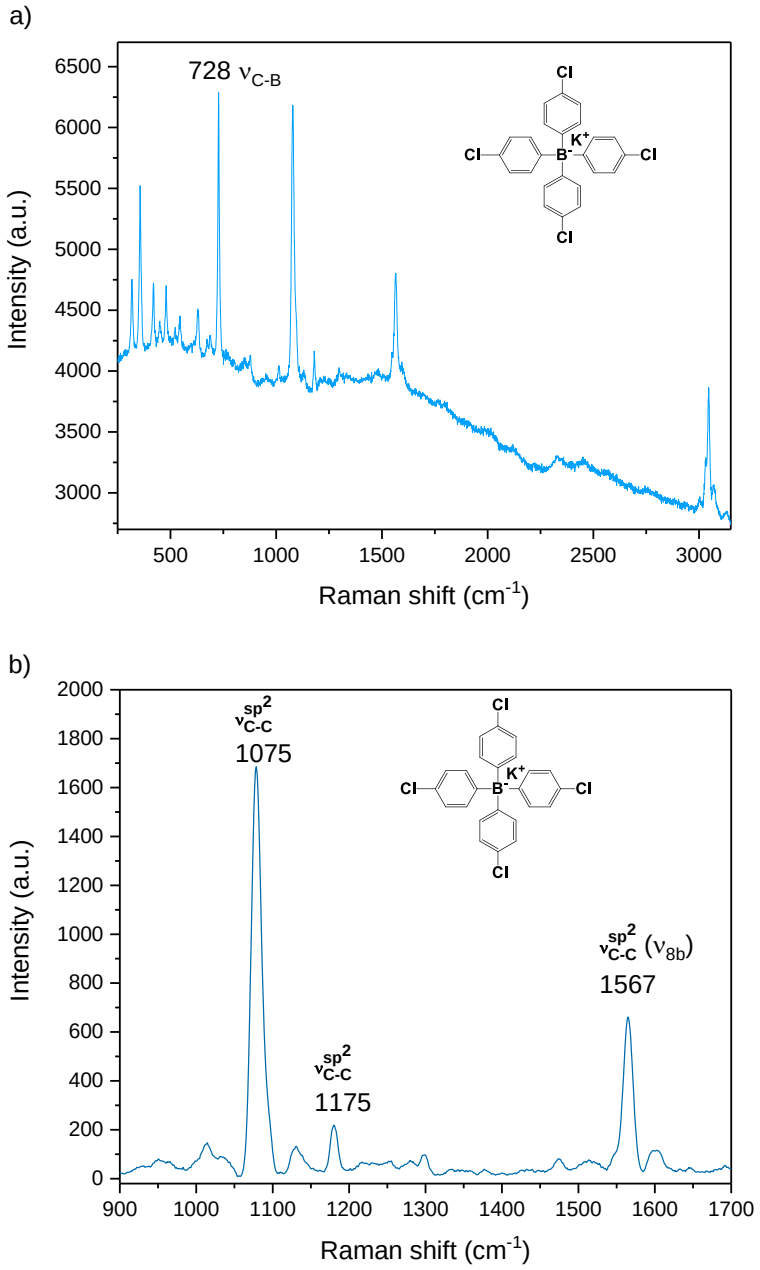

Figure 2.17. Spectrum of the potassium tetrakis-(4-chlorophenyl)borate (KTClPB): a) raw, 250–3250 cm^{-1}; b) 1000–1700 cm^{-1} (baseline removal using AsLS algorithm, 11-point Savitzky-Golay smoothing).

Then the spectra of the PVC-plasticized membrane having the standard composition were taken. Typical ligand content in ISE membranes is around 1-2 wt%. In spite of the high intensity of highly characteristic bands of the aromatic ring stretching modes of PDAM and KTClPB, they are not expected to appear in the NPOE-1 membrane spectrum due to overlapping with the corresponding bands of NPOE and their relatively low content in the membrane. However, in the spectrum of the standard ISE membrane (NPOE-1), only minor differences with the NPOE-0 (membrane without ligand) were observed, and the spectra in general were similar to the one of the reference (NPOE-0) (Fig. 2.18). For further investigations, it was decided to increase ligand concentration in all the membranes up to 10 wt% in order to observe the changes of the ligand bands directly. It can be seen in the Fig. 2.18 (blue color) that in this case the differences with the reference NPOE-0 are much more pronounced.

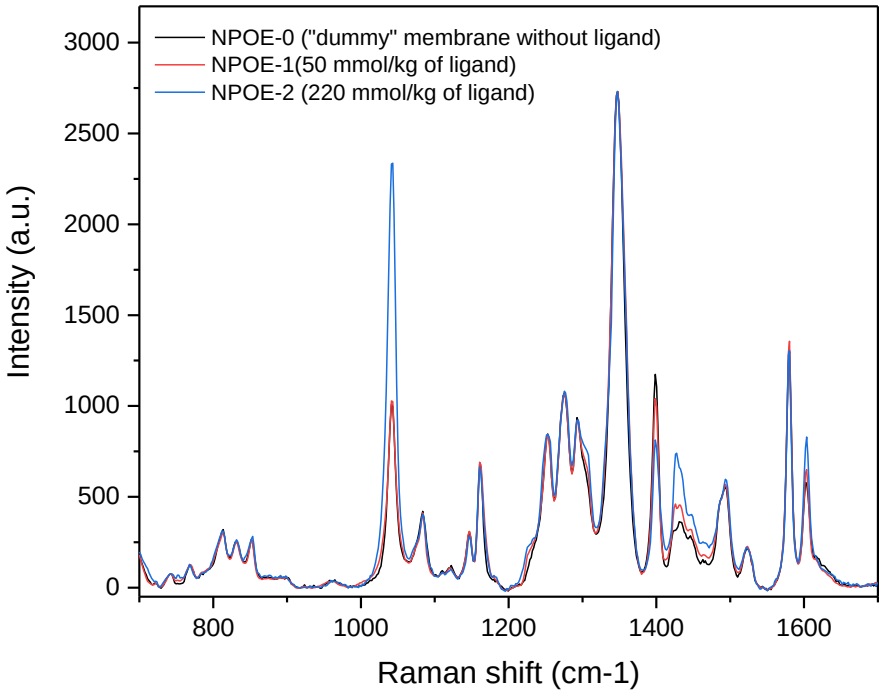

Figure 2.18. Spectra of the standard sensor membrane NPOE-1, NPOE-2 and the reference membrane NPOE-0 (without ligand).

Plasticizers, as a major membrane component, give the most noticeable contribution to the spectral signature of the membrane (Fig. 2.18). Since the nitro group is highly polarizable, it is not surprising that the -NO_{2symm} mode of NPOE molecule at 1350 cm^{-1} has the highest intensity in the membrane spectrum. This fact allows for using it as a reference band for normalization of the intensity all over the spectral set.

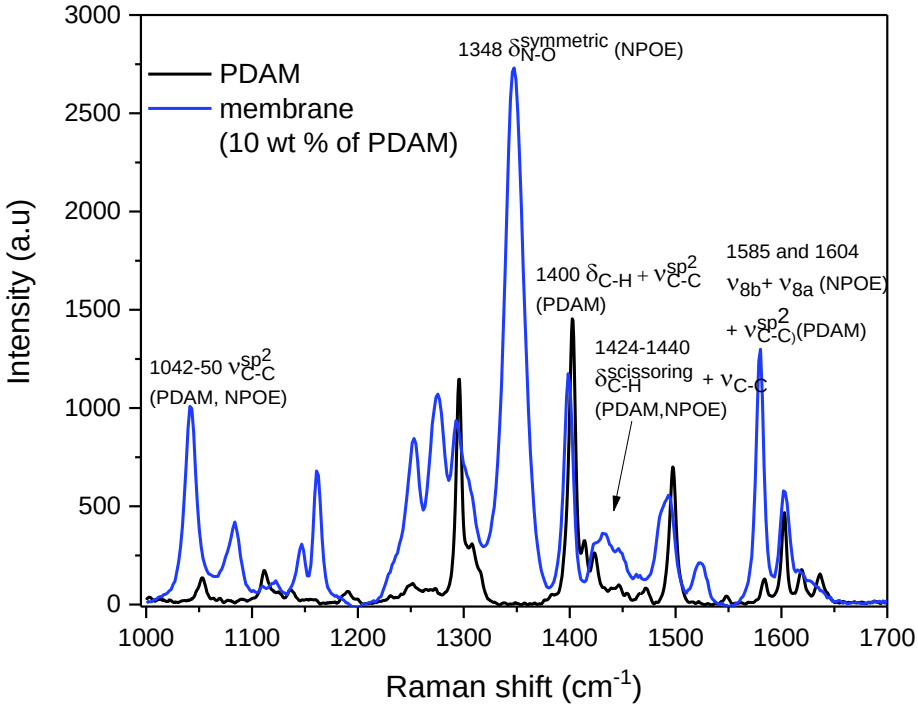

Figure 2.19. PDAM spectrum vs. spectrum of the sensor membrane NPOE-2. The preprocessing included baseline removal using AsLS algorithm and 11-point Savitzky-Golay smoothing.

At the next step, the spectra of the ligand-containing membrane in contact with aqueous cadmium solutions of different concentrations were registered. The variations in the spectral signature of the membrane after interaction with 10^{-4}, 10^{-3} and 10^{-2} M Cd^{2+} can be observed (Fig. 2.20). The complexation-induced evolution of the bands appears mainly in the 1380 – 1520 cm^{-1} range. It is important to mention, that spectral

reproducibility was quite good and the selected band intensity (1402 cm^{-1}) in replicated measurements did not vary more than 0.5%.

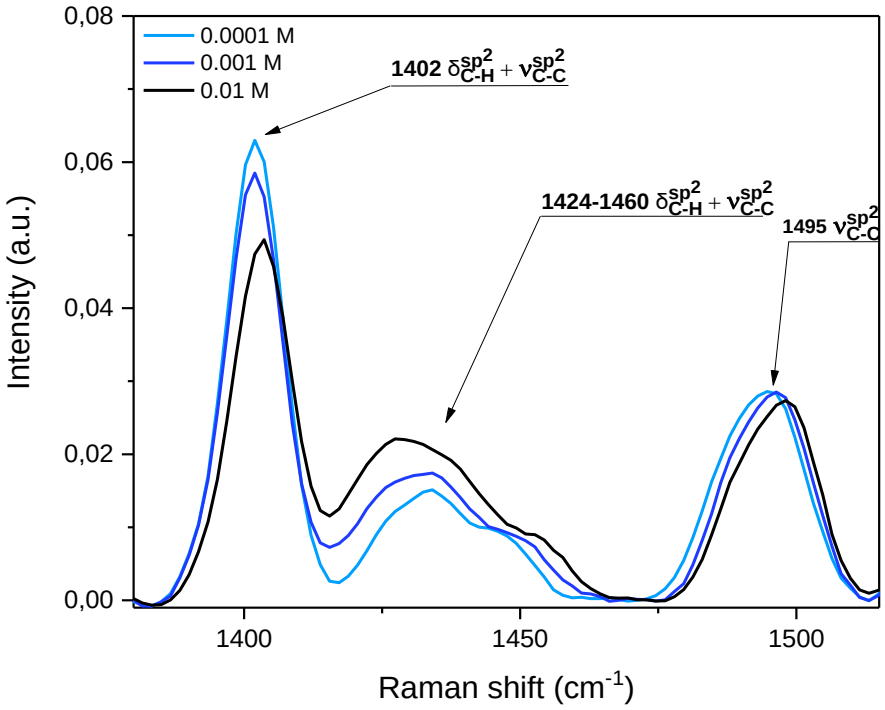

Figure 2.20. NPOE-2 membrane spectra evolution upon the interaction with 10^{-4}, 10^{-3} and 10^{-2} M $Cd(NO_3)_2$ aqueous solutions.

In order to evaluate the applicability of PVC-plasticized membranes for quantitative determination of metal cations by Raman spectroscopy, the analysis of membrane spectra after interaction with aqueous solutions with different Cd^{2+} concentration in the range 10^{-4} – 10^{-2} M was performed. Sample compositions are listed in Table 2.3.

Table 2.3. Cd^{2+} sample solutions.

Sample #	1	2	3	4	5	6	7	8	9	10	11	12
$[Cd^{2+}]$, 10^{-3} M	0,1	0,5	0,7	0,9	1,0	3,0	4,0	5,0	5,5	6,0	8,5	10

The spectra of the membrane corresponding to the composition in Table 2.3 are presented in the Fig. 2.21 in the range 1100 – 1650 cm^{-1}.

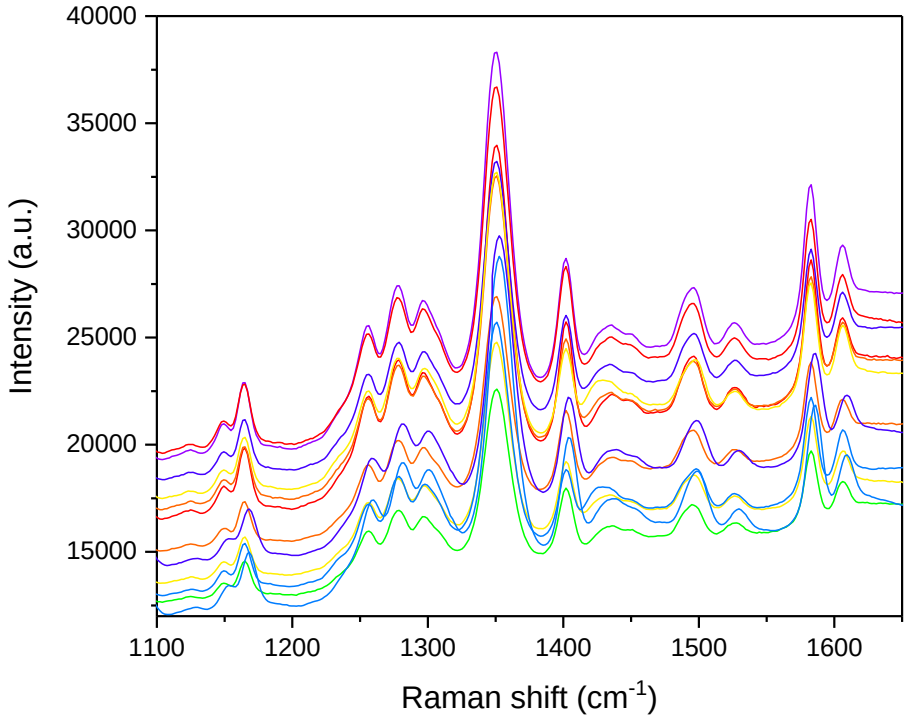

Figure 2.21. NPOE-2 membrane spectra upon the interaction with $Cd(NO_3)_2$ aqueous solutions (*10^{-3} M).

It can be seen from the Fig. 2.21 that only subtle changes in the 1380–1500 cm^{-1} range can be observed, and thus smoothing of the spectrum may have negative rather than beneficial effect on the multivariate calibration. Thus, the pre-processing routine consisted only in baseline correction (AsLS algorithm) and normalization along the intensity of 1350 cm^{-1} band (Fig. 2.22).

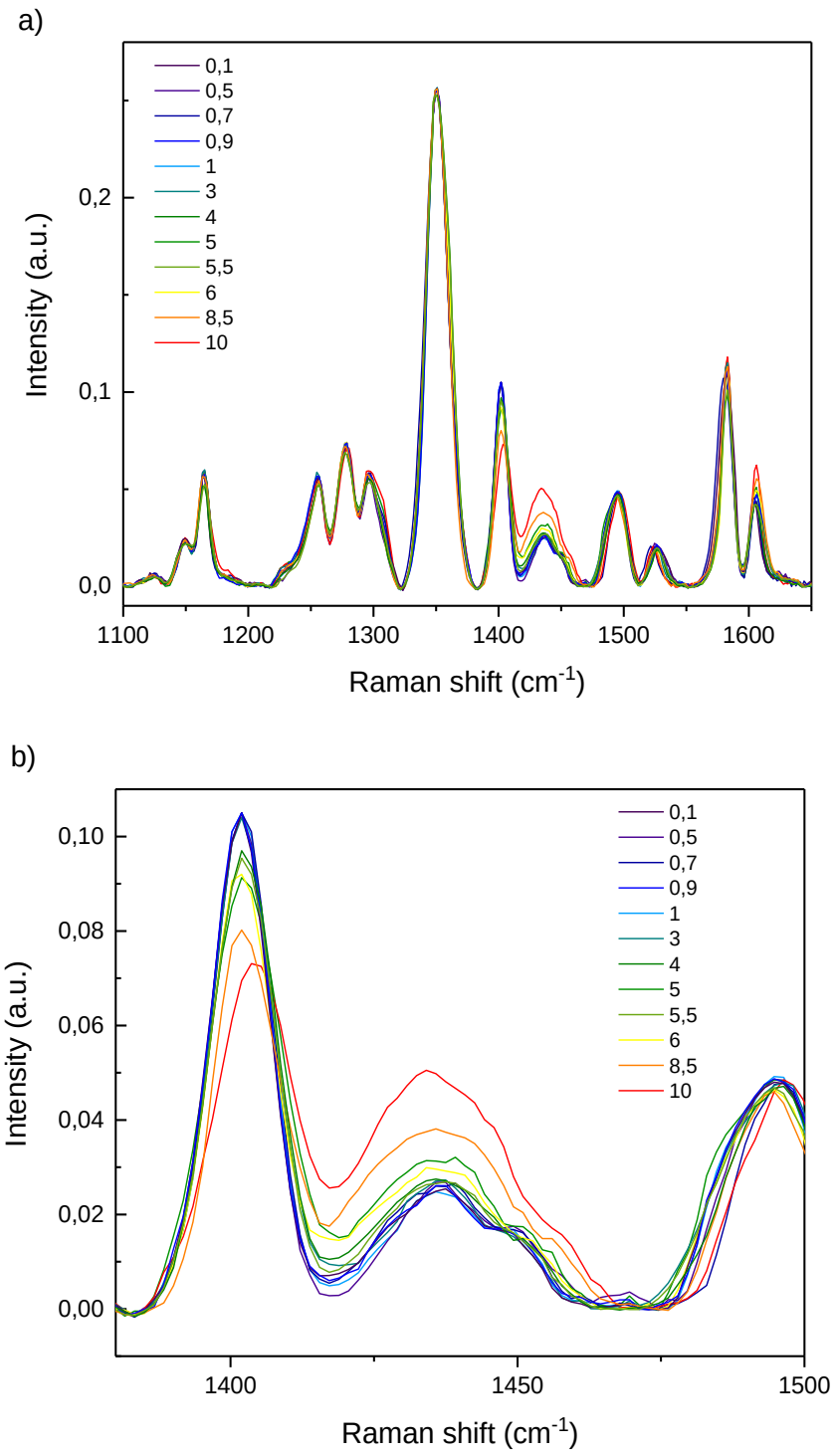

Figure 2.22. NPOE-2 membrane spectra upon the interaction with $Cd(NO_3)_2$ aqueous solutions (*10^{-3} M) (baseline correction, normalization): a) 1100–1700 cm^{-1} range; b) 1380–1500 cm^{-1} range.

Then the spectral set was processed with PLS regression in order to establish a relation between spectral signatures and Cd concentrations. The model was optimized using full cross-validation and a three-component PLS model was retained resulting in the following metrics: validation $R^2 = 0.97$ and root mean squared error of cross-validation RMSECV =$6.3*10^{-4}$ M.

Since the number of samples was not that large, the predictive performance of the model could not be evaluated independently. Nevertheless the obtained model demonstrates that the observed spectral evolution is highly correlated to the Cd^{2+} concentration of the sample in contact with the membrane. The total variance explained by the 3 components of the model was 69 % in **X**-variables and 99 % in **Y**-variables, which also confirms this correlation. It must be pointed out that the RMSECV, which is computed for the wide concentration range (10^{-4} – 10^{-2} mol/L), may provide a pessimistic error value, since it simultaneously takes into account concentration values that vary over two orders of magnitude.

As an additional validation of the model, we applied permutation testing. The RMSECV values were compared over 50 different 3-component PLS models for 50 different random permutations of the values in **Y**-vector (Cd concentrations) (Fig. 2.23). The average RMSECV was found to be $1.67*10^{-2}$ M, more than two orders of magnitude higher than the one obtained for the original model. Moreover, none of the permuted models had a better RMSECV than the original one. This confirms the relevance of the observed spectrum-concentration correlation.

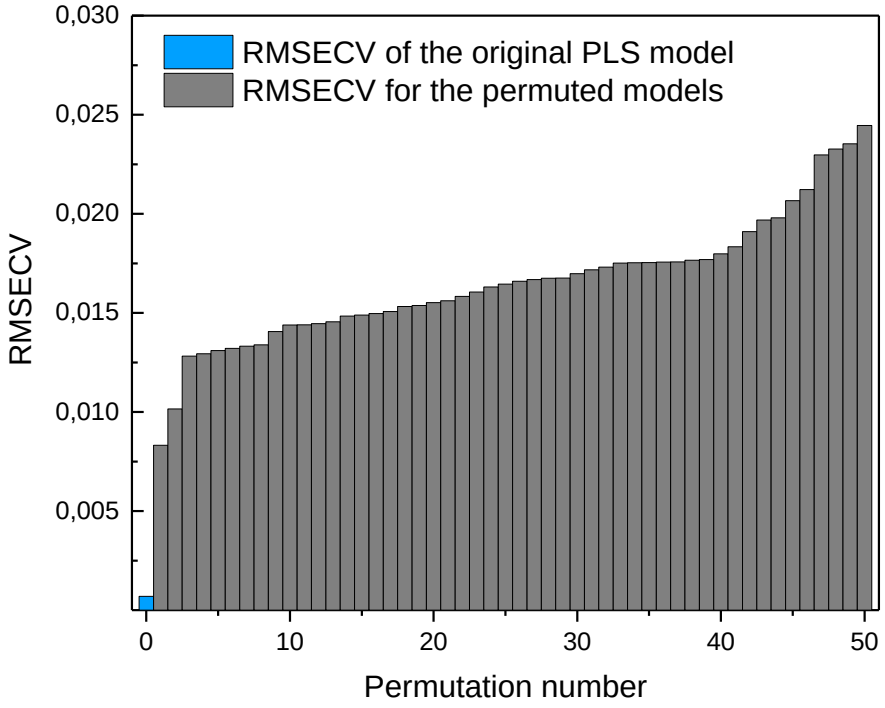

Figure 2.23. The RMSECV values calculated for random permutations of Cd concentrations vs. RMSECV of the original PLS model.

Evaluation of the VIP scores of the model (PC2) showed that the biggest contribution to the model is due to the spectral bands that referred to PDAM: δ (C-H) bending modes at 1402 cm^{-1}, 1424 – 1440 cm^{-1} of the phenanthroline skeleton (Fig. 2.24).

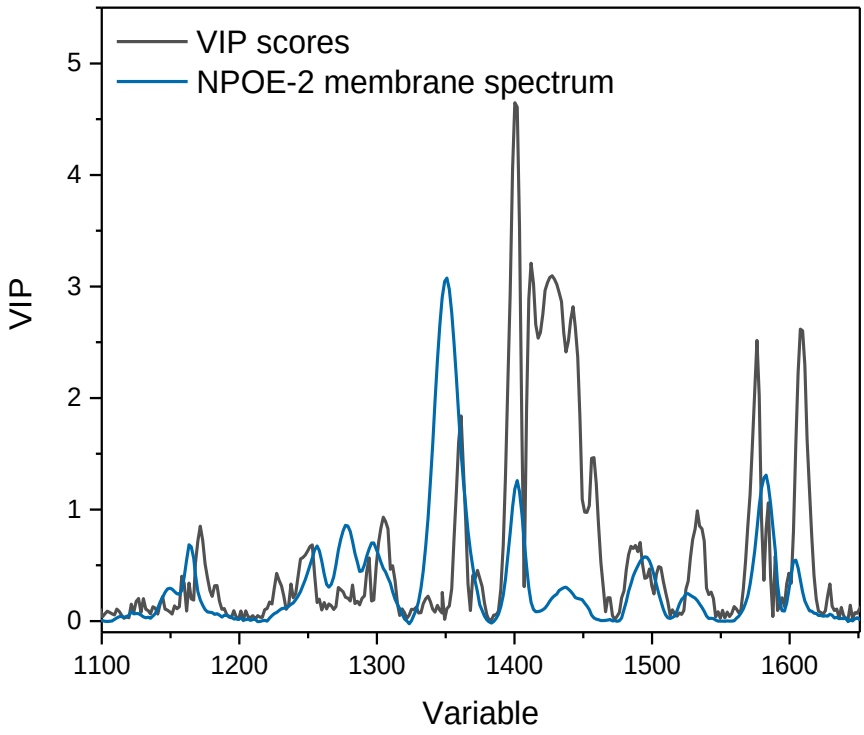

Figure 2.24. Comparison of a Raman spectrum of the NPOE-2 membrane with VIP scores.

VIP values in the 1585 – 1640 cm^{-1} region have relatively low values due to overlapping with ν_{8a} and ν_{8b} aromatic ring stretching modes, corresponding to NPOE plasticizer. The observed congruence in VIP values of the PLS model and membrane spectra may serve as an additional proof of the validity for the established correlation.

The “measured vs. predicted” plot for the PLS model is provided in Figure 2.25.

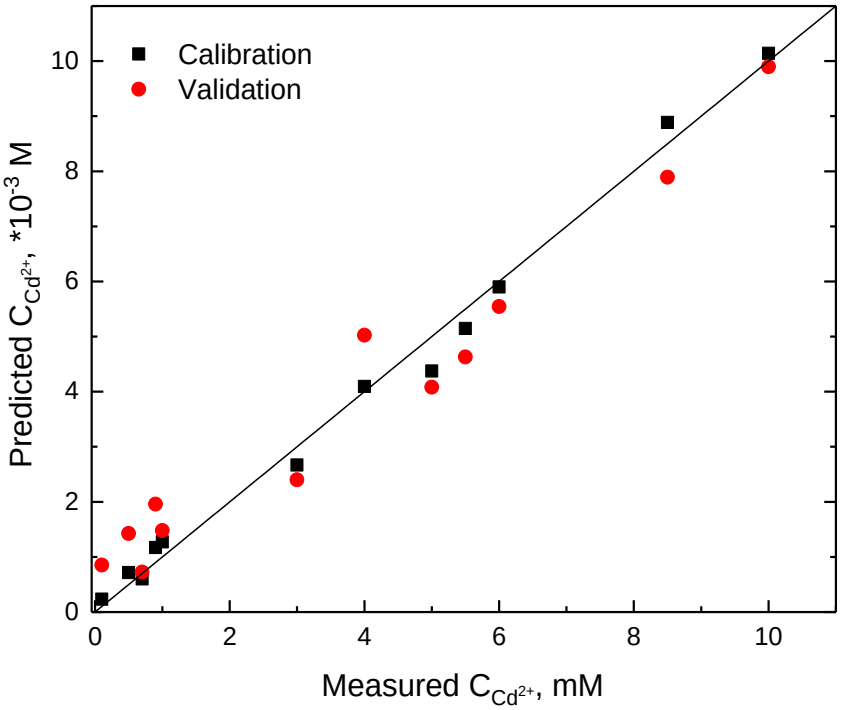

Figure 2.25. PLS regression model for the calibration in 10^{-4} – 10^{-2} M $Cd(NO_3)_2$ solutions.

As the most distinct changes in the membrane spectra are referred to the ligand, it was decided to investigate whether the proposed transduction principle could work for the membrane without the lipophilic additive as well. Within this assumption, the PVC-plasticized membrane without lipophilic additive was prepared (NPOE-3). It consisted of 30 wt% PVC, 60 wt% plasticizer (NPOE), and 10 wt% of ionophore. The ligand (ionophore) had a similar structure as the one in the PDAM-2 membrane but with ethyl- and (4-ethyl)phenyl substituents in the amide group instead of the butyl-one (Fig. 2.26). It was shown in [214] that these two ligands impart the same sensing properties of PVC-plasticized membranes (e.g. sensitivity towards Cd^{2+}).

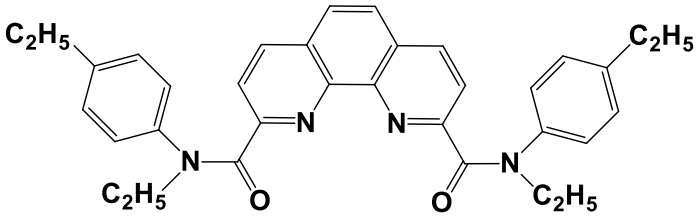

Figure 2.26. Structure of the N^2,N^9-diethyl- N^2,N^9-bis(4-ethylphenyl)-1,10-phenanthroline-2,9-dicarboxamide ionophore.

At first, the preliminary test on the interaction of the NPOE-3 membrane with the aqueous cadmium solution was performed. The spectra of the membrane in contact with 0.1 M cadmium nitrate were compared with those of the membrane in contact with water. Similar to the NPOE-2 membrane with the lipophilic additive in its composition, the spectral signature of NPOE-3 demonstrates certain changes upon contact with the cadmium solution. Fig. 2.27 shows the raw spectrum of NPOE-3, and Fig. 2.28 shows the spectrum of the NPOE-3 membrane upon the interaction with Cd^{2+} solution, processed with AsLS baseline correction, Savitzky-Golay smoothing and normalization (against NO_2 band of NPOE) algorithms.

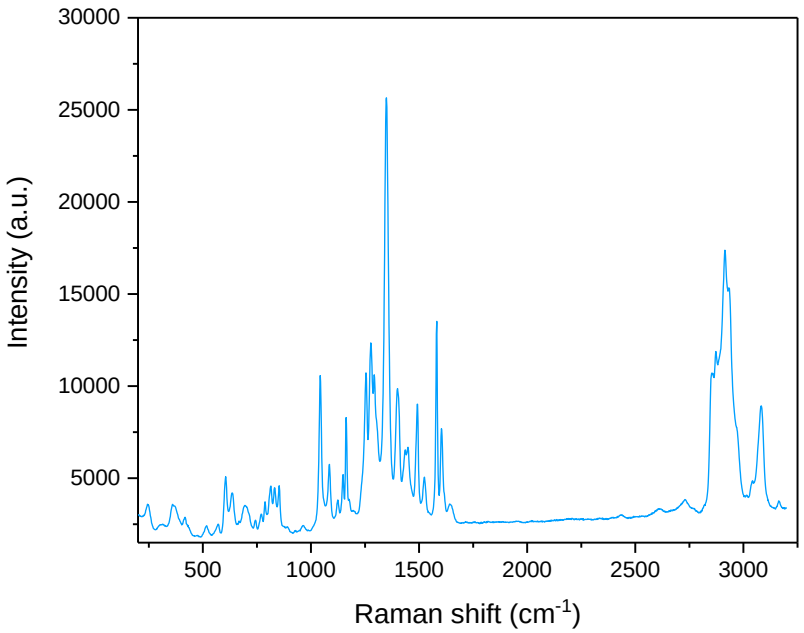

Figure 2.27. Raw spectrum of NPOE-3 membrane.

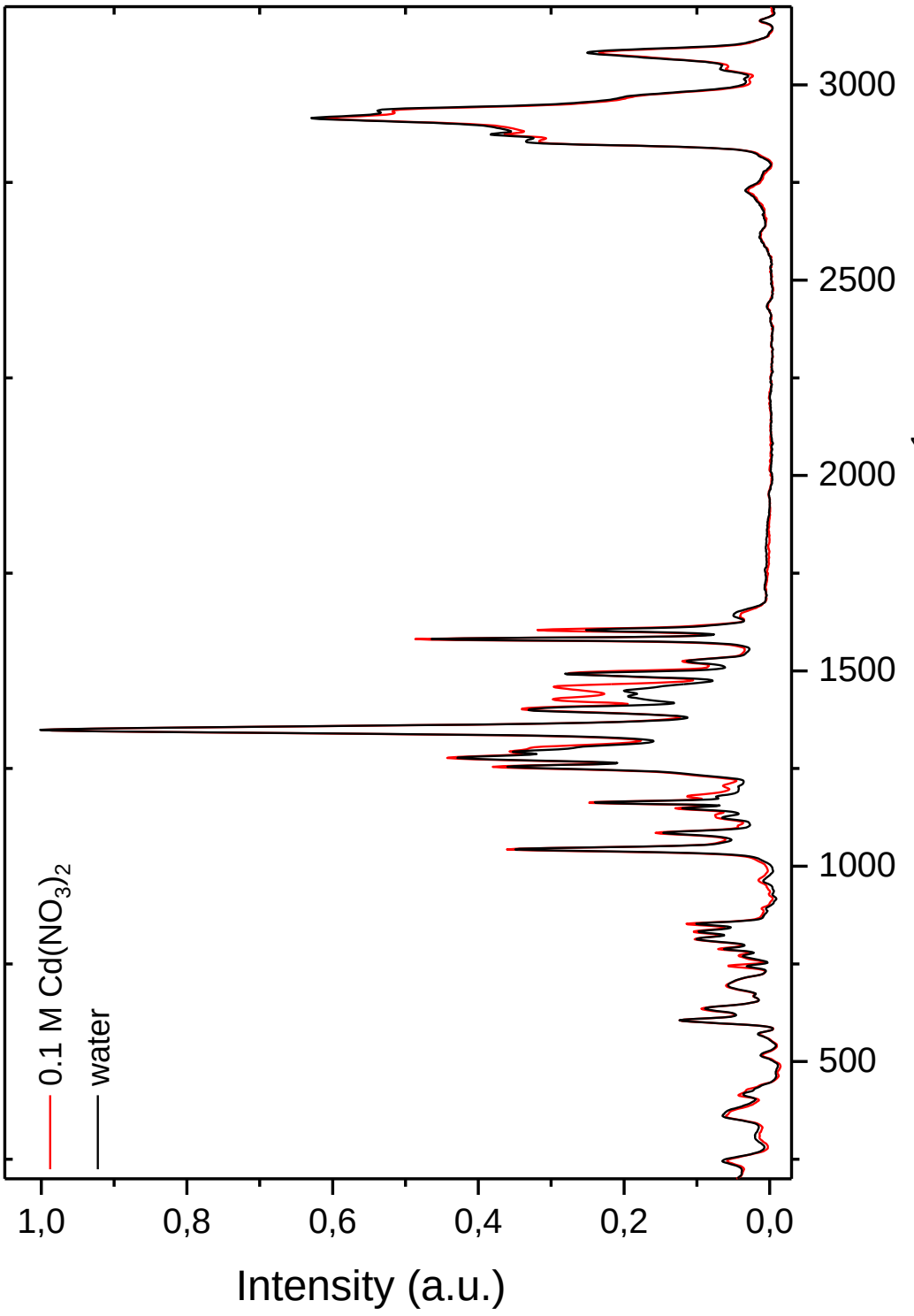

Figure 2.28. NPOE-3 membrane spectra evolution upon the interaction with a 0.1 M $Cd(NO_3)_2$ aq

Most of the spectral bands that are subjected to changes upon the interaction with Cd^{2+} are located in 1420–1500 cm^{-1} range. The shift of the bands position at 1437, 1450, 1492 cm^{-1}, together with their intensity changes could be attributed to the PDAM-Cd^{2+} interaction. The detailed representation of the above-mentioned bands is shown in the Fig. 2.29. The evolution of the Raman bands at 1420–1460 cm^{-1} can be due to the redistribution of the electronic density in the aromatic phenanthroline system of the ligand. In classical ISE membranes, the main function of the lipophilic ionic additive is to promote the transfer of ions from the aqueous phase into the membrane phase. The observed effect in the spectrum of NPOE-3, that does not contain the lipophilic additive, confirms the well-known fact that the primary contribution to the sensor response is generated on the membrane surface. Thus, in case of the sensing with Raman transduction, the presence of ion-exchanging sites in the membrane is not a prerequisite.

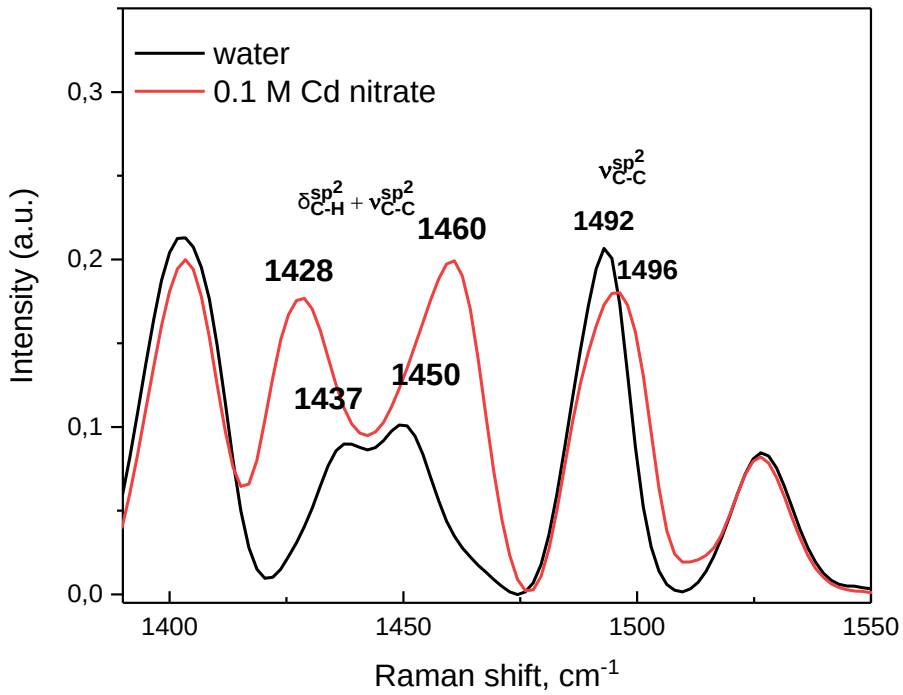

Figure 2.29. NPOE-3 membrane spectra evolution upon the interaction with a 0.1 M $Cd(NO_3)_2$ aqueous solution (1380–1550 cm^{-1} range).

The next step for testing our assumption was to estimate the changes in the membrane spectra upon the interaction with Cd^{2+} solutions of varying concentrations. The composition of the tested samples is given in Table 3.4.

Table 2.4. The concentrations of the Cd^{2+} solutions for the calibration.

Sample #	1	2	3	4	5	6	7	8	9	10	11
$[Cd^{2+}]$, 10^{-4} M	9,2	8,9	8,5	7,8	7,2	6,7	6,0	4,8	4,0	2,5	1,0

The obtained spectra (Fig. 2.30) were employed to construct PLS regression model relating the spectral signatures of the membrane with cadmium contents in the studied solutions.

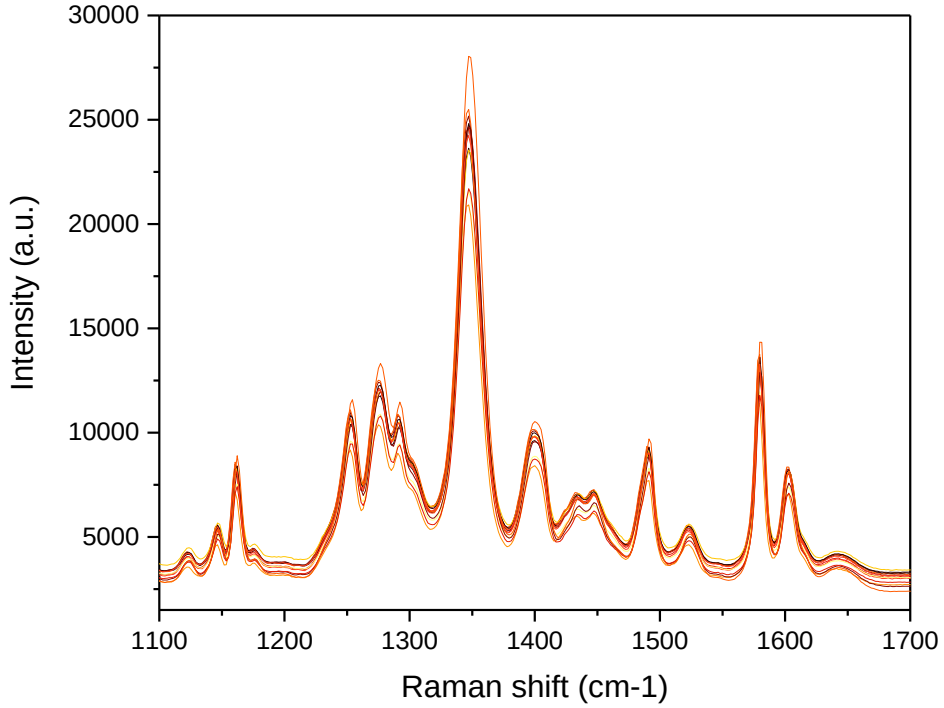

Figure 2.30. NPOE-3 membrane spectra upon the interaction with $Cd(NO_3)_2$ aqueous solutions (10^{-4} – 10^{-3} M)

The preprocessing procedure included a baseline correction (AsLS algorithm), smoothing (Savitzky-Golay algorithm, 7 points) and normalization by the intensity of the reference band (-NO_2 mode of NPOE at 1350 cm^{-1}). Smoothing with other number

of points in a window yielded poorer results in RMSECV just as with NPOE-2 membranes. As the spectral changes upon the interaction of the membrane with low concentration of Cd^{2+} were not strongly pronounced, it was decided to process the derivative spectra as well. Since the number of samples was not very high, “leave-one-out” validation procedure was employed. The parameters of the PLS models for two datasets (with and without derivatization) are provided in Table 2.5.

Table 2.5. Parameters of validation “measured vs. predicted” plot for PLS regression models. N − number of PLS factors.

	Slope	RMSECV, a	R^2	N
Zero order-derivative	0.95	$9.3*10^{-5}$	0.87	6
1^{st} order derivative	0.92	$1.3*10^{-4}$	0.84	2

In general, there is a reasonable correlation between the signals in the Raman spectra of the membrane and concentration of metal ion in contacting solution and this is an additional proof of validity of our assumptions. The PLS model for the zero order derivative spectra is characterized by RMSECV value close to 10^{-4} (in the “lg a” units). However, it is based on 6 latent variables and thus the model is most likely overfitting. On the other hand, the PLS model built on the derivative spectra is based on 2 latent variables only, and still yields reasonably low RMSECV value. This study may serve as an estimation of the lipophilic additive role in the membrane composition for Raman transduction of the analytical signal. First results show that the membrane spectral signature evolution upon the interaction with Cd^{2+} may be observed in a NPOE-3 membrane, consisting of a polymer, plasticizer and ligand only. Thus, the whole polymeric membrane is acting like a support for the lipophilic ligand which is responsible for the analytical signal manifestation and the addition of ion-exchanging sites in the membrane is not required.

2.4.2. Optimization of the membrane composition

The proposed approach to the Raman transduction of the analytical signal from the ISE membranes was shown to be viable for PVC-plasticized membranes. Nevertheless, the composition of the studied polymeric membranes is not fully optimized from the point of view of Raman spectra registration. The polymeric matrix is expected to give the biggest contribution to the membrane spectral signature as it is a major component of the membrane. The high content of the plasticizer in traditional PVC-plasticized membranes leads to the overlap of ligand spectral bands with those of the plasticizer, hereby hindering the study of the evolution of the Raman bands of the ligand upon contact with the sample. Lowering the plasticizer content in the membrane may potentially lead to more a sensitive and more precise detection of metals through the suggested procedure. In order to study this, we have performed several additional experiments.

ISE membranes based on silicon rubber

The next step of the investigation consisted of decreasing the plasticizer content, so that its contribution to the membrane spectral signature would be lower. For this purpose, poly(dimethylsiloxane), widely used for ISFET sensing elements was chosen. The plasticizer content was set at 15 %, as it was reported in [226], and a second membrane (SR-0) did not contain plasticizer at all, similar to ISFET matrices. The procedure of the membrane preparation was the same as for PVC-plasticized membranes, though the silicone rubber dissolution in THF takes much more time (about 1 h). The PDMS-based membrane composition was tested with PDAM ionophore and KTTClPB lipophilic additive.

Silicon rubber is one of the most frequently employed alternatives to the traditional PVC-based ISE membranes. The plasticizer content in the membranes based on silicon rubber (SR) normally does not exceed 20 %, which is three times lower than that in PVC-plasticized sensors. Besides, the Raman spectrum of the silicon

rubber does not contain any bands of high intensity in the 1300 – 1700 cm^{-1} range, where most of the ligand bands are situated.

We have studied the performance of the silicon rubber membrane (SR) containing 13 wt% of plasticizer (NPOE), 77 wt% silicon rubber and 10 wt% of the PDAM ionophore. The spectrum of the SR membrane was compared with that of the SR-0 membrane without ligand (Fig. 2.31). Except for the increase of the intensity of the band at 1400 cm^{-1} and appearance of the band at 1000 cm^{-1} (both referred to the phenanthroline aromatic ν_{C-C} modes), no ligand contribution to the SR membrane spectrum is observed. However, the plasticizer content is still too high for a more detailed registration of a ligand spectrum. Nevertheless, in order to determine if it will be possible to track the evolution of the ligand spectral signature, the spectra of the membrane in contact with 0.01, 0.1 and 1 M Cd solution were acquired.

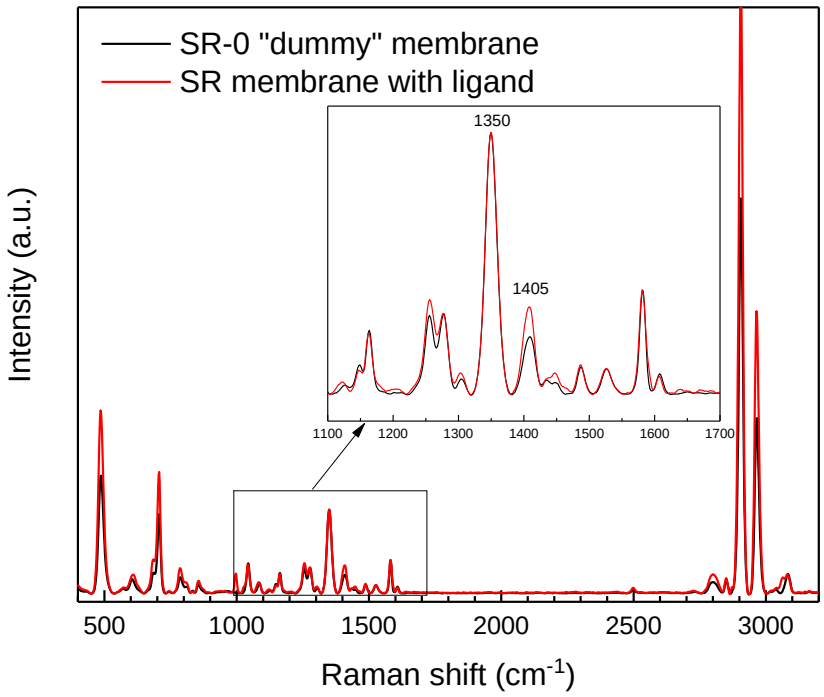

Figure 2.31. Spectrum of the SR-0 membrane and the SR membrane.

The main differences related to the presence of PDAM in the membrane are located in the 1400–1440 cm^{-1} region (δ(C-H) and ν(C-C) at 1405 cm^{-1} and ν (C--N) of the phenanthroline segment at 1424-1440 cm^{-1} region.

At the preprocessing stage, the normalization of the spectra by the intensity of the $-NO_2$ mode of NPOE (1350 cm^{-1}) did not result in the constant relative intensity of the bands assigned to the membrane matrix (Fig. 2.32).

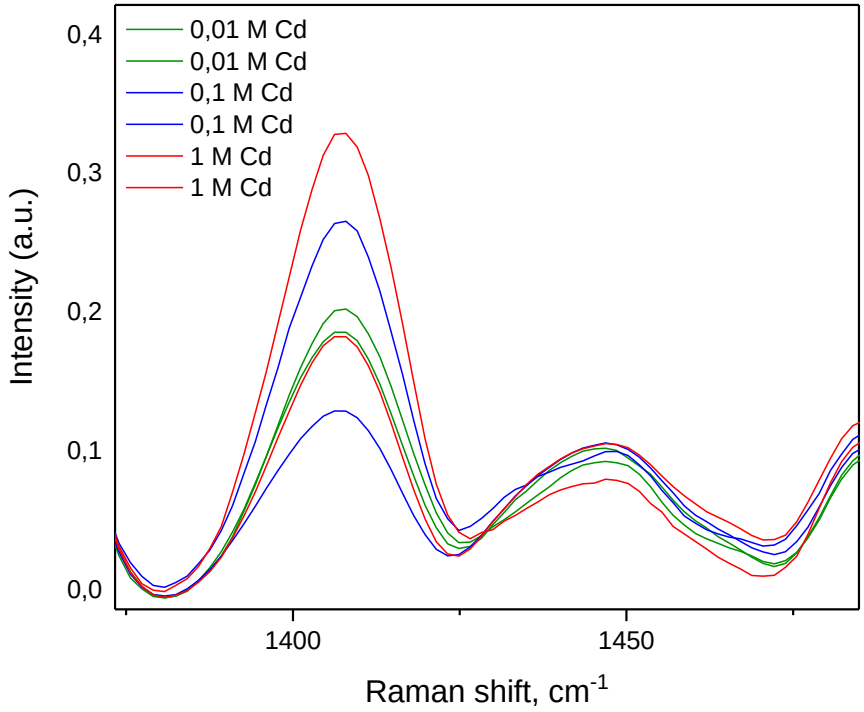

Figure 2.32. The fragment of the SR membrane spectra acquired in contact with 0.01, 0.1 and 1 M Cd (normalized by the intensity of the NPOE band at 1350 cm^{-1}).

The relative intensity values of the plasticizer and polymer bands are different in the spectra taken at the different points of the membrane under similar conditions. For example, the spectra of the membrane in contact with 1 M Cd have a very different intensity after normalization (red lines in Fig. 2.32). This can be due to the local inhomogeneity of the studied membrane. These local inhomogeneities hinder the quantitative analysis of the membrane spectra since the changes in the membrane

spectra can be due to both interaction with the analyte cation and non-uniformity of the membrane matrix. It was therefore decided that the silicon rubber-based membranes appear to be an inappropriate choice and their study was not further pursued.

Methacrylic-acrylic copolymer membranes

The previous sections have shown that the plasticizer may serve as the main factor hindering the application of the proposed approach to the detection of metal cations in the aqueous phase. At the same time, the preparation of the PVC-based ISE membranes without plasticizer is not possible, since the PVC glass transition temperature (T_g) is around 80 °C, and thus appropriate mechanical properties will not be achieved at room temperature without plasticizer. Some other polymers may contain the segments that act like a "built-in plasticizer", providing a lower T_g. Polyurethanes and acrylate polymers were actively studied in the so-called plasticizer-free membranes (see, e.g. [27, 38]) (Fig. 2.33). The reason for this choice is the simplicity and flexibility of the synthesis procedure of both polymers that allows varying the T_g values in a wide range, depending on the molecular weight of the selected monomer.

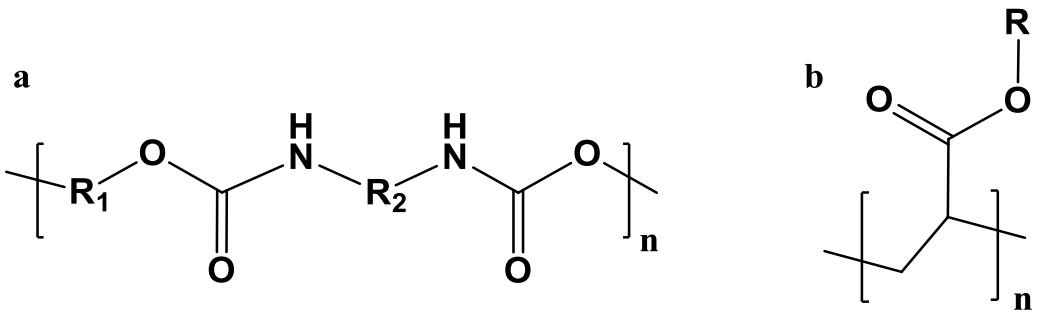

Figure 2.33. Schematic representations of polymeric structures: a – polyurethane; b – polyacrylate.

The most significant criteria for our study were the Raman spectrum of the polymeric matrix. The acrylate copolymer appears to be a better option for our purposes as its spectra should contain only C_{sp}^3–H, C=O and C–O modes referred to the aliphatic substituents, carbonyl and ester groups, respectively. Besides, the C=O

mode of acrylate compounds is located around 1730 cm^{-1} in Raman, and thus it would not overlap with the C=O mode of PDAM (1638 cm^{-1}).

During the next step of our study, the acrylate copolymer (AC) was employed. The copolymer AC was synthesized according to the procedure described in [101]. The molar ratio of methyl methacrylate and n-butyl acrylate was specified as 1:4 (Fig. 2.34). The monomer ratio 21:79 was confirmed by ^{1}H NMR spectroscopy (spectrum taken in $CDCl_3$, provided by Prof. S. Delbaere, University Lille 2 (Annex 3). The AC membrane cocktails were prepared by the dissolution of 90 wt% of AC and 10 wt% of PDAM ionophore in the dichloromethane under stirring. Then the mixture was poured in a glass Petri dish and left for 48 h for solvent evaporation.

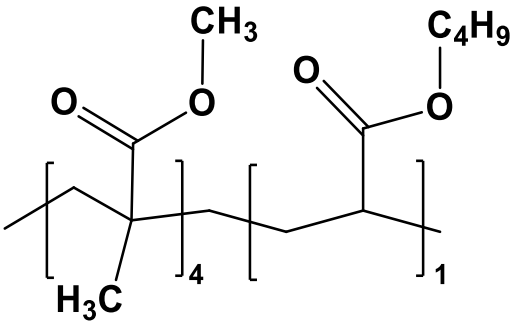

Figure 2.34. The schematic structure of the methacrylate – n-butyl acrylate copolymer (AC).

The Raman spectrum of the AC membrane was compared to the one of AC-0 (acrylate copolymer without a ligand added) (Fig. 2.35).

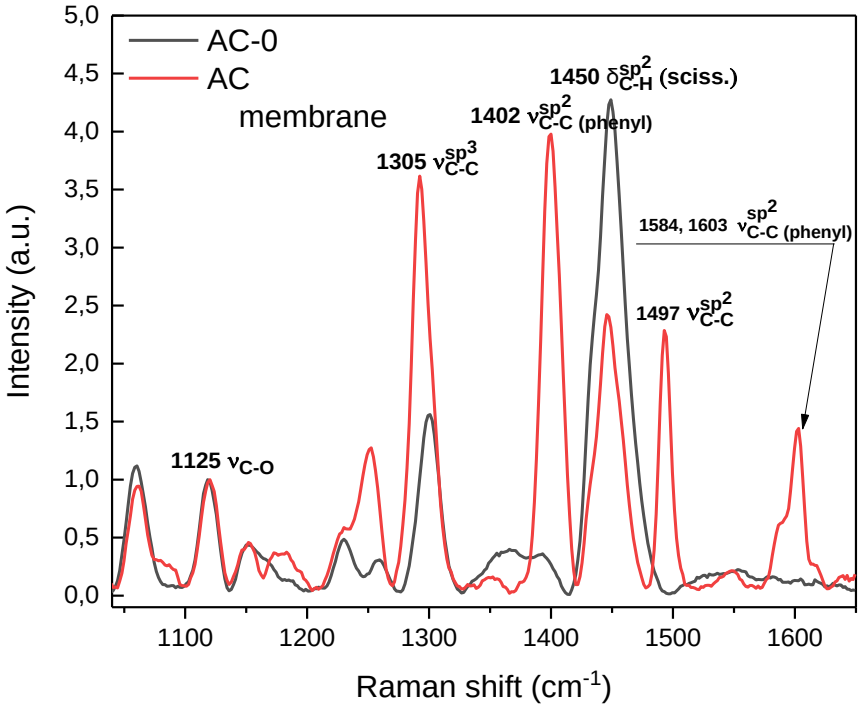

Figure 2.35. Spectra of the AC-0 and AC-based membranes (AC).

The observed contribution of PDAM to the AC-PDAM membrane spectrum is due to the fragments of the aromatic system, namely ν_{C-C} at 1402, 1497, 1584, 1603 cm^{-1} and ν_{C-H} at 1250 cm^{-1}. The aliphatic vibrational modes give bands with a bigger intensity in the spectrum of AC, compared to the ones of AC-PDAM. This can be explained by the bigger proportion of the aliphatic groups in its composition compared to PDAM.

Then, the spectra of the AC membrane in contact with Cd^{2+} solutions of 5 concentrations with ten-fold difference (from 10^{-1} to 10^{-5} M) were taken. At each concentration, the spectra were acquired at 3 different points in the 1100 – 1650 cm^{-1} range (Fig.2.36).

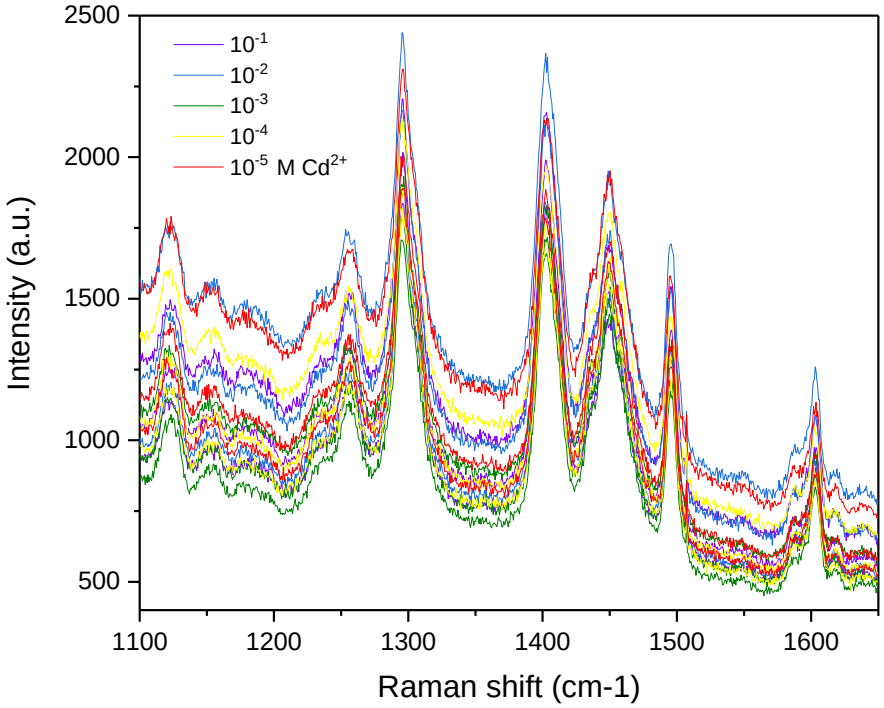

Figure 2.36. AC membranes spectra upon the interaction with $Cd(NO_3)_2$ aqueous solutions (10^{-5} – 10^{-1} M).

The preprocessing procedure included baseline correction (AsLS algorithm), 15-point Savitzky-Golay smoothing filter and normalization along 1125 cm^{-1} (C-O stretching mode of AC) (Fig.2.37). The smoothing window width for these spectra was bigger than that for NPOE-2 and NPOE-3, as the noise level of the spectra of AC membranes was way higher that for NPOE membranes.

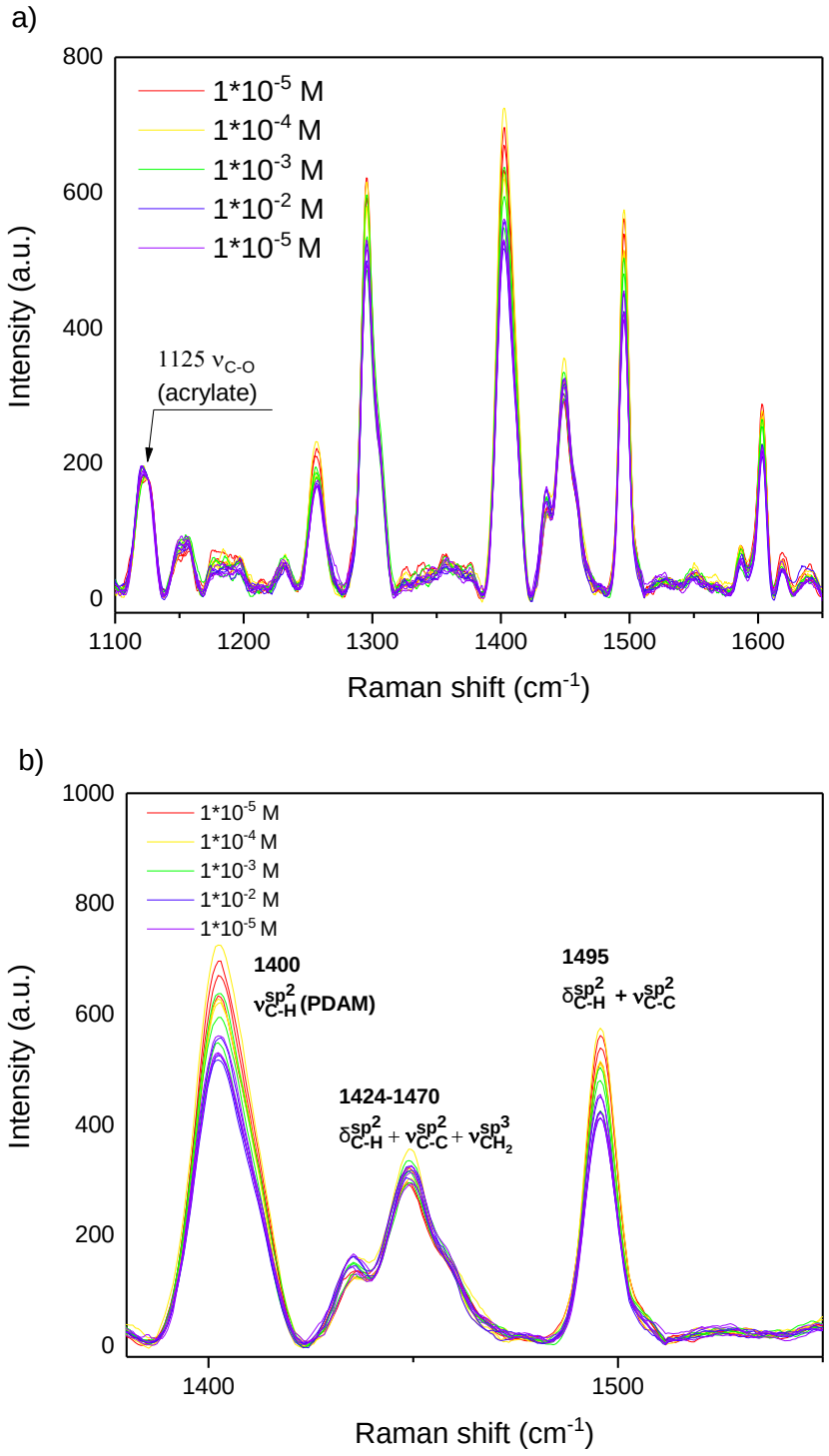

Figure 2.37. Spectra of AC-PDAM membrane in contact with 10^{-5} – 10^{-1} M $Cd(NO_3)_2$ aqueous solutions: a) 1100–1650 cm^{-1}; b) zoom in to the 1380–1550 cm^{-1} region.

The PCA model was then built on the resulting 15-points dataset. The results are presented in Fig. 2.33.

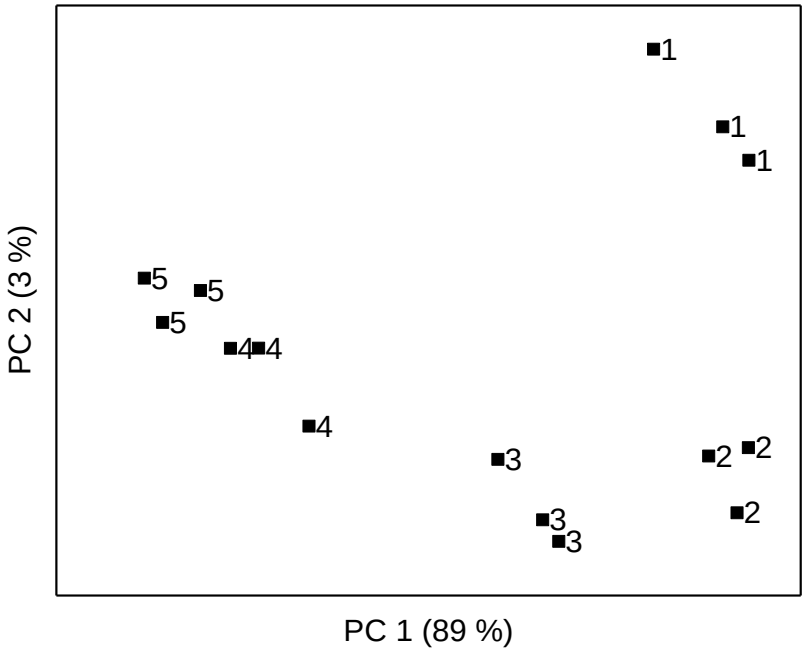

Figure 2.38. PCA scores plot for the set of AC membrane spectra in contact with Cd^{2+} solution (1 is for 10^{-1} M, 5 for 10^{-5} M Cd^{2+} concentration).

The samples formed clusters in the scores plot according to the Cd^{2+} concentration. This can be related to the evolution of the spectra upon interaction of the membrane with Cd^{2+} cations. The concentration dependence of the AC-PDAM spectral signatures was estimated with PLS algorithm. The spectra from the dataset employed for PCA were averaged over replicated measurements in the same Cd^{2+} concentration. The predictive ability of the PLS model was assessed with “leave-one-out” cross-validation. As the 10-fold Cd^{2+} concentration values were studied in this experiment, the $\log_{10}[Cd^{2+}]$ values were used for PLS modelling instead of $[Cd^{2+}]$ to avoid uneven distribution of the samples over the concentration range.

The PLS model was based on 1 latent variable and the R^2 value in cross-validation was 0.98. The percentage of the explained **X**-variance for the 1st PLS-component was 99 %, and 92 % for **Y**-variance. This can be considered as a proof of

correlation between the spectra and cadmium content in the contacting solution. However, in PLS regression, the use of 5 samples cannot ensure the reliable evaluation of the correlation and “leave-one-out” cross-validation most likely gave overoptimistic results. Further studies with extended set of samples are needed for the validation of the proposed approach with AC-PDAM membranes.

2.5. Conclusions

A novel type of analytical signal transduction for polymeric sensor membranes is suggested. The evolution of the Raman spectra of the sensor membranes in con tact with aqueous solutions of metals can be employed for ion content quantification. The advantages of the suggested approach lie in the possibility of indirect Raman quantification of metal ions in microliter sample volumes. It must be pointed out that the selectivity issue of the suggested approach requires a further dedicated study. Similar ions may induce similar spectral changes upon binding with the ligand, thus hindering selective quantification of a particular ion, especially in complex samples. A possible way to address this problem can be in the employment of mixture of ionophores, possessing a high selectivity towards components of a sample and having non-overlapping characteristic spectral bands. Simultaneous introduction of several ionophores together with multivariate data processing of resulting spectra may allow for selective quantification of particular ions.

CHAPTER 3. Ionophore-free ISE membranes

The ligand (ionophore) plays the most important role in the sensor membrane composition as it is the main responsible for the selective complexation of a target ion that provides sensor selectivity. Previously, the ionophores were always developed to reach the highest possible selective response in order to handle the analysis of complex multicomponent samples and even though there is huge variety of available ionophores, the number of unsolved analytical problems that these selective sensors were dedicated to still remains significant. Therefore, the design of new ligands that are selective for a particular analytical task remains an important research topic,but requires a significant amount of time and effort. In an attempt to overcome this limitation, we propose using ionophore-free sensor membranes. In these membranes, the selectivity of the sensor is regulated by the lipophilicity of the target ion, the ion-exchanger and the solvent-plasticizer. To investigate the influence of the membrane components on the sensor sensitivity, we prepared sensors based on two different types of lipophilic additives and various plasticizers and then tested their performance in the analysis of mixtures. Additionally, ionophore-free sensors were combined into the array to compensate for the insufficient selectivity of the before mentioned sensors in the multicomponent environment. With this set-up, we want to investigate its potential to determine the individual ion content in Ca^{2+}-Mg^{2+} mixtures, in the presence of 10^{-3} M of either Na^{+} or K^{+} ions, compared the results to those for the conventional ionophore-based sensors.

3.1. Experimental

3.1.1. Reagents

High molecular weight poly(vinyl chloride) (PVC), 2-nitrophenyl octyl ether (NPOE), (bis-(2-ethylhexyl) sebacate (DOS), 2-fluorophenyl-2-nitrodiphenyl ether (FNDPE), tris-(2-ethylhexyl) phosphate (TOP), bis(2-ethylhexyl) phthalate (DOP), tetrakis-(trifluoromethyl)phenyl borate (KTTFMPB), Calcium ionophore I ([(−)-(R,R)-

N,N′-bis-[11-(ethoxycarbonyl)undecyl]-N,N′-4,5-tetramethyl-3,6-dioxaoctanediamide]) and Magnesium ionophore I (N,N′-Diheptyl-N,N′-dimethyl-1,4-butanediamide) were purchased from Fluka (Switzerland). Chlorinated cobalt dicarbollide (CCD) was obtained from Katchem (Czech Republic) as a cesium salt and was converted to the acidic (H^+) form prior to the membrane preparation. NaCl, KCl, $CaCl_2$, $MgCl_2$ salts were purchased from Vekton (St. Petersburg, Russia) in an analytical grade. Tetrahydrofurane (THF) purchased from Merck (Germany) was freshly distilled before use.

3.1.2. Membrane preparation and potentiometric measurements

The ionophore-free polymeric membranes consisted of 33 wt% PVC, 66 % plasticizer and 1 % of a lipophilic additive. Ca^{2+}- and Mg^{2+}-selective sensor membranes were prepared using literature recipes [54, 227] based on corresponding ionophores (Fig. 3.1) and comprised 1.0 wt% of the ionophore, 0.5 wt% of KTFPB, 65.5 wt% NPOE and 33 wt% of PVC for Ca^{2+}-selective sensor and 1.4 wt% of the ionophore, 1.0 wt% of KTFPB, 64.5 wt% NPOE and 33.1 wt% of PVC for Mg^{2+}-selective sensor, respectively.

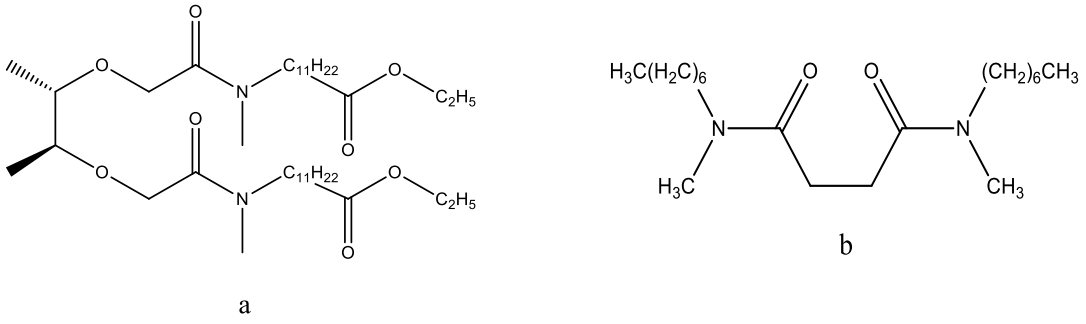

Figure 3.1. Structures of a) N,N-Dicyclohexyl-N′,N′-dioctadecyl-3-oxapentanediamide (Ca^{2+}-selective ionophore) ; b) N,N′-Diheptyl-N,N′-dimethyl-1,4-butanediamide (Mg^{2+}-selective ionophore).

It was shown that certain solvent-plasticizers can have an influence on the complexation in the membrane [43]. Therefore, the differences in sensor sensitivity patterns depend on the polarity and structure of the plasticizer. In order to investigate

the contribution of these factors, along with the lipophilic additive influence, the combinations of five various plasticizers and two lipophilic additives (Fig. 3.2) were used for the preparation of the ionophore-free sensor membranes. The selection of these plasticizers is based on their structural differences and polarity (e.g. polar or non-polar, containing aliphatic or aromatic fragments). The final composition of the membranes is shown in Table 3.1.

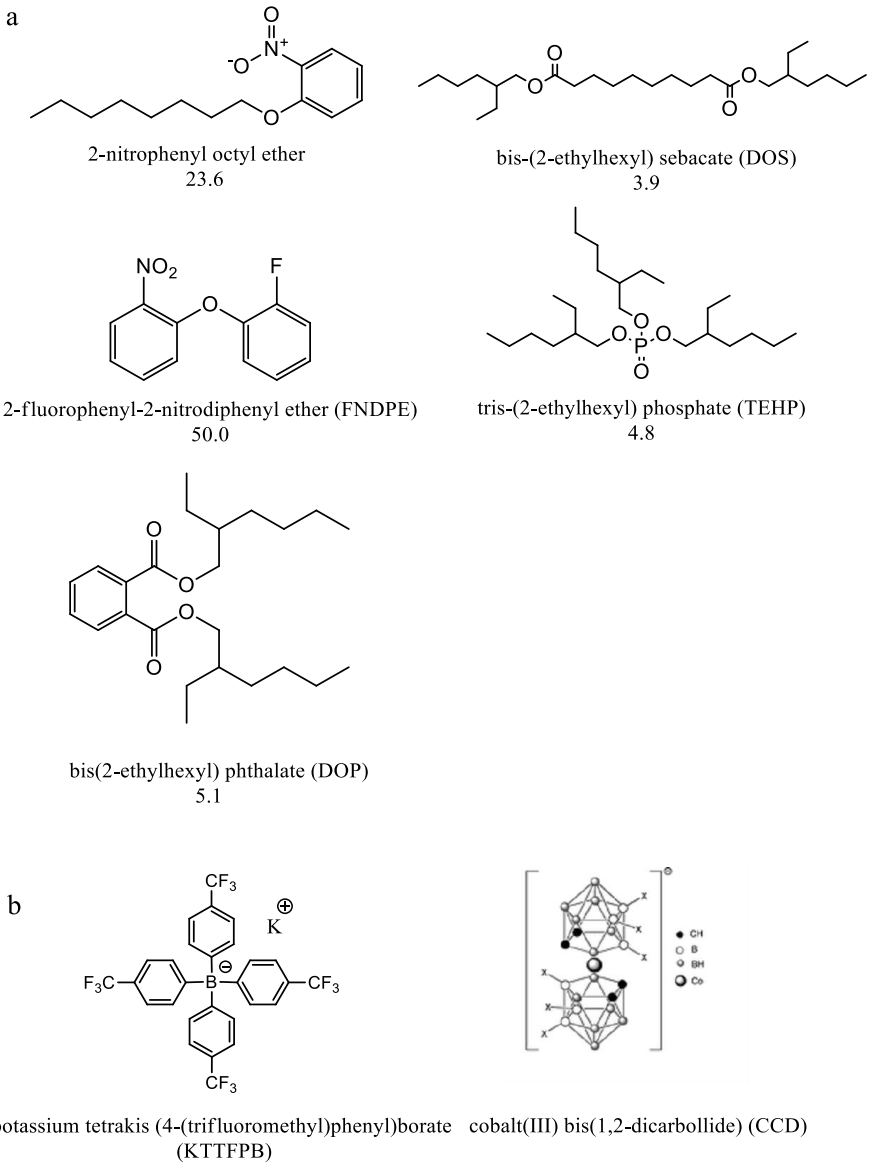

Figure 3.2. The structures of the ionophore-free membrane components; a – plasticizers and their dielectric constants (ε_r) [228], [229]; b – lipophilic additives.

Table 3.1. Ionophore-free sensor membrane compositions.

Name	Plasticizer	Lipophilic additive
1	NPOE	KTTFMPB
2		CCD
3	DOS	KTTFMPB
4		CCD
5	FNDPE	KTTFMPB
6		CCD
7	TEHP	KTTFMPB
8		CCD
9	DOP	KTTFMPB
10		CCD

For the preparation of the membrane, the components were weighed (300 mg in total) and dissolved under stirring in 3 mL THF. Then, the solution was poured into a Teflon cylindrical vessel and left to dry for 48 h, where after membranes of 7 mm in diameter (three of each composition) were cut from the resulting film. Solid inner contact made of copper wire in carbon paste was attached upon one side of each membrane. Finally, the resulting construction was glued into a PVC tube sensor body and conditioned by using a solution of 10^{-2} M sodium chloride (10^{-2} M calcium chloride for Ca^{2+}-selective and 10^{-2} M magnesium chloride for Mg^{2+}-selective sensors).

The electrochemical measurements were carried out in the following galvanic cell:

Cu | Ag ⋮ AgCl, KCl_{sat} | sample solution | membrane | carbon paste solid contact | Cu

The EMF measurements were performed against the standard reference Ag/AgCl (ZIP, Belorussia) electrode at room temperature (20 ^{o}C) using a multi-channel digital mV-meter with high input impedance (Sensor Systems LLC, St.Petersburg,

Russia). The electric potential was recorded with a 0.1 mV precision for 3 minutes in 10 sec intervals. The results are presented as an average of the last 3 EMF values during these 3 minutes. The standard glass pH electrode (ZIP, Belorussia) was used for pH control. Cation activity coefficients were calculated according to Debye–Hükkel theory.

Calibration of the sensors was performed in aqueous solutions of Ca^{2+}, Mg^{2+}, K^{+} and Na^{+} chloride salts in the concentration range between 10^{-7} and 10^{-2} M. The sensor sensitivity was calculated as the slope of the linear part of the electrode response function (mV per decade) according to the Nernst equation. The slope values were calculated for a metal ion concentration ranging between 10^{-4} and 10^{-2} M and were averaged over the three replica sensors of each composition and multiple replicated measurements.

The sensor array is comprised of 34 electrodes: two Ca^{2+}-selective sensors, two Mg^{2+}-selective ones and 30 cross-sensitive cationic sensors (10 types, 3 of each kind). To assess the correlation between the array response and Ca^{2+} and Mg^{2+} concentrations, the measurements were performed on a sample set containing 40 binary Ca-Mg mixtures (Table 3.2, Set 1). Additionally, the influence of the interfering ions K^{+} and Na^{+} was investigated, for which the same 40 samples were analyzed in the presence of 10^{-3} M of either Na^{+} or K^{+} (Table 3.2, Set 2 and 3, correspondingly). And lastly, the selectivity of the sensor to calcium and magnesium was determined in the presence of both monovalent cations. To do so, measurements were performed on a set of quaternary mixtures comprising Ca^{2+}, Mg^{2+}, K^{+} and Na^{+} ions (Table 3.2, Set 4).

Table 3.2. Mixtures composition (in logarithmic units). $p = -\log_{10}$.

№	Set 1		Set 2		Set 3		Set 4			
	$p\,a_{Ca^{2+}}$	$p\,a_{Mg^{2+}}$	$p\,a_{Ca^{2+}}$	$p\,a_{Mg^{2+}}$	$p\,a_{Ca^{2+}}$	$p\,a_{Mg^{2+}}$	$p\,a_{Ca^{2+}}$	$p\,a_{Mg^{2+}}$	$p\,a_{Na^{+}}$	$p\,a_{K^{+}}$
1	3.94	3.57	3.32	3.65	3.32	3.65	3.58	3.18	3.94	2.72
2	3.18	3.98	3.00	3.44	3.96	3.59	2.88	3.21	4.05	2.72
3	2.35	4.20	2.36	4.20	3.20	4.00	2.98	2.39	3.88	2.82
4	4.05	3.37	2.72	2.64	3.00	3.44	2.60	2.71	2.86	2.78
5	3.97	3.88	3.99	3.90	2.36	4.20	3.31	3.73	3.69	3.03
6	3.68	2.75	3.69	2.76	4.06	3.39	3.52	2.36	2.68	3.96
7	2.36	3.45	2.36	3.46	2.72	2.64	4.10	3.12	2.24	2.33
8	3.81	2.49	3.81	2.49	3.99	3.90	2.80	4.10	2.22	3.22
9	3.04	3.87	3.60	3.70	3.69	2.76	3.86	4.00	3.88	3.90
10	3.58	3.68	3.64	2.43	2.36	3.46	3.93	2.60	4.05	3.04
11	2.34	2.31	3.33	2.65	3.60	3.70	2.36	2.55	3.99	2.21
12	3.32	2.64	3.02	2.27	2.34	2.31	2.41	4.22	2.71	3.52
13	4.09	2.59	2.82	3.45	3.33	2.65	2.28	3.09	3.23	4.01
14	2.81	3.44	2.44	2.93	4.09	2.59	2.31	3.18	3.79	3.82
15	3.37	3.20	3.89	2.64	2.82	3.45	2.54	3.19	3.87	2.13
16	2.39	2.46	2.39	2.47	3.89	2.64	2.54	2.42	3.98	4.00
17	2.50	3.79	2.50	3.80	2.39	2.47	3.69	3.23	3.21	3.99
18	3.53	3.97	3.55	3.99	2.50	3.80	2.35	2.49	3.33	2.71
19	3.06	3.03	3.06	3.04	2.52	4.11	2.75	3.74	2.82	3.43
20	2.51	4.11	2.52	4.11	3.74	4.04	2.82	3.72	2.98	4.04
21	3.71	4.02	3.74	4.04	2.93	3.75	2.82	2.32	2.53	3.44
22	2.92	3.74	3.98	2.85	3.31	2.92	3.24	4.11	2.56	3.20
23	3.49	3.04	3.31	2.92	3.50	3.05	2.65	3.90	2.46	3.90
24	3.23	3.09	3.50	3.05	3.24	3.10	3.14	3.07	3.34	3.10
25	3.19	3.42	3.24	3.10	3.21	3.43	2.97	4.03	3.25	3.65

Table 3.2 (Cont.) Mixture composition (in logarithmic units). p = -$\log_{10}$.

№	Set 1		Set 2		Set 3		Set 4			
	p a_{Ca}^{2+}	p a_{Mg}^{2+}	p a_{Ca}^{2+}	p a_{Mg}^{2+}	p a_{Ca}^{2+}	p a_{Mg}^{2+}	p a_{Ca}^{2+}	p a_{Mg}^{2+}	p a_{Na}^{+}	p a_{K}^{+}
26	3.01	2.57	3.21	3.43	3.02	2.58	2.39	4.16	2.76	2.54
27	3.53	3.29	3.55	3.30	3.55	3.30	2.92	2.32	3.89	3.48
28	4.25	2.27	4.26	2.27	4.26	2.27	4.20	2.36	2.24	2.88
29	2.89	2.73	2.89	2.73	2.89	2.73	3.16	2.41	3.41	2.48
30	3.38	2.28	3.38	2.28	3.38	2.28	2.31	3.75	3.83	3.97
31	3.31	3.63	3.96	3.59	3.81	2.49	3.82	3.77	4.02	2.51
32	2.99	3.44	3.20	4.00	3.06	3.88	4.02	2.74	3.46	3.07
33	2.72	2.64	4.06	3.39	3.60	3.70	3.60	2.89	2.34	2.58
34	3.63	2.43	3.06	3.88	3.64	2.43	3.75	2.49	2.89	2.09
35	3.01	2.27	2.34	2.31	2.34	2.31	3.67	3.81	3.08	3.10
36	2.43	2.93	4.09	2.59	3.33	2.65	2.29	4.15	2.43	3.04
37	3.88	2.64	3.38	3.21	4.09	2.59	3.69	3.23	3.21	3.99
38	2.57	3.57	2.58	3.57	3.02	2.27	2.39	3.62	2.58	2.73
39	3.97	2.84	2.93	3.75	2.82	3.45	2.58	3.33	3.56	2.63
40	3.30	2.91	3.02	2.58	2.44	2.93	2.73	2.30	3.08	2.35

3.1.3. Data processing

Each dataset contains the responses of 10 types of sensors measured over 40 samples. The composition of the solutions was determined according to the procedure described in reference [230] to ensure the uniform distribution of the calibration points in the chosen concentration space (10^{-4} – 10^{-2} M) defined by the content of two ions. In the absence of an ionophore, the response of the sensor is supposed to be non-equilibrated, as the ion migration in the membrane is mainly driven by the hydrophilicity of the ions. To eliminate response fluctuations, the EMF value before calibration was measured in water and subtracted from the sample EMF value ($\Delta E = E_{sample} - E_{water}$). The average value of three replicas was taken, forming a 40 x 10 matrix which was used for further processing.

The ability to quantify [Ca^{2+}] and [Mg^{2+}] was explored using PLS modelling. Regression models were based on 30 training samples (#1-30 in Table 3.2.) and validated with 10 independent test samples (samples #31-40 in Table 3.2.). The precision of the model was assessed with the Root Mean Square Error of prediction (RMSEP) value and R^2 parameter.

Data from parallel measurements using Ca^{2+} and Mg^{2+}-selective sensors were assessed with Ordinary Least Squares (OLS). The RMSEP and R^2 values calculated by this model were compared to those derived from the data of ionophore-free sensor arrays. All calculations were performed in The Unscrambler 9.7 (CAMO, Norway).

3.2. Results and discussion

3.2.1. Sensitivity of ionophore-free sensors

The results of the ionophore-free sensors' sensitivity assessment in individual ion solutions are presented in Table 3.3. Two tendencies can be observed considering sensor sensitivities. Highly polar plasticizers (NPOE, FNDPE – compositions 1, 2, 5, 6) promote extraction of cations into the membrane of the sensor according to the lipophilicity series. The highest sensor sensitivity values can be observed in potassium solutions for all sensor compositions (besides 7 and 8) which is in a good agreement with lipophilicity series: $K^+ > Na^+ > Ca^{2+} > Mg^{2+}$ [231].

Table 3.3. Sensitivity (±1 mV/dec) of the sensors towards individual ions.

Ion / Sensor	1 NPOE / KTFPB	2 NPOE / CCD	3 DOS / KTFPB	4 DOS / CCD	5 FNDPE / KTFPB	6 FNDPE / CCD	7 TEHP / KTFPB	8 TEHP / CCD	9 DOP / KTFPB	10 DOP / CCD	Ca^{2+}-selective	Mg^{2+}-selective
K^+	46	35	47	43	46	41	24	25	46	46	1	11
Na^+	20	14	44	42	20	14	46	46	42	35	2	5
Ca^{2+}	18	10	14	28	18	19	19	18	15	7	28	29
Mg^{2+}	16	6	25	21	19	19	24	24	15	15	18	22

The deviation observed for the two TEHP-plasticized sensors can be explained by the fact that TEHP possesses its own complexing properties [232]. This may reverse the selectivity pattern from bigger to smaller ions as was reported for some compounds containing P=O groups [233]. Besides, the membranes containing non-polar plasticizers demonstrate a sensitivity to Mg^{2+} which is equal or even surpasses the corresponding value for the standard Mg^{2+}-selective sensor plasticized by NPOE. For the compositions 1, 2, 5, 6 (containing polar plasticizers) the KTFPB-based sensors demonstrate a higher sensitivity to potassium compared to the CCD-based ones. No significant difference between two lipophilic additives was found for the membranes containing non-polar plasticizers. Moreover, the long-term stability of sensor response was reasonable and sensitivity values remained constant within 3 months of the study.

In the absence of the ionophore, the sensor response is governed by ion interactions with the plasticizer, lipophilic additives and by the lipophilicity of the target ion itself. Therefore, it is normal that the sensitivity values decrease when the ion lipophilicity decreases.

3.2.2. Mixture analysis

In order to assess the performance of the ionophore-free sensor arrays for the quantification of individual ions in complex mixtures, potentiometric measurements were performed in sample sets 1-4 (Table 3.2.). The model parameters obtained for binary mixtures (Set 1) are given in Table 3.4.

Table 3.4. Parameters of “measured vs. predicted” plot for the test set validation of regression models for ionophore-free sensor array (PLS) and separate selective sensors (OLS) in Ca-Mg mixtures. *N* − number of PLS factors.

	Ca				***Mg***			
	Slope	RMSEP, lg a	R^2	*N*	Slope	RMSEP, lg a	R^2	*N*
Ionophore-free array (PLS)	0.95	0.21	0.84	2	0.89	0.17	0.90	2
Selective sensor (OLS)	0.99	0.08	0.99	-	0.10	>180	9E-06	-

The OLS model based on the selective Ca^{2+} sensor response allows for the reliable quantification of the calcium concentration in binary mixtures. At the same time, the Mg-selective sensor response shows poor sensitivity to the Mg^{2+} concentration in presence of Ca^{2+} ions in solution. On the other hand, the response of the ionophore-free array demonstrates a reasonable correlation with the concentration of both ions (R^2 values were equal 0.84 for Ca and 0.90 for Mg). Measured vs predicted plots for these regression models are given in Fig. 3.3. The RMSEP value for Ca^{2+} determination with ionophore-free array was somewhat higher than that for the Ca-selective sensor (0.21 vs 0.08). By contrast to the Mg-selective sensors, the ionophore-free array allows to determine Mg^{2+} concentration in the presence of Ca^{2+}.

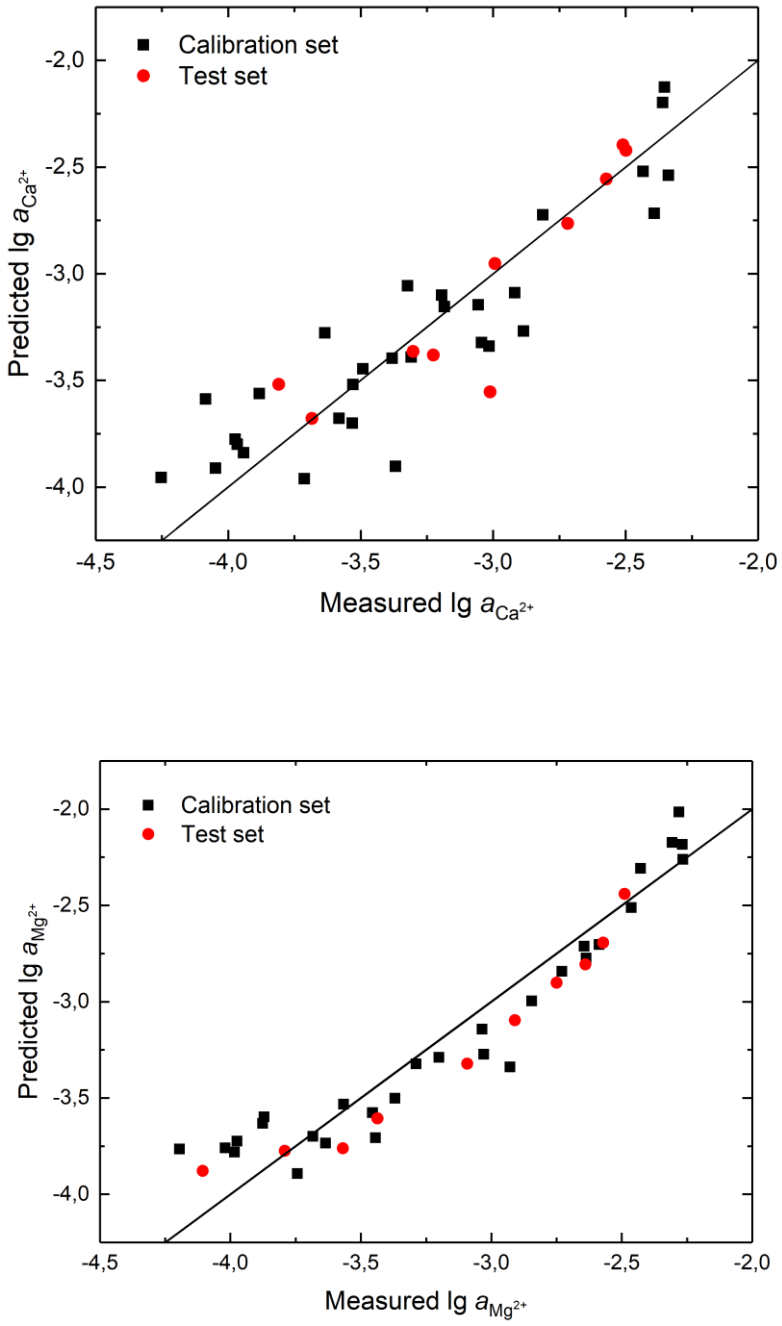

Figure 3.3. PLS modelling results for the a) Ca^{2+} b) Mg^{2+} concentration prediction by ionophore-free sensors.

For the PLS model of Mg^{2+}, we observe obvious deviations from linearity in the predicted-measured plot. This effect on the sensitivity of the ionophore-free sensors to Mg^{2+} may be caused by changing background of the more lipophilic Ca^{2+}. The non-linear relations between **X** and **Y** can be modelled by **X** variable transformations. To consider non-linear contributions with the model, the matrix containing the transformed **X** variables is augmented to the original X matrix [234]. In our case, the correction for non-linearities was performed by augmentation of the **X** matrix with its squared elements, so the model was based on 20 predictor variables instead of 10. The predicted vs. measured plot for this PLS model is shown in Fig. 3.4. The bias at the edges of the concentration range, corresponding to the non-linear shape in the original model, is much lower for the model built on the transformed variables, while the RMSEP was comparable (0.15).

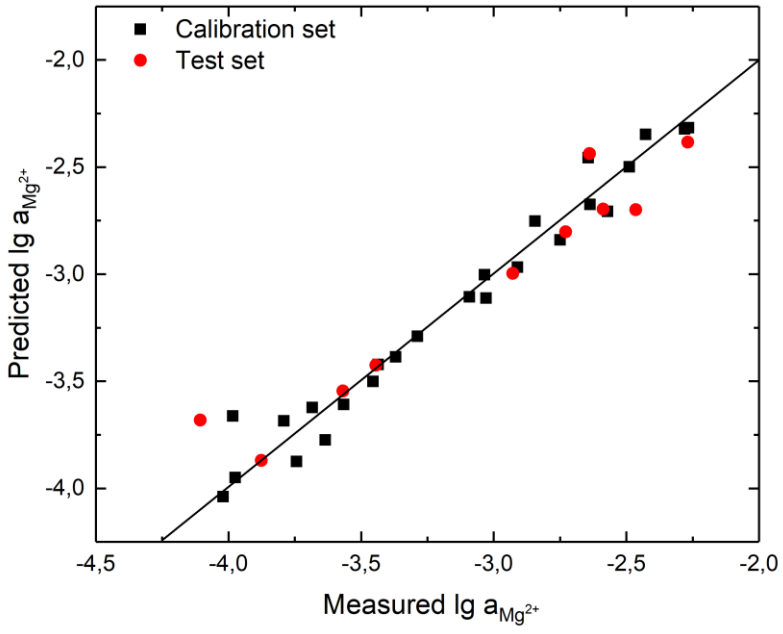

Figure 3.4. PLS modelling results for the Mg^{2+} concentration prediction for the ionophore-free sensor data with the augmented second order term.

3.2.3. Results of calcium and magnesium quantification in sample sets 2-4.

To assess the feasibility of a selective determination of Ca^{2+} and Mg^{2+}, a series of additional measurements in the presence of constant concentrations of Na^+ and K^+ interfering ions were performed. Both Ca- and Mg-selective sensors demonstrate a higher sensitivity to calcium than to magnesium. The PLS model for the prediction of the calcium concentration in mixtures containing 10^{-3} M Na^+ (Set 2) is characterized by the relatively low RMSEP = 0.15. In contrast, the analogous modelling for the Mg^{2+} failed (R^2 = 0.09), due to the interference from Na^+. As follows from the data presented in the Table 3.5, the measurements performed in the presence of potassium show a significant deterioration of model parameters for both calcium and magnesium due to the presence of these potassium ions. This can be explained by the fact that potassium is more lipophilic than both Ca^{2+} and Mg^{2+}, and thus it will have a bigger contribution to the response of ionophore-free sensors.

Table 3.5. Parameters of the test set validation of regression models for ionophore-free sensor array (PLS) and separate selective sensors (OLS) in Ca-Mg mixtures with various interferences. (RMSEP – Root Mean Square Error of prediction, R^2 – squared correlation coefficient, *N* – number of PLS factors).

Set №	Mixture type	Model type	Ca				Mg			
			Slope	RMSEP, lg *a*	R^2	N	Slope	RMSEP, lg *a*	R^2	N
1	Ca-Mg	OLS	0.99	0.08	0.99		0.10	>180	9E-06	
		PLS	0.95	0.21	0.84	2	0.89	0.17	0.90	2
2	Ca-Mg + Na	OLS	0.99	0.04	0.99		0.01	10.7	0.01	
		PLS	0.88	0.15	0.94	2	0.33	0.66	0.09	2
3	Ca-Mg + K	OLS	1.02	1.50	0.96		0.02	5.60	0.00	
		PLS	0.87	0.00	0.72	1	0.13	0.00	0.02	1
4	Ca-Mg + Na + K	OLS	0.96	0.07	0.96		0.6	82.5	0.60	
		PLS	0.09	0.63	0.06	1	0.68	0.35	0.69	1

3.3. Conclusions

Using PLS regression modelling, we have shown that the ionophore-free sensor array with polymeric sensor membranes based on various cation-exchangers and solvent-plasticizers allows for simultaneous quantification of both Ca and Mg in their aqueous mixtures. We observed a high correlation between Ca^{2+} concentration and ionophore-free sensor data, not only for binary mixtures, but also in the presence of the less lipophilic Na^{+} interference. For instance, the root mean squared error of prediction did not surpass 0.15 in lg *a* units for the Ca^{2+} determination. Besides, the combination of the proposed approach with PLS regression method can effectively compensate for the lack of selectivity in the case of the determination of Mg^{2+} concentration in mixtures by the conventional selective sensors. Therefore, we conclude that the potentiometric selectivity can be attained in principle without using selective ligands. Nevertheless, the presence of interfering cations (e.g. K^{+}) reduces the reliable quantification of calcium and magnesium significantly. However, using a wider range of plasticizers and ion-exchangers seems to be the advantageous way to increase the variability of sensitivity patterns of the sensors, which should be further explored in future research.

CHAPTER 4. Multi-ionophore potentiometric sensor membranes

The main idea of this part of the thesis is based on programming the sensor properties by mixing several ionophores within one sensor membrane. However, similarly to the extraction systems containing several extracting agents, it is expected that the sensor sensitivity patterns of multi-ionophore sensors are subjective to certain non-additive effects.

Three ligands traditionally used in the rare earth element extraction procedure were employed as ionophores for the PVC-plasticized sensor membranes. Introducing several ionophores into the sensor membranes seems to be a feasible way of designing the sensor sensitivity patterns, and thus, this approach has the potential to be used in multisensor systems. Moreover, it was decided to evaluate the potential of this approach with the analysis of lanthanide cations, a series of cations that demonstrate a strong mutual interference when present in mixtures. A sensor array consisting of both mono- and multi-ionophore sensors was used for the analysis of two- and three component solutions and the results were compared to those obtained with conventional mono-ionophore sensors. Additionally, a multivariate data processing approach was used to selectively quantify particular lanthanide cations in the multisensory data.

4.1. Experimental

4.1.1. Reagents

Considering numerous cases where extraction agents were used as ionophores for ISE membranes, three compounds were selected for the analysis of rare earth metal cations. The chosen ionophores were: diphenyl-N,N-di-n-butylcarbamoylmethylphoshine oxide (DPCMPO), 3-oxapentadicarbonic acid tetraoctyldiamide (TODGA) and N,N′-diethyl-N,N′-di(p)-fluorophenyl dipicolinamide (DPA) (Fig. 4.1. a, b and c, respectively). The sensor membranes were based on 33 wt% PVC and 66 % NPOE with 10 mmol/kg of potassium

tetrakis[3,5-bis(trifluoromethyl)phenyl] borate (KTTFPB) as a lipophilic additive, and 50 mmol/kg of the ionophores in total.

High-molecular weight polyvinyl chloride (PVC), o-nitrophenyloctyl ether (NPOE) and potassium tetrakis[3,5-bis(trifluormethyl)phenyl]borate (KTTFPB) were obtained from Fluka Chemical (Switzerland). DPCMPO was synthesized at the Institute of Chemical Reagents and Special Purity Chemical Substances (IREA, Moscow). TODGA was kindly provided by Dr. B. Casensky (Katchem, Czech Republic) and DPA was kindly provided by Khlopin Radium Institute.

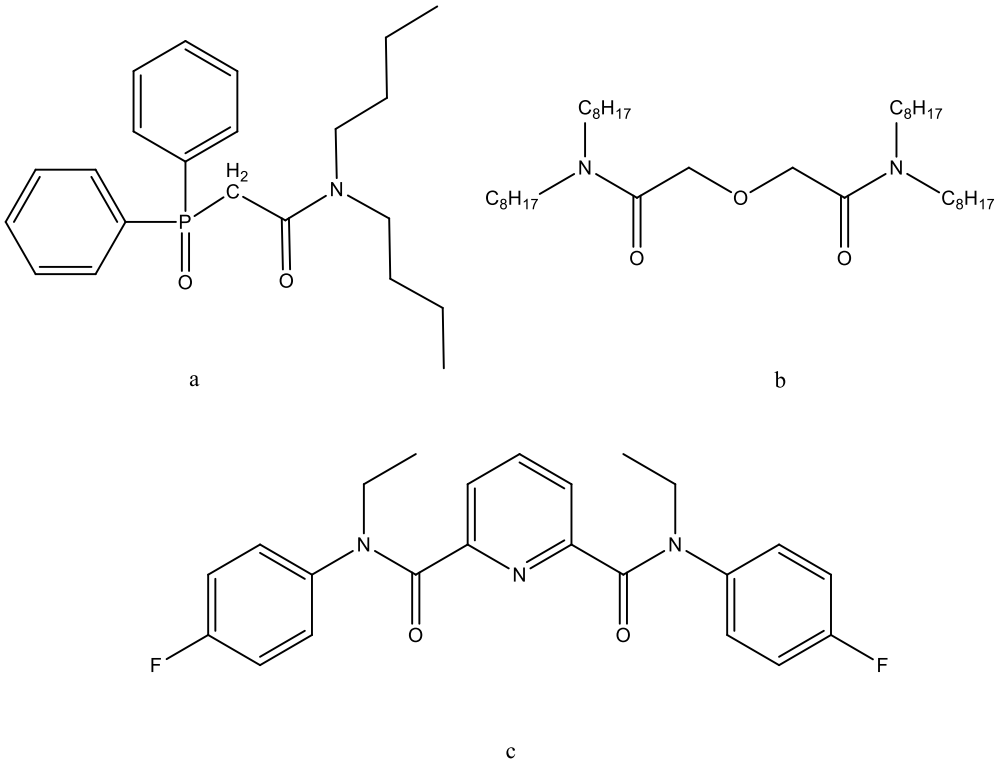

Figure 4.1. The structure of the ionophores used for the multi-ionophore sensor membranes. a – DPCMPO, b – TODGA, c – DPA.

4.1.2. Membrane composition and preparation

The sensor array consisted of 21 sensors: 7 membrane compositions with 3 pieces of each type. The membranes M1–M3 contained single ionophores, the membranes M5–M7 contained binary mixtures of ionophores, and the membrane M4 simultaneously contained three ionophores. All the studied compositions are listed in Table 4.1.

The sensor membranes were prepared according to the standard procedure. All the weighed components were dissolved in freshly distilled tetrahydrofuran (THF) under stirring. After complete dissolution of the components, the membrane cocktails were poured into 3 ml Teflon cylindrical vessels and left for 48h until THF was completely evaporated. Further, 7-mm diameter circles of the membranes (3 per composition) were cut and glued onto the sensor body using the mixture of PVC and cyclohexanone. All sensors were conditioned in 0.01 M NaCl prior to measurements.

Table 4.1. Multi-ionophore sensor membrane compositions.

#	$m_{ionophore}$, mg ($C_{ionophore}$, mmol/kg)			$m_{plasticizer}$	m_{PVC}	$m_{lipophilic\ additive}$
	DPCMPO	TODGA	DPA			
1	5.6 (50)	-	-	194.5	97.2	1.5
2	-	8.7 (50)	-	192.4	96.2	1.5
3	-	-	6.1 (50)	194.1	97.1	1.5
4	1.8 (16.67)	2.9 (16.67)	2.0 (16.67)	193.7	96.8	1.5
5	2.8 (25)	4.4 (25)	-	193.4	96.7	1.5
6	2.8 (25)	-	3.1 (25)	194.3	97.1	1.5
7	-	4.4 (25)	3.1 (25)	193.2	96.6	1.5

4.1.3. Potentiometric measurements and data processing

Potentiometric measurements were performed using digital mV-meter HAN-11 (Sensor Systems LLC, St. Petersburg, Russia) against standard Ag/AgCl reference electrode (Izmeritelnaya Tekhnika, Moscow, Russia) in the following galvanic cell:

Ag | AgCl, KCl_{sat}| sample solution | membrane | NaCl, 0.01 M, AgCl | Ag

The standard glass pH electrode (Izmeritelnaya Tekhnika, Moscow, Russia) was used for pH control during the measurements as the pH values were fixed at 2 with nitric acid to suppress hydrolysis. The sensitivity of the sensors M1–M7 towards lanthanide and transition metal cations was investigated in 10^{-6} – 10^{-3} M aqueous solutions of the corresponding metal nitrates. Lanthanide nitrates were used as 1M stock solutions in 10^{-2} M HNO_3. The sensitivity values (expressed as the slope of the linear part of the response function) were averaged over the three replica sensors of the same composition and three repeated measurements. The standard deviation did not exceed 1 mV/dec. In order to investigate the characteristics of the proposed array in the analysis of a mixture, two sets of lanthanide mixtures were analyzed: the binary set of the "light" La^{3+} and Nd^{3+}, and the tertiary set containing "light" Nd^{3+}, "heavy" Er^{3+} cations and Eu^{3+} from the middle segment of the lanthanide range. The experimental set contained 35 samples and was designed according to the procedure described in [230] for the 10^{-5} – 10^{-3} M concentration range. It consisted of Calibration (points 1-25) and Validation (points 26-35) subsets for PLS regression modeling (Table 4.2.).

Table 4.2. Compositions of the La-Nd and Nd-Eu-Er mixtures.

	Binary mixtures		Tertiary mixtures		
№	$-\lg C_{La^{3+}}$, M	$-\lg C_{Nd^{3+}}$, M	$-\lg C_{Nd^{3+}}$, M	$-\lg C_{Eu^{3+}}$, M	$-\lg C_{Er^{3+}}$, M
1	4,45	4,97	4,83	3,34	4,32
2	4,31	4,59	4,58	4,67	3,01
3	3,87	4,78	3,57	3,06	3,08
4	3,52	4,81	4,28	4,59	3,90
5	3,17	4,80	5,00	4,65	5,00

Table 4.2 (Cont.). Compositions of the La-Nd and Nd-Eu-Er mixtures.

	Binary mixtures		Tertiary mixtures		
№	$-\lg C_{La^{3+}}$, M	$-\lg C_{Nd^{3+}}$, M	$-\lg C_{Nd^{3+}}$, M	$-\lg C_{Eu^{3+}}$, M	$-\lg C_{Er^{3+}}$, M
6	4,97	4,51	4,95	4,67	3,65
7	4,65	4,65	4,24	4,81	4,57
8	3,87	4,43	3,77	4,48	3,03
9	3,52	4,43	3,06	4,51	4,54
10	3,16	4,39	4,49	5,00	3,49
11	4,98	4,00	4,97	3,86	3,98
12	4,30	3,84	3,81	3,25	4,19
13	4,13	4,16	3,10	3,46	5,00
14	3,71	3,91	4,84	5,00	4,55
15	3,29	3,49	3,43	4,86	3,71
16	4,92	3,60	3,12	4,04	4,89
17	4,48	3,15	3,96	5,00	3,24
18	4,00	3,47	4,47	3,01	4,64
19	3,64	3,57	3,38	4,79	4,94
20	3,04	4,06	4,78	4,52	4,21
21	4,83	3,20	4,99	3,07	4,91
22	4,45	3,50	3,03	3,15	3,31
23	4,04	3,05	3,34	4,88	3,09
24	3,64	3,22	4,42	3,42	3,25
25	3,00	3,30	3,26	3,73	3,22
26	3,25	3,37	4,73	3,61	4,86
27	4,97	3,55	4,68	3,11	3,07
28	4,99	4,93	3,58	3,98	3,11
29	3,29	3,91	3,77	4,09	4,77
30	3,31	4,85	3,04	4,98	4,64
31	4,33	3,71	3,86	4,80	3,97
32	3,67	4,35	4,98	4,94	4,17
33	4,18	4,22	4,62	4,12	3,57
34	3,92	3,37	4,27	4,97	3,00
35	4,83	4,09	3,07	3,04	3,14

The calibration and validation sets were designed independently so as lgC values would both have a uniform distribution in the given concentration range. To assess the model prediction performance, the RMSEP was calculated.

4.2. Results and discussion

4.2.1. Sensitivity of ionophore-free sensors to lanthanide cations

The sensitivity of the sensors M1—M7 towards Ln^{3+} cations was determined for the 10^{-6} — 10^{-3} M range. The typical (theoretical) sensor calibration curve for Ln^{3+} cation analysis is presented in Fig. 4.2. This curve corresponds to a theoretical value of the Nernstian response to the trivalent lanthanide cations equal to 19 mV/dec. The experimentally observed sensor sensitivity values are reported in Fig. 4.3. and Fig. 4.4.

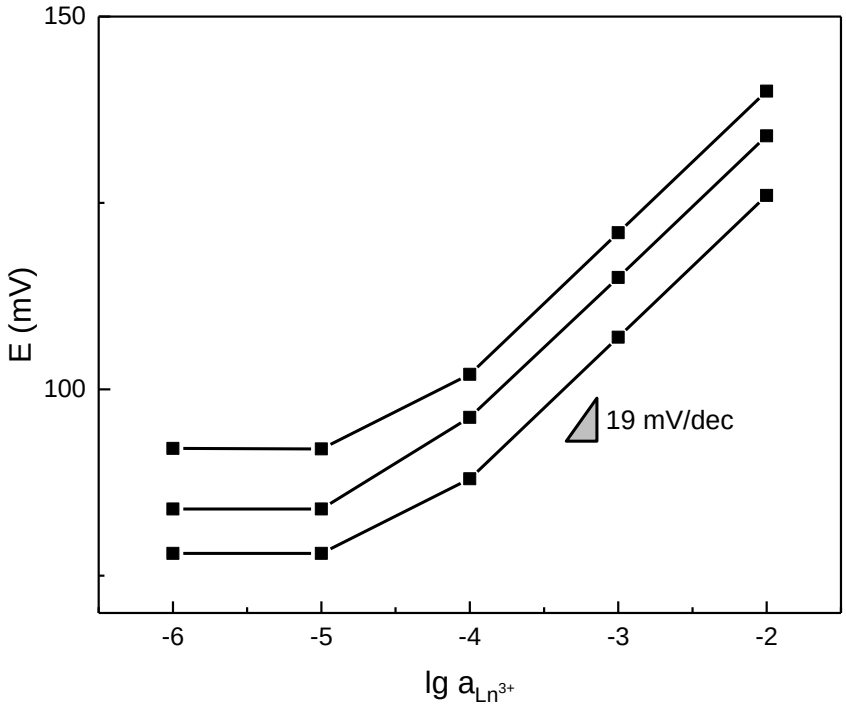

Figure 4.2. The typical calibration curve for the Ln^{3+} for 3 replicate sensors with the same composition.

Sensors M4, M5 and M7 containing TODGA in mixture with other ligands demonstrate a sensitivity pattern identical to the M2 sensor that only contains TODGA. This pattern is characterized with an increase in sensitivity from «light» to «heavy» lanthanides, in line with the growth of the atomic number of the element (Fig. 4.3). Besides, TODGA-based sensors have the highest sensitivity values towards “heavy”

lanthanides over the whole sensor array. According to reference [235], in which TODGA is used as an extracting agent, TODGA tends to extract heavier lanthanides rather than the "light" ones. Moreover, regarding the "heavy" lanthanides, its distribution ratio (D) is several orders larger than the one of DPCMPO [7] and DPA [236, 237] under similar experimental conditions. This fact explains the prevalence of the TODGA sensitivity pattern over the sensitivity patterns of DPCMPO and DPA.

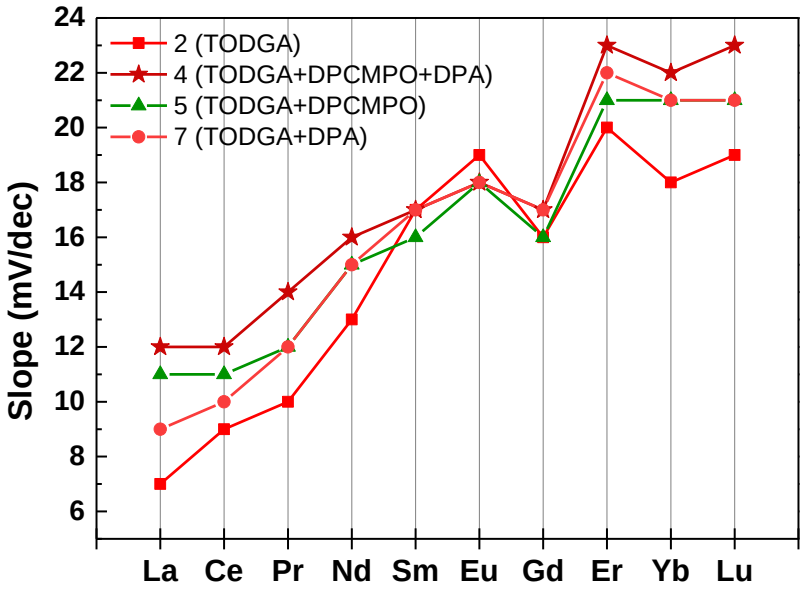

Figure 4.3. Sensor sensitivity patterns for TODGA-containing sensors, ± 1 mV/dec.

Concerning the DPCMPO-based sensors, its sensitivity values decrease with the atomic number of the lanthanide. For instance, the sensitivity pattern for the sensor M6, containing DPCMPO and DPA, is similar to the pattern of the DPCMPO-based sensor M1 but not to the DPA-based sensor M3. The similarities in the sensitivity patterns within the DPCMPO-based sensor membranes are shown in Fig. 4.4.

It is known that D_{Ln3+} distribution ratios for extraction with carbamoyl phosphine oxides decrease from "light" to "heavy" lanthanides [238, 239], whereas Dipicolinamides demonstrate moderate sensitivity over the whole lanthanide range [240, 241]. In general, the D values are normally proportional to the stability constants

of “ionophore-Ln^{3+}” complex. As they decrease in the TODGA >> DPCMPO > DPA series, one can expect similar tendencies for the sensor sensitivity patterns. In practice, the sensitivity pattern of TODGA being mixed with either DPCMPO or DPA prevails over two other ones. In its turn, sensors containing both DPCMPO and DPA tend to have the DPCMPO sensitivity pattern. Therefore, we can conclude that the DPA-sensitivity pattern can only be observed for the mono-ionophore membrane without additional ligands.

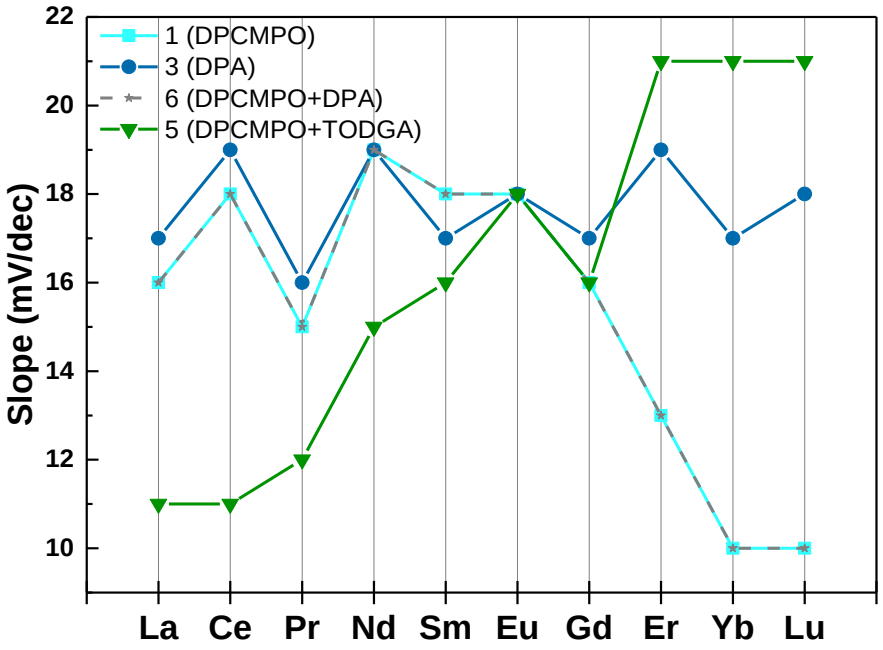

Figure 4.4. The sensitivity patterns for the sensors M1, M3, M6 (DPCMPO-based membranes).

Moreover, the selectivity characteristics of the sensors were evaluated using the fixed interference method [74]. Selectivity coefficients were calculated from the calibration measurements in lanthanide solutions with the presence of 10^{-5} M La^{3+} and are reported in Table 4.3.

Table 4.3. The selectivity coefficients $K_{Ln/La}$ determined in the 10^{-5} M Ln^{3+} solutions.

Primary Ln^{3+} ion/sensor #	M1	M2	M3	M4	M5	M6	M7
Ce	0.4	3.2	0.4	0.8	1.6	0.4	0.4
Pr	0.8	>>10	1.6	>>10	>>10	3.2	10.0
Nd	0.3	0.2	0.6	0.3	0.5	0.5	0.3
Sm	1.6	0.3	1.0	0.6	0.6	1.3	0.6
Eu	0.5	0.1	0.2	0.1	0.1	1.0	0.1
Gd	1.0	0.3	0.3	0.2	0.2	1.0	0.2
Er	3.9	0.4	1.0	0.4	0.2	5.0	0.1

As expected, TODGA-based sensors (M4, M5, M7) demonstrate a higher selectivity towards the “heavy” lanthanides. For instance, the $K_{Ln/La} < 1$ in case of lanthanides “heavier” than Nd^{3+}. Sensors M1 and M6 with a more pronounced “light” lanthanide sensitivity have $K_{Ln/La} > 1$, which confirms the fact that they prefer the “lighter” lanthanum over the “heavier” lanthanides. In case of Ce^{3+}, the preference to “lighter” ions is clear ($K_{Ce/La} < 1$). These interesting results are demonstrated by the DPA-based M3 sensor. In most cases the $K_{Ln/La}$ value is about 1, which is in agreement with its moderate sensitivity to the whole range of the lanthanide cations observed before.

It is clear that some of the lanthanide cations will demonstrate a strong mutual interference in their mixtures. For instance, both “light”- and “heavy”-sensitive sensors demonstrate a high sensitivity to neodymium in the presence of Ln^{3+}. To analyze the impact of the multi-ionophore sensor membrane composition on the lanthanide mixture analysis, a set of La-Nd binary mixtures was analyzed.

4.2.2. Mixture analysis

The ability of the sensor array to quantify individual lanthanides in mixtures was first studied for La-Nd binary mixtures. A set of 35 La-Nd solutions was analyzed and

the acquired data were analyzed with PLS regression to relate the sensor responses with the metal content. The resulting PLS models demonstrated a sufficient precision in prediction for both Nd^{3+} and La^{3+} concentrations (RMSEP = 0.15 and 0.12, respectively).

As the sensors of the array formed groups according to their sensitivity patterns, the additional PLS regression models were built based on the following subsets of the sensor array: “light Ln”-sensitive (M1, M3, M6), and “heavy Ln”-sensitive (M2, M4, M5, M7). The parameters of the models were compared to those for the complete array (M1–M7) (Table 4.4).

Table 4.4. Comparison of PLS models based on the complete sensor array data and partial data from sensor subsets for La-Nd binary mixtures analysis. RMSEP – Root Mean Square Error of prediction, R^2 – squared correlation coefficient, *N* – number of PLS factors.

Sensor set	La^{3+}				Nd^{3+}			
	Slope	RMSEP, lgC	R^2	N	Slope	RMSEP, lgC	R^2	N
Complete array (M1-M7)	0.69	0.12	0.85	4	1.14	0.15	0.89	2
M1 + M3 + M6 (“light” - sensitive set)	0.84	0.09	0.90	3	0.31	0.35	0.40	3
M2 + M4 + M5 + M7 (“heavy” - sensitive set)	0.37	0.24	0.55	2	1.06	0.13	0.91	2

The PLS model built by using the “light”-sensitive sensor subset for the prediction of the neodymium concentration demonstrated a higher RMSEP value compared to the one obtained by using the complete array (0.29 and 0.15 lgC, respectively). The dominance of the TODGA sensitivity pattern for most of the sensors resulted in comparable RMSEP values for both the “heavy”-sensitive set and the complete array (0.13 and 0.15 lgC, respectively). For the determination of the “lighter” La^{3+}, TODGA-based sensors do not demonstrate a high precision (RMSEP = 0.24)

and the RMSEP obtained when using the full array is two times lower (0.12). However, the model is based on 4 latent variables, which may cause overfitting of the signal by the model. As a conclusion, the “light”-sensitive part of the array is best suited for the La^{3+} determination, as this is the subset of sensors for which the PLS model gives the lowest RMSEP values (i.e. 0.09 lgC).

VIP values of the PLS regression model based on the complete array were compared for the variables M1–M7 (Fig. 4.5). Indeed, as shown before, the most significant variables for the Nd determination correspond to the sensors M2, M4, M5, M7. Similarly, the biggest VIP values for the PLS model for the La^{3+} determination correspond to the “light-sensitive” sensors M1, M3, M6. Thus, the complete array (M1-M7) provides reliable estimation of both ions concentration and the analysis precision may be further improved by excluding “non-sensitive” variables from the model, as shown in Table 5.4.

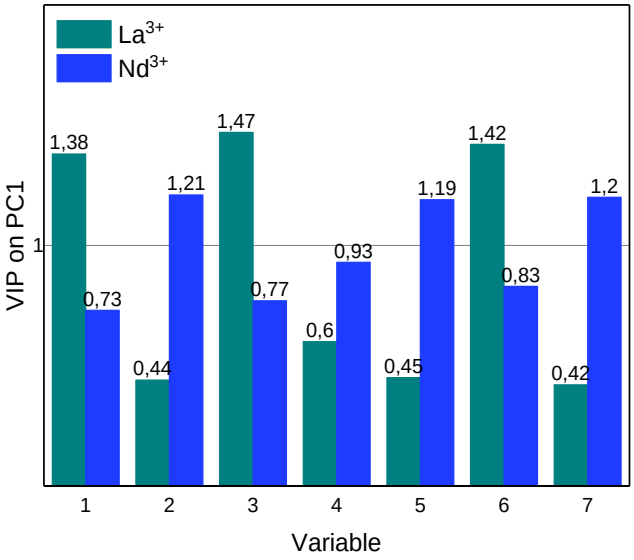

Figure 4.5. VIP values for the La^{3+} and Nd^{3+} mixture analysis.

In the next step of the study, a multi-ionophore sensor array was applied for the analysis of ternary Ln^{3+} mixtures. Three metals were chosen: one in the beginning (Nd^{3+}), one in the middle (Eu^{3+}) and one in the end of the lanthanide series (Er^{3+}). The results of the PLS regression modelling of the sensor responses in the studied mixtures are given in Table 4.5.

Table 4.5. PLS results for Nd-Eu-Er mixtures analysis. RMSEP – Root Mean Square Error of prediction, R^2 – squared correlation coefficient, N – number of PLS factors.

Ion	Slope	RMSEP, lg C	R^2	N
Nd^{3+}	0.09	0.29	0.26	1
Eu^{3+}	0.39	0.46	0.50	3
Er^{3+}	1.01	0.08	0.97	2

From the results shown in this table, it is clear that only the Er^{3+} determination can be performed with a sufficient precision (RMSEP = 0.08 lgC). This can be explained by the prevalence of the TODGA sensitivity pattern over the other ligands. In order to confirm this, the VIP scores for the 1st latent variable of the PLS model were determined (shown in Fig. 4.6). The highest VIP values correspond to the sensors M2, M4, M5, M7 – namely TODGA-based sensors – exhibiting a high sensitivity towards “heavy” lanthanide cations.

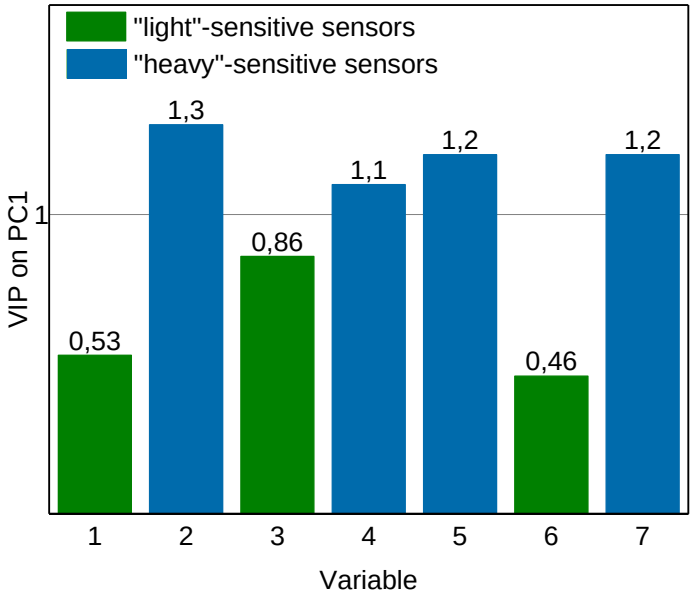

Figure 4.6. The VIP scores of the PLS model built on data Er^{3+} analysis in tertiary Nd-Eu-Er mixtures.

4.3. Conclusions

This study contributes to the understanding of sensitivity patterns of sensor membranes containing multiple ionophores. The proposed multi-ionophore membrane compositions do not provide new sensitivity patterns compared to the mono-ionophore sensors. However, the slight differences in the sensors performance, depending on the membrane composition, are still sufficient for a multisensory analysis of mixtures. For instance, the analysis of binary La^{3+} and Nd^{3+} mixtures yielded a reasonable precision.

The analysis of ternary lanthanide mixtures is not possible with the suggested sensor array due to the fact that TODGA-based sensors are highly selective to the “heavy” lanthanides. This will therefore provide a dominating sensitivity pattern for four (M2, M4, M5, M7) sensors out of seven, since TODGA has a very strong complexation ability compared to the other two ligands, DPCMPO and DPA. In the future, this new understanding should help to improve the polymeric membrane compositions (e.g. use alternative ionophores) in order to perform the analysis of mixtures in a more flexible way.

CHAPTER 5. Conclusion

Nowadays, there is an ongoing process of switching to the paradigm of so-called “Industry 4.0” or the fourth industrial revolution. The main concept of this process is an ever-increasing automation associated with information technologies in all fields of human activities. This process has already led to the Internet of things, cloud computing and cyber-physical systems. The implementation of these concepts in the industry requires the development of advanced monitoring and control systems, that could operate continuously in an on-line mode, yield reliable data, exchange these data through the networks, and all of this being done without human input.

The development of such systems would allow monitoring chemical parameters in various industrial processes, environmental samples or biological systems, and is therefore of special importance. Throughout the last decades, there was a tremendous growth of process analytical technology (PAT) and multivariate statistical process control (MSPC) in all industrial fields. These techniques are aimed at the substitution of traditional sampling-based control which is not capable of yielding timely chemical information in an express way. Application of modern spectroscopic tools with appropriate data processing algorithms allows reliable estimation of chemical composition of industrial streams in on-line mode. This automation trend is also clearly seen in modern analytical chemistry: more and more studies are aiming at the development of analytical methods suitable for fast and simple measurements of several key quality parameters instead of research on traditional “heavy” analytical tools providing super-selective and super-sensitive but super-expensive information on the exhaustive chemical composition of a sample. The development of such chemical monitoring systems is closely associated with data analysis and machine learning (chemometrics in the context of chemical studies). Application of chemometrics enables deriving reliable chemical information from noisy and poorly resolved analytical signals which are typical for simple instruments, and since “math is cheaper than physics”, this paradigm appears to be very powerful and effective.

Due to the above mentioned trends, the number of studies devoted to the development of various chemical sensors and sensor systems has grown exponentially over the last decade. A very representative example where simplicity of the device still allows very effective performance is the multisensor approach. Multisensor systems are made of a set of cross-sensitive chemical sensors combined with chemometrics. This concept proved to be very powerful in various real-life applications, where the evaluation of global quality parameters is often needed instead of the information on the precise composition of the sample. For example, arrays of cross-sensitive sensors may be used for the estimation of the water toxicity in ecological monitoring, while the content of the individual toxicants in water is not directly correlated with the reaction and survival rate of biological objects. Some of these quality parameters, such as taste for food products, do not even have a clearly defined measurement unit. Taste is correlated with multivariate data from sensor arrays rather than with concentrations of individual constituents. In industrial processes monitoring, along with the determination of key components, compliance of general process quality to appropriate standards is checked.

Further successful developments of multisensor approaches and their implementation into good industrial practices require addressing several important issues such as: 1) novel sensor signal transduction schemes to produce more informative sensor response; 2) novel approaches for programmable sensor properties.

The present thesis was devoted to the developing of new approaches to signal transduction in potentiometric sensors. This type of sensors is the most popular and widely applied due to very simple construction and measurement process, yet very prominent analytical performance in terms of selectivity and detection limits. The manuscript consists of three parts each one addressing particular issues in modern potentiometric sensor technology.

The first part proposed a new way of analytical signal transduction from potentiometric sensor membranes. The aim of the present research was to examine

the evolution of the Raman spectral signature of a polymeric sensor membrane upon contact with the sample solution. The feasibility study was performed using a ligand (PDAM) immobilized in the plasticized PVC sensor membrane. As a model analyte, Cd^{2+} was chosen since metal cations do not inherently have vibrational modes and therefore no Raman spectral signature. It was found that the formation of the complex between Cd^{2+} in sample solution and PDAM induces quantitative changes in the Raman spectrum of the membrane. Multivariate regression applied to membrane spectra in contact with Cd^{2+} solutions allowed the estimation of the metal content in a sample. The main advantage of the proposed approach is the possibility of working with very small sample volumes, in the order of microliter. Further perspectives of this research could be devoted to the adaptation of the membrane composition for the determination of other analytes, e.g. using new polymers and ligands. Besides, an additional study could assess the selectivity of the PDAM-Cd^{2+} complex formation, as the presence of other transition metal cations may induce similar changes in the spectrum.

Both the second and the third part of the thesis were aimed at developing sensor arrays with programmable cross-sensitivity properties, providing easy adaptation of the array to a particular analytical task, by changing the composition of the sensor membrane.

The second part of the study was focused on ionophore-free sensor array applications, where sensor membranes were based on the polymer, plasticizer and lipophilic additive only. As the cross-sensitivity of these sensors is defined by the combination of the plasticizer and the lipophilic additive in the membrane, the ionophore-free approach may eventually circumvent the tedious and cumbersome procedure of ionophore selection. The proposed array was tested in the analysis of Ca^{2+} and Mg^{2+} cations demonstrating high mutual interference in mixtures, and the results were compared with characteristics of individual selective sensors with conventional membrane compositions. It was found that the proposed procedure yields reasonable precision in the quantification of both calcium and magnesium in

double mixtures even without ionophores. Application of PLS regression can effectively compensate for the lack of selectivity in case of Mg^{2+} determination in mixtures, by contrast to the use of selective sensors. Nevertheless, since selectivity of the ionophore-free sensors is governed by the lipophilicity of target ions, in more complex mixtures containing sodium and potassium interfering background, reliable quantification of calcium and magnesium is still not possible. A way to circumvent this limitation could be to apply a wider range of plasticizers and ion-exchangers in order to increase the variability of sensitivity patterns of the sensors. In general, the suggested approach of attaining potentiometric selectivity without ionophores should be studied further.

The third part introduced multi-ionophore sensors, containing several ionophores in one PVC-plasticized membrane. The goal was to assess the effect of the presence of several ionophores on the sensor sensitivity patterns. This multi-ionophore approach was tested in the analysis of rare earth element cations mixtures and compared to the results of conventional mono-ionophore sensor. It was shown that even slight differences in sensitivity patterns for the mono-and multi-ionophore sensors result in a significant increase in the sensor performance, as shown for the analysis of La^{3+} and Nd^{3+} mixtures. The main limitation of the designed sensors was related to the dominance of the sensitivity patterns of one of the chosen ionophores (TODGA), providing the selectivity towards “heavy” lanthanide cations rather than “light” ones in their mixtures. Further studies with other ligands should be carried out in order to determine whether a bigger diversity of the sensitivity patterns – and thus a better performance of the sensor array – can be achieved.

These approaches being combined with multivariate data analysis techniques may become competitive with the traditional ISE applications. Further development may allow achieving wide range programmable sensitivity patterns in an array, allowing a more flexible adaptation to particular analytical tasks.

Annex 1. The NIPALS algorithm (PCA).

1) Initialize the scores vector $\mathbf{t}_1$;
2) Obtain the loading vector $\mathbf{p}_1$ regressing the $\mathbf{X}$ on the scores vector $\mathbf{t}_1$ and normalize the result (Eq.28):

$$\mathbf{p}_1 = \frac{\mathbf{X}^T\mathbf{t}_1}{\left\|\mathbf{X}^T\mathbf{t}_1\right\|} \quad \text{(Eq.28)}$$

3) Recalculate t_1 by the projection of $\mathbf{X}$ on $\mathbf{p}_1$ (Eq.28):

$$\mathbf{t}_{1new} = \mathbf{X}\mathbf{p}_1 \quad \text{(Eq.29)}$$

4) Check if the convergence achieved, e.g. the difference between the recalculated $\mathbf{t}_{new}$ and the initial one is below some threshold value (most often $\boldsymbol{\varepsilon} = 0.00001$) (Eq.30):

$$\left|\mathbf{t}_1 - \mathbf{t}_{1new}\right| < \boldsymbol{\varepsilon} \quad \text{(Eq.30)}$$

5) remove the first PC from the initial $\mathbf{X}$ matrix (Eq.31):

$$\mathbf{E} = \mathbf{X} - \mathbf{t}_1\mathbf{p}_1^T \quad \text{(Eq.31)}$$

The t_i and p_i for the next principal component are estimated basing on the residuals matrix E from the previous iteration.

Annex 2. NIPALS algorithm (PLS regression)

1) Choose a starting vector $\mathbf{u_i}$, (one of the **Y** columns)
2) Estimate the X-weights, **w**:

$$\mathbf{w_i} = \mathbf{X}^T\mathbf{u_i} / \| \mathbf{X}^T\mathbf{u_i} \| \quad \text{(Eq.32)}$$

3) Calculate **X**-scores, **t**:

$$\mathbf{t_i} = \mathbf{X}\mathbf{w_i} \quad \text{(Eq.33)}$$

4) Estimate the **Y**-loadings, $\mathbf{q_i}$:

$$\mathbf{q_i} = \mathbf{u_i}^T\mathbf{t_i} / \| \mathbf{u_i}^T\mathbf{t_i} \| \quad \text{(Eq.34)}$$

5) Estimate the **Y**-scores, q_i:

$$\mathbf{u_i} = \mathbf{Y}\mathbf{q_i} \quad \text{(Eq.35)}$$

6) Check if the convergence of **t** is achieved (difference between two consecutive iterations is below selected threshold value ε):

$$\| \mathbf{t}_{i-1} - \mathbf{t}_i \| / \| \mathbf{t}_i \| < \varepsilon \quad \text{(Eq.36)}$$

If **t** has not converged, then return to 1)

if **t** has converged, then

7) compute the loadings for X:

$$\mathbf{p_i} = \mathbf{X}^T\mathbf{t_i} / \| \mathbf{t_i}^T\mathbf{t_i} \| \quad \text{(Eq.37)}$$

8) remove the resulting component from **X,** so the residuals can be used**:**

$$\mathbf{E_i} = \mathbf{X_{i+1}} - \mathbf{t_i}\mathbf{p}_i^T$$
$$\mathbf{F_i} = Y_{\mathbf{i+1}} - \mathbf{u_i}\mathbf{q_i}^T \quad \text{(Eq.38)}$$

repeat with the next component until $\mathbf{F_i}$ is below a certain pre-determined threshold, which would mean that sufficient percentage of Y-variance is explained.

The regression coefficient vector **B** is calculated according to:

$$b_i = \mathbf{W_i}\left(\mathbf{P_i^T}\mathbf{W_i}\right)^{-1}\mathbf{q_i} \quad \text{(Eq.39)}$$

Annex 3. NMR spectrum of the acrylate copolymer

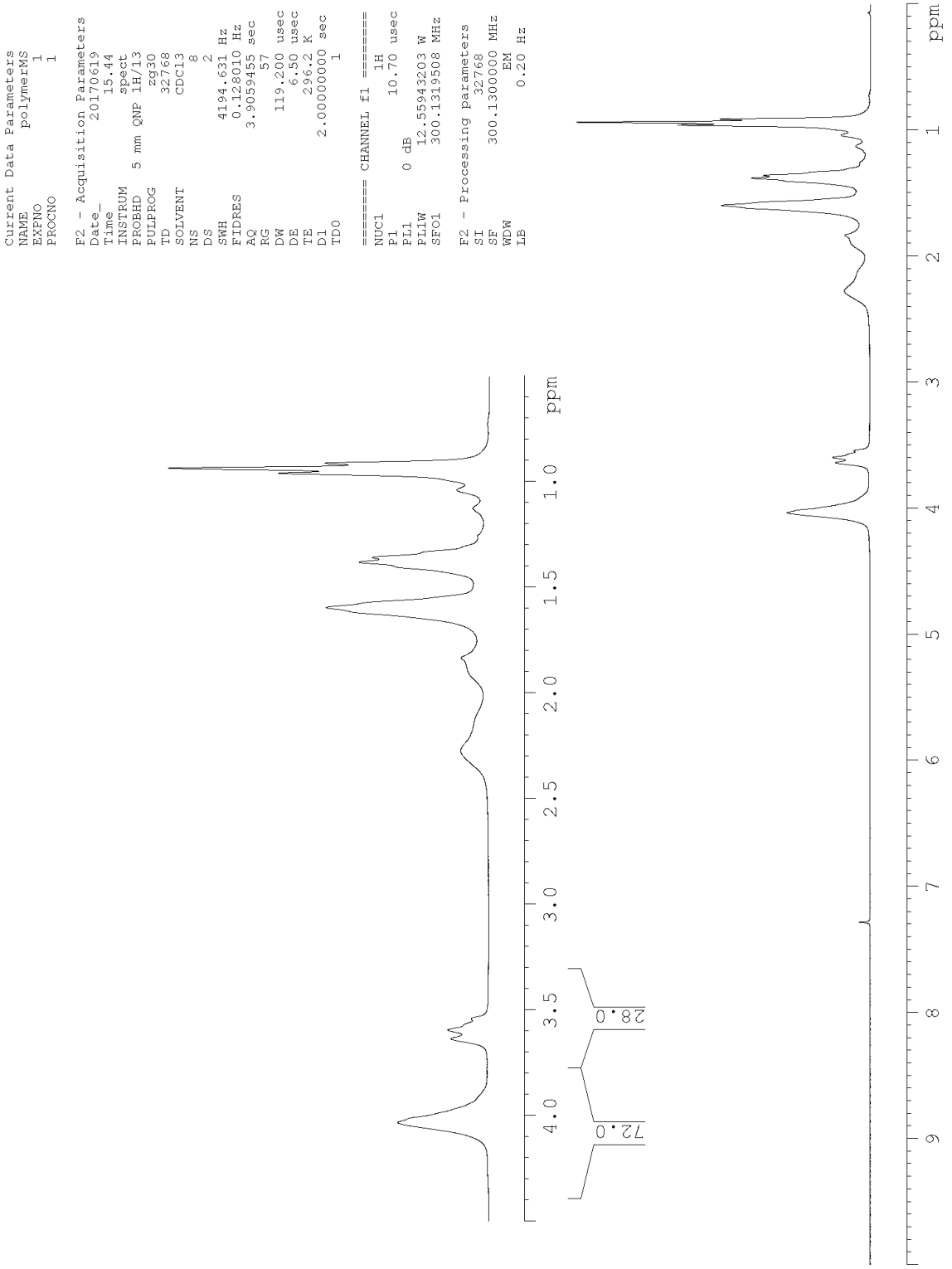

Annex 4. Original contributions

Peer-reviewed publications

1. M. Alyapyshev, J. Ashina, D. Dar'in, E. Kenf, D. Kirsanov, L. Tkachenko, A. Legin, G. Starova, V. Babain, 1,10-Phenanthroline-2,9-dicarboxamides as ligands for separation and sensing of hazardous metals, RSC Advances, 6 (2016) 68642-68652

2. J. Ashina, D. Kirsanov, M. Moreau, V. Koverga, K. Mikhelson, C. Ruckebusch, A. Legin, Raman transduction for polymeric ion-selective sensor membranes: Proof of concept study, Sensors and Actuators, B: Chemical, 253 (2017) 697-702

Conference abstracts:

3. J. Ashina, D. Kirsanov, M. Moreau, C. Ruckebusch, A. Legin. «Raman transduction for ISE polymeric membranes: feasibility study». Book of abstracts of Matrafured 2017 Conference On Electrochemical Sensors. June 11-16, 2017, Budapest, Hungary.

4. J. Ashina, D. Kirsanov, V.Babain, C. Ruckebusch, A. Legin. «Polymeric Membrane Sensors with Two Ionophores: Case Study in Lanthanide Mixtures Analysis». Book of abstracts of Matrafured 2017 Conference On Electrochemical Sensors. June 11-16, 2017, Budapest, Hungary.

5. J. Ashina, D. Kirsanov, C. Ruckebusch, A. Legin. «Attaining potentiometric selectivity by ionophore-free sensors». Book of abstracts of Matrafured 2017 Conference On Electrochemical Sensors. June 11-16, 2017, Budapest, Hungary.

References:

1. Gründler, P., *Chemical Sensors: An Introduction for Scientists and Engineers*. 2007: Springer Berlin Heidelberg.
2. Janata, J., *Principles of Chemical Sensors*. Principles of Chemical Sensors. 2009. 1-373.
3. Wang, Y., et al., *Electrochemical Sensors for Clinic Analysis.* Sensors (Basel, Switzerland), 2008. **8**(4): p. 2043-2081.
4. Thompson, M.E., *Magnesium in sea water: an electrode measurement.* Science, 1966. **153**(3738): p. 866-7.
5. Hui, X., et al., *A miniature all-solid-state calcium electrode applied to in situ seawater measurement.* Measurement Science and Technology, 2013. **24**(12): p. 125105.
6. Kumar, P. and Y.B. Shim, *A novel Mg(II)-selective sensor based on 5,10,15,20-tetrakis(2-furyl)-21, 23-dithiaporphyrin as an electroactive material.* Journal of Electroanalytical Chemistry, 2011. **661**(1): p. 25-30.
7. Lewenstam, A., *Routines and Challenges in Clinical Application of Electrochemical Ion-Sensors.* Electroanalysis, 2014. **26**(6): p. 1171-1181.
8. Wackerlig, J. and P.A. Lieberzeit, *Molecularly imprinted polymer nanoparticles in chemical sensing - Synthesis, characterisation and application.* Sensors and Actuators, B: Chemical, 2015. **207**(Part A): p. 144-157.
9. Wojciechowski, M., et al., *Microspheres aided introduction of ionophore and ion-exchanger to the ion-selective membrane.* Talanta, 2012. **88**: p. 66-72.
10. Otto, M. and J.D.R. Thomas, *Model studies on multiple channel analysis of free magnesium, calcium, sodium, and potassium at physiological concentration levels with ion-selective electrodes.* Analytical Chemistry, 1985. **57**(13): p. 2647-2651.
11. del Valle, M., *Electronic tongues employing electrochemical sensors.* Electroanalysis, 2010. **22**(14): p. 1539-1555.
12. Kirsanov, D., et al., *Water toxicity evaluation in terms of bioassay with an Electronic Tongue.* Sensors and Actuators B-Chemical, 2013. **179**: p. 282-286.
13. Schazmann, B., et al., *Robust, Bridge-Less Ion-Selective Electrodes with Significantly Reduced Need for Pre- and Post-Application Handling.* Electroanalysis: p. n/a-n/a.
14. Natale, C.D., et al. *DATA ANALYSIS FOR CHEMICAL SENSOR ARRAYS*. in *Advances in Sensing with Security Applications*. 2006. Dordrecht: Springer Netherlands.
15. Lvova, L., et al., *Multi-transduction sensing films for Electronic Tongue applications.* Sensors and Actuators B: Chemical, 2015. **207**: p. 1076-1086.
16. Lvova, L., et al., *Towards Hyphenated Sensors Development: Design and Application of Porphyrin Electropolymer Materials.* Electroanalysis, 2012. **24**(4): p. 776-789.

17. D'Orazio, P., *Biosensors in clinical chemistry.* Clin Chim Acta, 2003. **334**(1-2): p. 41-69.
18. Michael, D.J. and R.M. Wightman, *Electrochemical monitoring of biogenic amine neurotransmission in real time.* J Pharm Biomed Anal, 1999. **19**(1-2): p. 33-46.
19. Márquez, A., et al., *Electrodepositable alginate membranes for enzymatic sensors: An amperometric glucose biosensor for whole blood analysis.* Biosensors and Bioelectronics, 2017. **97**: p. 136-142.
20. Climent, V. and J.M. Feliu, *Cyclic Voltammetry*, in *Reference Module in Chemistry, Molecular Sciences and Chemical Engineering*. 2015, Elsevier.
21. Yoo, E.-H. and S.-Y. Lee, *Glucose Biosensors: An Overview of Use in Clinical Practice.* Sensors (Basel, Switzerland), 2010. **10**(5): p. 4558-4576.
22. Turner, A.P., B. Chen, and S.A. Piletsky, *In vitro diagnostics in diabetes: meeting the challenge.* Clin Chem, 1999. **45**(9): p. 1596-601.
23. van de Leest, R.E., *Solid-state ion-selective electrodes for metal ions.* Analyst, 1977. **102**(1216): p. 509-514.
24. Brosel-Oliu, S., et al., *Impedimetric label-free sensor for specific bacteria endotoxin detection by surface charge registration.* Electrochimica Acta, 2017. **243**: p. 142-151.
25. Varshney, M. and Y. Li, *Interdigitated array microelectrodes based impedance biosensors for detection of bacterial cells.* Biosensors and Bioelectronics, 2009. **24**(10): p. 2951-2960.
26. Nikolskii, B.P., *Theory of the glass electrode. I. Theoretical.* J. Phys. Chem. (U.S.S.R.), 1937(3): p. 495-50.
27. Haber, F. and Z. Hlemensiewicz, *Über elektrische phasengrenzkräfte.* Zeitschrift für physikalische Chemie, 1909. **67**(1): p. 385-431.
28. Růžička, J. and C.G. Lamm, *A new type of solid-state ion-selective electrodes with insoluble sulphides or halides.* Analytica Chimica Acta, 1971. **53**(1): p. 206-208.
29. Martin, S.F. and James W. Ross, Jr., *Electrode for Sensing Fluoride Ion Activity in Solution.* Science, 1966. **154**(3756): p. 1553-1555.
30. Faridbod, F., et al., *Developments in the Field of Conducting and Non-conducting Polymer Based Potentiometric Membrane Sensors for Ions Over the Past Decade.* Sensors, 2008. **8**(4): p. 2331.
31. Bonner, O.D. and D.C. Lunney, *A study of some concentration cells with liquid ion-exchanger membranes.* Journal of Physical Chemistry, 1966. **70**(4): p. 1140-1150.
32. Ross, J.W., *Calcium-Selective Electrode with Liquid Ion Exchanger.* Science, 1967. **156**(3780): p. 1378-1379.
33. Wang, X., et al., *A polymeric liquid membrane electrode responsive to 3,3',5,5'-tetramethylbenzidine oxidation for sensitive peroxidase/peroxidase mimetic-based potentiometric biosensing.* Anal Chem, 2014. **86**(9): p. 4416-22.

34. Bloch, R., A. Shatkay, and H.A. Saroff, *Fabrication and Evaluation of Membranes as Specific Electrodes for Calcium ions.* Biophysical Journal, 1967. **7**(6): p. 865-877.
35. Moody, G.J., R.B. Oke, and J.D.R. Thomas, *A calcium-sensitive electrode based on a liquid ion exchanger in a poly(vinyl chloride) matrix.* Analyst, 1970. **95**(1136): p. 910-918.
36. Yan, R., et al., *Review of progresses on clinical applications of ion selective electrodes for electrolytic ion tests: From conventional ISEs to graphene-based ISEs.* Chemical Speciation and Bioavailability, 2016. **28**(1-4): p. 72-77.
37. Lee, K.S., et al., *Asymmetric carbonate ion-selective cellulose acetate membrane electrodes with reduced salicylate interference.* Analytical Chemistry, 1993. **65**(21): p. 3151-3155.
38. Yun, S.Y., et al., *Potentiometric Properties of Ion-Selective Electrode Membranes Based on Segmented Polyether Urethane Matrices.* Analytical Chemistry, 1997. **69**(5): p. 868-873.
39. Jun Yoon, I., et al., *Potentiometric behavior of metalloporphyrin-based ion-selective electrodes: Use of silicone rubber matrix for serum chloride analysis.* Analytica Chimica Acta, 1998. **367**(1-3): p. 175-181.
40. van den Berg, A., A. Grisel, and E. Verney-Norberg, *An ISFET-based calcium sensor using a photopolymerized polysiloxane membrane.* Sensors and Actuators B: Chemical, 1991. **4**(3): p. 235-238.
41. Tietje-Girault, J., et al., *Photopolymerisation of ion-selective membranes onto silicon nitride surfaces for ISFET fabrication.* Electrochimica Acta, 1990. **35**(4): p. 777-783.
42. Simon, W., *Selective Ion Sensitive Electrodes. Von G. J. Moody und J. D. R. Thomas. Merrow Publ. Co. Ltd., Watford 1971. 1. Aufl., VII, 140 S., zahlr. Abb., geb. £ 2.25.* Angewandte Chemie, 1973. **85**(23): p. 1063-1063.
43. Eugster, R., et al., *Plasticizers for liquid polymeric membranes of ion-selective chemical sensors.* Analytica Chimica Acta, 1994. **289**(1): p. 1-13.
44. Dearden, J.C., *Partitioning and lipophilicity in quantitative structure-activity relationships.* Environmental health perspectives, 1985. **61**: p. 203-228.
45. Harsanyi, G., *Polymer Films in Sensor Applications*. 1995: Taylor & Francis.
46. Bakker, E. and E. Pretsch, *Lipophilicity of tetraphenylborate derivatives as anionic sites in neutral carrier-based solvent polymeric membranes and lifetime of corresponding ion-selective electrochemical and optical sensors.* Analytica Chimica Acta, 1995. **309**(1–3): p. 7-17.
47. Lyczewska, M., et al., *Comparison of trihexadecylalkylammonium iodides as ion-exchangers for polyacrylate and poly(vinyl chloride) based iodide-selective electrodes.* Sensors and Actuators B: Chemical, 2010. **146**(1): p. 283-288.
48. Legin, A., et al., *Solvent polymeric membranes based on tridodecylmethylammonium chloride studied by potentiometry and electrochemical impedance spectroscopy.* Analytica Chimica Acta, 2004. **514**(1): p. 107-113.

49. Ozawa, S., et al., *Anion-Selective Electrodes Based on Long-Chain Methyltrialkylammonium Salts.* Analytical Chemistry, 1996. **68**(23): p. 4149-4152.
50. Buck, R.P. and E. Lindner, *Recomendations for nomenclature of ion-selective electrodes (IUPAC recommendations 1994).* Pure and Applied Chemistry, 1994. **66**(12): p. 2527-2536.
51. Buck, R.P. and E. Lindner, *Tracing the history of selective ion sensors.* Analytical Chemistry, 2001. **73**(3): p. 88A-97A.
52. Buhlmann, P., E. Pretsch, and E. Bakker, *Carrier-based ion-selective electrodes and bulk optodes. 2. Ionophores for potentiometric and optical sensors.* Chemical Reviews, 1998. **98**(4): p. 1593-1687.
53. Umezawa, Y., et al., *Potentiometric selectivity coefficients of ion-selective electrodes part I. Inorganic cations (technical report).* Pure and Applied Chemistry, 2000. **72**(10): p. 1851-2082.
54. Erne, D., et al., *Lipophilic Di- and Triamides as Ionophores for Alkaline Earth Metal Cations.* Helvetica Chimica Acta, 1980. **63**(8): p. 2271-2279.
55. Hancock, R.D., et al., *Ligand design for complexation in aqueous solution. 1. Neutral oxygen donor bearing groups as a means of controlling size-based selectivity for metal ions.* Inorganic Chemistry, 1989. **28**(2): p. 187-194.
56. Blažek Bregović, V., N. Basarić, and K. Mlinarić-Majerski, *Anion binding with urea and thiourea derivatives.* Coordination Chemistry Reviews, 2015. **295**: p. 80-124.
57. Nishizawa, S., et al., *Application of a bis-thiourea ionophore for an anion selective electrode with a remarkable sulfate selectivity.* Analytica Chimica Acta, 1998. **358**(1): p. 35-44.
58. Hay, B.P. and J.R. Rustad, *Why the addition of neutral oxygen donor groups promotes selectivity for larger metal ions.* Supramolecular Chemistry, 1996. **6**(3-4): p. 383-390.
59. Ding, W.-Q. and S.E. Lind, *Metal ionophores – An emerging class of anticancer drugs.* IUBMB Life, 2009. **61**(11): p. 1013-1018.
60. Malinowska, E., et al., *Lead selective electrodes based on thioamide functionalized calix[4]arenes as ionophores.* Analytica Chimica Acta, 1994. **298**(2): p. 253-258.
61. Merrill, D. and R.D. Hancock, *Metal ion selectivities of the highly preorganized tetradentate ligand 1,10-phenanthroline-2,9-dicarboxamide with lanthanide(III) ions and some actinide ions.* Radiochimica Acta, 2011. **99**(3): p. 161-166.
62. Hancock, R.D., et al., *Ligand design for complexation in aqueous solution. 2. Chelate ring size as a basis for control of size-based selectivity for metal ions.* Inorganic Chemistry, 1990. **29**(10): p. 1968-1974.
63. Kirsanov, D., et al., *Potentiometric Sensor Array for Analysis of Complex Rare Earth Mixtures.* Electroanalysis, 2012. **24**(1): p. 121-130.
64. Ustynyuk, Y.A., et al., *Pyridinedicarboxylic Acid Diamides as Selective Ligands for Extraction and Separation of Trivalent Lanthanides and Actinides: DFT Study.* Solvent Extraction and Ion Exchange, 2014. **32**(5): p. 508-528.

65. Bakker, E., P. Bühlmann, and E. Pretsch, *The phase-boundary potential model.* Talanta, 2004. **63**(1): p. 3-20.
66. Lindner, E. and Y. Umezawa, *Performance evaluation criteria for preparation and measurement of macro- and microfabricated ion-selective electrodes (IUPAC Technical Report).* Pure and Applied Chemistry, 2008. **80**(1): p. 85-104.
67. Lrving, H.M.N.H., et al., *Recommendations for nomenclature of ion-selective electrodes (recommendations 1975).* Pure and Applied Chemistry, 1976. **48**(1): p. 127-132.
68. Szigeti, Z., et al., *Approaches to Improving the Lower Detection Limit of Polymeric Membrane Ion-Selective Electrodes.* Electroanalysis, 2006. **18**(13-14): p. 1254-1265.
69. Shvarev, A. and E. Bakker, *Reversible Electrochemical Detection of Nonelectroactive Polyions.* Journal of the American Chemical Society, 2003. **125**(37): p. 11192-11193.
70. Amemiya, S., P. Bühlmann, and Y. Umezawa, *A Phase Boundary Potential Model for Apparently "Twice-Nernstian" Responses of Liquid Membrane Ion-Selective Electrodes.* Analytical Chemistry, 1998. **70**(3): p. 445-454.
71. Sokalski, T., et al., *Lowering the Detection Limit of Solvent Polymeric Ion-Selective Membrane Electrodes. 2. Influence of Composition of Sample and Internal Electrolyte Solution.* Analytical Chemistry, 1999. **71**(6): p. 1210-1214.
72. Johnson, R.D. and L.G. Bachas, *Ionophore-based ion-selective potentiometric and optical sensors.* Anal Bioanal Chem, 2003. **376**(3): p. 328-41.
73. Eisenman, G., D.O. Rudin, and J.U. Casby, *Glass electrode for measuring sodium ion.* Science, 1957. **126**(3278): p. 831-834.
74. Bakker, E., E. Pretsch, and P. Bühlmann, *Selectivity of potentiometric ion sensors.* Analytical Chemistry, 2000. **72**(6): p. 1127-1133.
75. Horvai, G., *The matched potential method, a generic approach to characterize the differential selectivity of chemical sensors.* Sensors and Actuators B: Chemical, 1997. **43**(1): p. 94-98.
76. Crespo, G.A., *Recent Advances in Ion-selective membrane electrodes for in situ environmental water analysis.* Electrochimica Acta, 2017. **245**: p. 1023-1034.
77. Cuartero, M. and E. Bakker, *Environmental water analysis with membrane electrodes.* Current Opinion in Electrochemistry, 2017.
78. De Marco, R., G. Clarke, and B. Pejcic, *Ion-Selective Electrode Potentiometry in Environmental Analysis.* Electroanalysis, 2007. **19**(19-20): p. 1987-2001.
79. Cardwell, T.J., et al., *A multi-ion sensor cell and data-acquisition system for flow injection analysis.* Analytica Chimica Acta, 1988. **214**: p. 359-366.
80. Yang, X., D. Brynn Hibbert, and P.W. Alexander, *Flow injection potentiometry by poly(vinyl chloride)-membrane electrodes with substituted azacrown ionophores for the determination of lead(II) and mercury(II) ions.* Analytica Chimica Acta, 1998. **372**(3): p. 387-398.

81. Lukow, S.R. and S.P. Kounaves, *Analysis of simulated martian regolith using an array of ion selective electrodes.* Electroanalysis, 2005. **17**(15-16): p. 1441-1449.
82. Kounaves, S.P., *Electrochemical approaches for chemical and biological analysis on Mars.* Chemphyschem, 2003. **4**(2): p. 162-8.
83. Bakker, E. and E. Pretsch, *Modern Potentiometry.* Angewandte Chemie (International ed. in English), 2007. **46**(30): p. 5660-5668.
84. Young, C.C., *Evolution of Blood Chemistry Analyzers Based on Ion Selective Electrodes.* Journal of Chemical Education, 1997. **74**(2): p. 177.
85. Shim, J.H., et al., *Glass nanopore-based ion-selective electrodes.* Anal Chem, 2007. **79**(10): p. 3568-74.
86. Bakker, E. and E. Pretsch, *Modern potentiometry.* Angew Chem Int Ed Engl, 2007. **46**(30): p. 5660-8.
87. Malon, A., et al., *Potentiometry at trace levels in confined samples: Ion-selective electrodes with subfemtomole detection limits.* Journal of the American Chemical Society, 2006. **128**(25): p. 8154-8155.
88. Bratov, A., et al., *Ion-selective field effect transistor (ISFET)-based calcium ion sensor with photocured polyurethane membrane suitable for ionised calcium determination in milk.* Analytica Chimica Acta, 2000. **408**(1–2): p. 57-64.
89. Liu, Y., et al., *An extended CMOS ISFET model incorporating the physical design geometry and the effects on performance and offset variation.* IEEE Transactions on Electron Devices, 2011. **58**(12): p. 4414-4422.
90. Spanu, A., et al., *A reference-less pH sensor based on an organic field effect transistor with tunable sensitivity.* Organic Electronics: physics, materials, applications, 2017. **48**: p. 188-193.
91. Bratov, A., et al., *Photocurable polymers applied as encapsulating materials for ISFET production.* Sensors and Actuators: B. Chemical, 1995. **25**(1-3): p. 823-825.
92. Miller, P.R., et al., *Microneedle-based transdermal sensor for on-chip potentiometric determination of K+.* Advanced Healthcare Materials, 2014. **3**(6): p. 876-881.
93. Nouman, M., et al., *Exudation of additives to the surface of medical devices: impact on biocompatibility in the case of polyurethane used in implantable catheters.* Journal of Biomedical Materials Research - Part A, 2016. **104**(12): p. 2954-2967.
94. Fang, L., et al., *A needle-type glucose biosensor based on PANI nanofibers and PU/E-PU membrane for long-term invasive continuous monitoring.* Biosensors and Bioelectronics, 2017. **97**: p. 196-202.
95. Arakawa, T., et al., *Mouthguard biosensor with telemetry system for monitoring of saliva glucose: A novel cavitas sensor.* Biosensors and Bioelectronics, 2016. **84**(Supplement C): p. 106-111.
96. Matzeu, G., L. Florea, and D. Diamond, *Advances in wearable chemical sensor design for monitoring biological fluids.* Sensors and Actuators B: Chemical, 2015. **211**: p. 403-418.

97. Sempionatto, J.R., et al., *Eyeglasses based wireless electrolyte and metabolite sensor platform.* Lab on a Chip, 2017. **17**(10): p. 1834-1842.
98. Kim, J., et al., *Advanced Materials for Printed Wearable Electrochemical Devices: A Review.* Advanced Electronic Materials, 2017. **3**(1).
99. Novell, M., et al., *Paper-Based Ion-Selective Potentiometric Sensors.* Analytical Chemistry, 2012. **84**(11): p. 4695-4702.
100. Bandodkar, A.J., et al., *Epidermal tattoo potentiometric sodium sensors with wireless signal transduction for continuous non-invasive sweat monitoring.* Biosensors and Bioelectronics, 2014. **54**: p. 603-609.
101. Heng, L.Y. and E.A.H. Hall, *Methacrylic–acrylic polymers in ion-selective membranes: achieving the right polymer recipe.* Analytica Chimica Acta, 2000. **403**(1–2): p. 77-89.
102. Heng, L.Y. and E.A.H. Hall, *Taking the Plasticizer out of Methacrylic-Acrylic Membranes for K+-Selective Electrodes.* Electroanalysis, 2000. **12**(3): p. 187-193.
103. Escuder-Gilabert, L. and M. Peris, *Review: Highlights in recent applications of electronic tongues in food analysis.* Analytica Chimica Acta, 2010. **665**(1): p. 15-25.
104. Esbensen, K., et al., *Fermentation monitoring using multisensor systems: feasibility study of the electronic tongue.* Analytical and Bioanalytical Chemistry, 2004. **378**(2): p. 391-395.
105. Legin, A., et al., *Tasting of beverages using an electronic tongue.* Sensors and Actuators B: Chemical, 1997. **44**(1–3): p. 291-296.
106. Legin, A., et al., *Application of electronic tongue for qualitative and quantitative analysis of complex liquid media.* Sensors and Actuators B: Chemical, 2000. **65**(1–3): p. 232-234.
107. Ciosek, P. and W. Wroblewski, *Sensor arrays for liquid sensing - electronic tongue systems.* Analyst, 2007. **132**(10): p. 963-978.
108. Tahara, Y. and K. Toko, *Electronic Tongues-A Review.* Ieee Sensors Journal, 2013. **13**(8): p. 3001-3011.
109. Riul Jr, A., et al., *Recent advances in electronic tongues.* Analyst, 2010. **135**(10): p. 2481-2495.
110. Legin, A., et al., *Multicomponent analysis of fermentation growth media using the electronic tongue (ET).* Talanta, 2004. **64**(3): p. 766-772.
111. Kirsanov, D., et al., *Towards reliable estimation of an "electronic tongue" predictive ability from PLS regression models in wine analysis.* Talanta, 2012. **90**: p. 109-116.
112. Pein, M., et al., *Independent comparison study of six different electronic tongues applied for pharmaceutical analysis.* Journal of Pharmaceutical and Biomedical Analysis, 2015. **114**: p. 321-329.
113. Gallardo, J., et al., *Use of an Electronic Tongue Based on All-Solid-State Potentiometric Sensors for the Quantitation of Alkaline Ions.* Electroanalysis, 2005. **17**(4): p. 348-355.

114. Ciosek, P. and W. Wroblewski, *Performance of selective and partially selective sensors in the recognition of beverages.* Talanta, 2007. **71**(2): p. 738-46.
115. Woertz, K., et al., *Taste sensing systems (electronic tongues) for pharmaceutical applications.* International Journal of Pharmaceutics, 2011. **417**(1): p. 256-271.
116. Kirsanov, D., et al., *A combination of dynamic measurement protocol and advanced data treatment to resolve the mixtures of chemically similar analytes with potentiometric multisensor system.* Talanta, 2014. **119**: p. 226-231.
117. Rudnitskaya, A., et al., *Detection of ultra-low activities of heavy metal ions by an array of potentiometric chemical sensors.* Microchimica Acta, 2008. **163**(1-2): p. 71-80.
118. Buczkowska, A., et al., *The monitoring of methane fermentation in sequencing batch bioreactor with flow-through array of miniaturized solid state electrodes.* Talanta, 2010. **81**(4): p. 1387-1392.
119. Abramova, N., et al., *Integrated multi-sensor chip with photocured polymer membranes containing copolymerised plasticizer for direct pH, potassium, sodium and chloride ions determination in blood serum.* Talanta, 2009. **79**(4): p. 984-989.
120. Rudnitskaya, A., et al., *Detection of ultra-low activities of heavy metal ions by an array of potentiometric chemical sensors.* Microchimica Acta, 2008. **163**(1): p. 71-80.
121. Gallardo, J., S. Alegret, and M. del Valle, *A flow-injection electronic tongue based on potentiometric sensors for the determination of nitrate in the presence of chloride.* Sensors and Actuators B: Chemical, 2004. **101**(1): p. 72-80.
122. Gallardo, J., S. Alegret, and M. Del Valle, *Application of a potentiometric electronic tongue as a classification tool in food analysis.* Talanta, 2005. **66**(5): p. 1303-1309.
123. Krantz-Rülcker, C., et al., *Electronic tongues for environmental monitoring based on sensor arrays and pattern recognition: A review.* Analytica Chimica Acta, 2001. **426**(2): p. 217-226.
124. Moreno, L., et al., *Multi-sensor array used as an "electronic tongue" for mineral water analysis.* Sensors and Actuators, B: Chemical, 2006. **116**(1-2): p. 130-134.
125. Gutiérrez, M., et al., *Remote environmental monitoring employing a potentiometric electronic tongue.* International Journal of Environmental Analytical Chemistry, 2008. **88**(2): p. 103-117.
126. Pankratova, N., et al., *Potentiometric sensing array for monitoring aquatic systems.* Environmental Science: Processes & Impacts, 2015. **17**(5): p. 906-914.
127. Kirsanov, D., et al., *Mimicking Daphnia magna bioassay performance by an electronic tongue for urban water quality control.* Analytica Chimica Acta, 2014. **824**: p. 64-70.

128. Zadorozhnaya, O., et al., *Water pollution monitoring by an artificial sensory system performing in terms of Vibrio fischeri bacteria.* Sensors and Actuators B: Chemical, 2015. **207**: p. 1069-1075.
129. Ribeiro, M.C.C., L.F.C. de Oliveira, and P.S. Santos, *Raman bandshape analysis of oxocarbon ions in aqueous solutions.* Chemical Physics, 1997. **217**(1): p. 71-81.
130. Madic, C., et al., *Raman spectroscopy of neptunyl and plutonyl ions in aqueous solution: hydrolysis of neptunium(VI) and plutonium(VI) and disproportionation of plutonium(V).* Inorganic Chemistry, 1984. **23**(13): p. 1914-1921.
131. Schmidt, C. and T.M. Seward, *Raman spectroscopic quantification of sulfur species in aqueous fluids: Ratios of relative molar scattering factors of Raman bands of H2S, HS−, SO2, HSO4−, SO42−, S2O32−, S3− and H2O at ambient conditions and information on changes with pressure and temperature.* Chemical Geology, 2017. **467**(Supplement C): p. 64-75.
132. Uibel, R.H. and J.M. Harris, *In situ Raman spectroscopy studies of metal ion complexation by 8-hydroxyquinoline covalently bound to silica surfaces.* Analytical Chemistry, 2002. **74**(19): p. 5112-5120.
133. Foley, S. and M. Enescu, *A Raman spectroscopy and theoretical study of zinc–cysteine complexation.* Vibrational Spectroscopy, 2007. **44**(2): p. 256-265.
134. Zeravik, J., et al., *State of the Art in the Field of Electronic and Bioelectronic Tongues – Towards the Analysis of Wines.* Electroanalysis, 2009. **21**(23): p. 2509-2520.
135. Legin, A.V., et al., *The features of the electronic tongue in comparison with the characteristics of the discrete ion-selective sensors.* Sensors and Actuators B: Chemical, 1999. **58**(1–3): p. 464-468.
136. Pol'shin, E.N., et al., *Comparison of the Analytical Potential of Individual Sensors and a Multisensor System of the "Electronic Tongue" Type for the Example of Determination of the Perchlorate Ion.* Russian Journal of Applied Chemistry, 2010. **83**(9): p. 1563-1569.
137. Ceresa, A. and E. Pretsch, *Determination of formal complex formation constants of various Pb2+ ionophores in the sensor membrane phase.* Analytica Chimica Acta, 1999. **395**(1–2): p. 41-52.
138. Żubrowska, M., W. Wróblewski, and K. Wojciechowski, *The effect of lipophilic salts on surface charge in polymeric ion-selective electrodes.* Electrochimica Acta, 2011. **56**(17): p. 6114-6122.
139. Ciosek, P., M. Janczyk, and W. Wroblewski *Classification of amino acids and oligopeptides with the use of multi-mode chemical images obtained with ion selective electrode array*. Analytica Chimica Acta, 2011. **699**, 26-32 DOI: 10.1016/j.aca.2011.05.013.
140. Kutyła-Olesiuk, A., et al., *Monitoring of beer fermentation based on hybrid electronic tongue.* Bioelectrochemistry, 2012. **87**: p. 104-113.
141. Beebe, K., et al., *Sparingly selective ion-selective electrode arrays for multicomponent analysis.* Analytical Chemistry, 1988. **60**(1): p. 66-71.

142. Dimeski, G., T. Badrick, and A.S. John, *Ion Selective Electrodes (ISEs) and interferences—A review.* Clinica Chimica Acta, 2010. **411**(5–6): p. 309-317.
143. Ross, J.W., *Calcium-selective electrode with liquid ion exchanger.* Science, 1967. **156**(3780): p. 1378-9.
144. Legin, A.V., et al., *Cross-sensitive rare earth metal ion sensors based on extraction systems.* Sensors and Actuators B-Chemical, 2008. **131**(1): p. 29-36.
145. Alyapyshev, M.Y., et al., *Calixarenes functionalized with phosphine oxide and diamide functions as extractants and ionofores for rare-earth metals.* Journal of Inclusion Phenomena and Macrocyclic Chemistry, 2010. **67**(1-2): p. 117-126.
146. Nilsson, M. and K.L. Nash, *Review Article: A Review of the Development and Operational Characteristics of the TALSPEAK Process.* Solvent Extraction and Ion Exchange, 2007. **25**(6): p. 665-701.
147. Lumetta, G.J., et al., *Combining Octyl(phenyl)-N,N-diisobutylcarbamoylmethylphosphine oxide and bis-(2-ethylhexyl)phosphoric acid extractants for recovering transuranic elements from irradiated nuclear fuel*, in *ACS Symposium Series*. 2010. p. 107-118.
148. Lumetta, G.J., et al., *The TRUSPEAK Concept: Combining CMPO and HDEHP for Separating Trivalent Lanthanides from the Transuranic Elements.* Solvent Extraction and Ion Exchange, 2013. **31**(3): p. 223-236.
149. Lee, K.S., et al., *Multiionophore-based solid-state potentiometric ion sensor as a cation detector for ion chromatography.* Sensors and Actuators B: Chemical, 1994. **20**(2): p. 239-246.
150. Hyun Han, S., et al., *Potentiometric detection in ion chromatography using multi-ionophore membrane electrodes.* Journal of Chromatography A, 1993. **648**(1): p. 283-288.
151. Cuartero, M., G.A. Crespo, and E. Bakker, *Ionophore-Based Voltammetric Ion Activity Sensing with Thin Layer Membranes.* Anal Chem, 2016. **88**(3): p. 1654-60.
152. Jadhav, S. and E. Bakker, *Selectivity Behavior and Multianalyte Detection Capability of Voltammetric Ionophore-Based Plasticized Polymeric Membrane Sensors.* Analytical Chemistry, 2001. **73**(1): p. 80-90.
153. Bakker, E. and E. Pretsch, *Ion-Selective Electrodes Based on Two Competitive Ionophores for Determining Effective Stability Constants of Ion−Carrier Complexes in Solvent Polymeric Membranes.* Analytical Chemistry, 1998. **70**(2): p. 295-302.
154. Wang, J., *Electrochemical Sensors*, in *Analytical Electrochemistry*. 2006, John Wiley & Sons, Inc. p. 201-243.
155. Mallard, P.J.L.a.W.G., *NIST Chemistry WebBook, NIST Standard Reference Database Number 69, National Institute of Standards and Technology.*
156. for, S.D. and O.C.S.N.I.o.A.I.S.a. Technology, https://sdbs.db.aist.go.jp
157. Lin-Vien, D., et al., *CHAPTER 1 - Introduction*, in *The Handbook of Infrared and Raman Characteristic Frequencies of Organic Molecules*. 1991, Academic Press: San Diego. p. 1-7.

158. Raman, C.V. and K.S. Krishnan, *A New Type of Secondary Radiation.* Nature, 1928. **121**: p. 501.
159. Smith, E. and G. Dent, *The Raman Experiment – Raman Instrumentation, Sample Presentation, Data Handling and Practical Aspects of Interpretation*, in *Modern Raman Spectroscopy – A Practical Approach*. 2005, John Wiley & Sons, Ltd. p. 23-70.
160. Miller, F.A., *Introduction*, in *Course Notes on the Interpretation of Infrared and Raman Spectra*. 2004, John Wiley & Sons, Inc. p. 1-32.
161. Arora, R., et al., *Improving sensitivity in nonlinear Raman microspectroscopy imaging and sensing.* Journal of biomedical optics, 2011. **16**(2): p. 021114-021114.
162. Smith, E. and G. Dent, *Modern Raman Spectroscopy - A Practical Approach*. Modern Raman Spectroscopy - A Practical Approach. 2005. 1-210.
163. Guendouz, M., et al., *Oxidised porous silicon/disperse red 1 composite material: fabrication and micro-Raman spectrometry analysis.* physica status solidi (c), 2005. **2**(9): p. 3453-3456.
164. Yang, D. and Y. Ying, *Applications of raman spectroscopy in agricultural products and food analysis: A review.* Applied Spectroscopy Reviews, 2011. **46**(7): p. 539-560.
165. Moore, D.S. and R.J. Scharff, *Portable Raman explosives detection.* Analytical and Bioanalytical Chemistry, 2009. **393**(6-7): p. 1571-1578.
166. de Veij, M., et al., *Reference database of Raman spectra of pharmaceutical excipients.* Journal of Raman Spectroscopy, 2009. **40**(3): p. 297-307.
167. Skoulika, S.G. and C.A. Georgiou, *Rapid, Noninvasive Quantitative Determination of Acyclovir in Pharmaceutical Solid Dosage Forms Through their Poly(vinyl chloride) Blister Package by Solid-State Fourier Transform Raman Spectroscopy.* Applied Spectroscopy, 2003. **57**(4): p. 407-412.
168. Welter, N., U. Schüssler, and W. Kiefer, *Characterisation of inorganic pigments in ancient glass beads by means of Raman microspectroscopy, microprobe analysis and X-ray diffractometry.* Journal of Raman Spectroscopy, 2007. **38**(1): p. 113-121.
169. Vandenabeele, P., H.G.M. Edwards, and L. Moens, *A decade of Raman spectroscopy in art and archeology.* Chemical Reviews, 2007. **107**(3): p. 675-686.
170. Perez-Rodriguez, J.L., et al., *Wall paintings studied using Raman spectroscopy: A comparative study between various assays of cross sections and external layers.* Spectrochimica Acta Part A: Molecular and Biomolecular Spectroscopy, 2014. **120**: p. 602-609.
171. Vandenabeele, P., F. Verpoort, and L. Moens, *Non-destructive analysis of paintings using fourier transform Raman spectroscopy with fibre optics.* Journal of Raman Spectroscopy, 2001. **32**(4): p. 263-269.
172. Pozzi, F. and M. Leona, *Surface-enhanced Raman spectroscopy in art and archaeology.* Journal of Raman Spectroscopy, 2016. **47**(1): p. 67-77.

173. Schwab, S.D. and R.L. McCreery, *Versatile, efficient Raman sampling with fiber optics.* Analytical Chemistry, 1984. **56**(12): p. 2199-2204.
174. Shim, M.G., et al., *Study of Fiber-Optic Probes for in vivo Medical Raman Spectroscopy.* Applied Spectroscopy, 1999. **53**(6): p. 619-627.
175. Matthäus, C., et al., *Label-Free Detection of Mitochondrial Distribution in Cells by Nonresonant Raman Microspectroscopy.* Biophysical Journal, 2007. **93**(2): p. 668-673.
176. Mariani, M.M., P.J.R. Day, and V. Deckert, *Applications of modern micro-Raman spectroscopy for cell analyses.* Integrative Biology, 2010. **2**(2-3): p. 94-101.
177. Mikoliunaite, L., et al., *The substrate matters in the Raman spectroscopy analysis of cells.* Scientific Reports, 2015. **5**: p. 13150.
178. Edwards, H.G.M., et al., *Ancient biodeterioration: an FT–Raman spectroscopic study of mammoth and elephant ivory.* Analytical and Bioanalytical Chemistry, 2005. **383**(4): p. 713-720.
179. Butler, H.J., et al., *Using Raman spectroscopy to characterize biological materials.* Nature Protocols, 2016. **11**: p. 664.
180. Schrader, B., et al., *Non-destructive Raman analyses – polyacetylenes in plants.* Spectrochimica Acta Part A: Molecular and Biomolecular Spectroscopy, 2005. **61**(7): p. 1395-1401.
181. Jarvis, R.M., A. Brooker, and R. Goodacre, *Surface-enhanced Raman scattering for the rapid discrimination of bacteria.* Faraday Discussions, 2006. **132**(0): p. 281-292.
182. Puppels, G.J., et al., *Studying single living cells and chromosomes by confocal Raman microspectroscopy.* Nature, 1990. **347**: p. 301.
183. Wang, H., et al., *A Method for accurate in vivo micro-Raman spectroscopic measurements under guidance of advanced microscopy imaging.* 2013. **3**: p. 1890.
184. de Oliveira Penido, C.A.F., et al., *Raman spectroscopy in forensic analysis: identification of cocaine and other illegal drugs of abuse.* Journal of Raman Spectroscopy, 2016. **47**(1): p. 28-38.
185. Harvey, S.D., et al., *Blind field test evaluation of Raman spectroscopy as a forensic tool.* Forensic Science International, 2002. **125**(1): p. 12-21.
186. Zhao, J., et al., *Using Raman Spectroscopy to Detect and Diagnose Skin Cancer In Vivo.* Dermatologic Clinics, 2017. **35**(4): p. 495-504.
187. Nijssen, A., et al., *Towards oncological application of Raman spectroscopy.* Journal of Biophotonics, 2009. **2**(1-2): p. 29-36.
188. Haka, A.S., et al., *In vivo margin assessment during partial mastectomy breast surgery using Raman spectroscopy.* Cancer Research, 2006. **66**(6): p. 3317-3322.
189. Hanlon, E.B., et al., *Prospects for in vivo Raman spectroscopy.* Physics in Medicine & Biology, 2000. **45**(2): p. R1.
190. Barker, I.K., V. Fawcett, and D.A. Long, *Solvent dependence of the resonance Raman spectra of azobenzene, 4-aminoazobenzene, 4-methylaminobenzene*

and 4-dimethylaminoazobenzene. Journal of Raman Spectroscopy, 1987. **18**(1): p. 71-75.
191. Estienne, F., et al., *Multivariate calibration with Raman spectroscopic data: a case study.* Analytica Chimica Acta, 2000. **424**(2): p. 185-201.
192. Fleischmann, M., P.J. Hendra, and A.J. McQuillan, *Raman spectra of pyridine adsorbed at a silver electrode.* Chemical Physics Letters, 1974. **26**(2): p. 163-166.
193. Henry, A.-I., et al., *Surface-Enhanced Raman Spectroscopy Biosensing: In Vivo Diagnostics and Multimodal Imaging.* Analytical Chemistry, 2016. **88**(13): p. 6638-6647.
194. Khan, M.A., et al., *Surface Plasmon Structures for Surface-Enhanced Raman Scattering.* MRS Proceedings, 2007. **1055**.
195. Xu, X., et al., *Fabrication and Robotization of Ultrasensitive Plasmonic Nanosensors for Molecule Detection with Raman Scattering.* Sensors (Basel, Switzerland), 2015. **15**(5): p. 10422-10451.
196. Abramczyk, H. and B. Brozek-Pluska, *Raman imaging in biochemical and biomedical applications. Diagnosis and treatment of breast cancer.* Chemical Reviews, 2013. **113**(8): p. 5766-5781.
197. Goubert, G. and R.P. Van Duyne, *Tipping point.* Nature Nanotechnology, 2016. **12**: p. 100.
198. Duncan, M.D., J. Reintjes, and T.J. Manuccia, *Scanning coherent anti-Stokes Raman microscope.* Optics Letters, 1982. **7**(8): p. 350-352.
199. Matousek, P., et al., *Noninvasive Raman Spectroscopy of Human Tissue in vivo.* Applied Spectroscopy, 2006. **60**(7): p. 758-763.
200. *Handbook of Chemometrics and Qualimetrics*. 1997: Elsevier Science.
201. Wold, H., *Estimation of Principal Components and Related Models by Iterative Least squares*, in *Multivariate Analysis.* 1966, Academic Press. p. 391-420.
202. Bro, R. and A.K. Smilde, *Principal component analysis.* Analytical Methods, 2014. **6**(9): p. 2812-2831.
203. Wold, S., M. Sjöström, and L. Eriksson, *PLS-regression: a basic tool of chemometrics.* Chemometrics and Intelligent Laboratory Systems, 2001. **58**(2): p. 109-130.
204. Geladi, P. and B.R. Kowalski, *Partial least-squares regression: a tutorial.* Analytica Chimica Acta, 1986. **185**: p. 1-17.
205. Wold, S., et al., *DNA and peptide sequences and chemical processes multivariately modelled by principal component analysis and partial least-squares projections to latent structures.* Analytica Chimica Acta, 1993. **277**(2): p. 239-253.
206. Farrés, M., et al., *Comparison of the variable importance in projection (VIP) and of the selectivity ratio (SR) methods for variable selection and interpretation.* Journal of Chemometrics, 2015. **29**(10): p. 528-536.
207. Devos, O. and L. Duponchel, *Parallel genetic algorithm co-optimization of spectral pre-processing and wavelength selection for PLS regression.* Chemometrics and Intelligent Laboratory Systems, 2011. **107**(1): p. 50-58.

208. Zeaiter, M. and D. Rutledge, *3.04 - Preprocessing Methods A2 - Brown, Steven D*, in *Comprehensive Chemometrics*, R. Tauler and B. Walczak, Editors. 2009, Elsevier: Oxford. p. 121-231.
209. H C Eilers, P. and H. F M Boelens, *Baseline Correction with Asymmetric Least Squares Smoothing*. 2005.
210. Devos, O., et al., *Baseline correction methods to deal with artifacts in femtosecond transient absorption spectroscopy.* Analytica Chimica Acta, 2011. **705**(1-2): p. 64-71.
211. Savitzky, A. and M.J.E. Golay, *Smoothing and Differentiation of Data by Simplified Least Squares Procedures.* Analytical Chemistry, 1964. **36**(8): p. 1627-1639.
212. Isaksson, T. and T. Næs, *The Effect of Multiplicative Scatter Correction (MSC) and Linearity Improvement in NIR Spectroscopy.* Applied Spectroscopy, 1988. **42**(7): p. 1273-1284.
213. Barnes, R.J., M.S. Dhanoa, and S.J. Lister, *Correction to the Description of Standard Normal Variate (SNV) and De-Trend (DT) Transformations in Practical Spectroscopy with Applications in Food and Beverage Analysis—2nd Edition.* NIR news, 1994. **5**(3): p. 6-6.
214. Alyapyshev, M., et al., *1,10-Phenanthroline-2,9-dicarboxamides as ligands for separation and sensing of hazardous metals.* RSC Advances, 2016. **6**(73): p. 68642-68652.
215. Frisch, M.J., et al., *Gaussian 09*. 2009, Gaussian, Inc.: Wallingford, CT, USA.
216. Zhao, Y. and D.G. Truhlar, *Density Functionals with Broad Applicability in Chemistry.* Accounts of Chemical Research, 2008. **41**(2): p. 157-167.
217. Zhao, Y. and D.G. Truhlar, *The M06 suite of density functionals for main group thermochemistry, thermochemical kinetics, noncovalent interactions, excited states, and transition elements: two new functionals and systematic testing of four M06-class functionals and 12 other functionals.* Theoretical Chemistry Accounts, 2008. **120**(1): p. 215-241.
218. Chase, H.M., et al., *Assessment of DFT for Computing Sum Frequency Generation Spectra of an Epoxydiol and a Deuterated Isotopologue at Fused Silica/Vapor Interfaces.* The Journal of Physical Chemistry B, 2016. **120**(8): p. 1919-1927.
219. Reiher, M., G. Brehm, and S. Schneider, *Assignment of vibrational spectra of 1,10-phenanthroline by comparison with frequencies and Raman intensities from density functional calculations.* Journal of Physical Chemistry A, 2004. **108**(5): p. 734-742.
220. Gomleksiz, M., C. Alkan, and B. Erdem, *Synthesis, Characterization and Antibacterial Activity of 2-P-Tolyl-1h-Imidazo[4,5f][1,10] Phenanthroline and Its Co(Ii), Ni(Ii) and Cu(Ii) Complexes.* Bulletin of the Chemical Society of Ethiopia, 2013. **27**(2): p. 213-220.
221. Wu, Q., et al., *Intensities of E. coli Nucleic Acid Raman Spectra Excited Selectively from Whole Cells with 251-nm Light.* Analytical Chemistry, 2000. **72**(13): p. 2981-2986.

222. Awual, M.R., et al., *Selective lanthanide sorption and mechanism using novel hybrid Lewis base (N-methyl-N-phenyl-1,10-phenanthroline-2-carboxamide) ligand modified adsorbent.* Journal of Hazardous Materials, 2013. **252–253**: p. 313-320.
223. Acheson, R.M., *An introduction to the chemistry of heterocyclic compounds*. 1976: Wiley.
224. Arora, J.S. and V.G. Gaikar, *Molecular design of a novel ligand for Menshutkin complexation of Bi(iii) from aqueous acidic copper sulfate electrolyte solutions and experimental investigations.* RSC Advances, 2016. **6**(46): p. 39663-39674.
225. Lin-Vien, D., et al., *CHAPTER 17 - Aromatic and Heteroaromatic Rings*, in *The Handbook of Infrared and Raman Characteristic Frequencies of Organic Molecules*. 1991, Academic Press: San Diego. p. 277-306.
226. Reinhoudt, D.N., et al., *Development of Durable K+-Selective Chemically Modified Field Effect Transistors with Functionalized Polysiloxane Membranes.* Analytical Chemistry, 1994. **66**(21): p. 3618-3623.
227. Bedlechowicz-Sliwakowska, I., et al., *Ion-selective electrode for measuring low Ca^{2+} concentrations in the presence of high K^{+}, Na^{+} and Mg^{2+} background.* Anal Bioanal Chem, 2006. **385**(8): p. 1477-82.
228. de los A. Arada Pérez, M.a., et al., *Influence of different plasticizers on the response of chemical sensors based on polymeric membranes for nitrate ion determination.* Sensors and Actuators B: Chemical, 2003. **89**(3): p. 262-268.
229. Wróblewski, W., et al., *Uranyl salophenes as ionophores for phosphate-selective electrodes.* Sensors and Actuators, B: Chemical, 2000. **68**(1): p. 313-318.
230. Kirsanov, D., et al., *A sample-effective calibration design for multiple components.* Analyst, 2014. **139**(17): p. 4303-4309.
231. Smith, D.W., *Ionic hydration enthalpies.* Journal of Chemical Education, 1977. **54**(9): p. 540-542.
232. Buøen, S., J. Dale, and W. Lund, *Ion-selectivity of plasticizers in poly(vinyl chloride) membrane electrodes.* Analytica Chimica Acta, 1986. **185**(C): p. 347-349.
233. Kazuhisa, H., O. Tatsuhiro, and S. Hideki, *Di-n-octyl Phenyl Phosphonate: A Plasticizer of Poly(vinyl chloride) Matrix Membrane Electrodes Behaving As a Li+-selective Agent.* Bulletin of the Chemical Society of Japan, 1986. **59**(6): p. 2015-2016.
234. Geladi, P., L. Hadjiiski, and P. Hopke, *Multiple regression for environmental data: Nonlinearities and prediction bias.* Chemometrics and Intelligent Laboratory Systems, 1999. **47**(2): p. 165-173.
235. Suzuki, H., H. Naganawa, and S. Tachimori, *Role of hydrophobic counteranions in the ion pair extraction of lanthanides(III) with an electrically neutral extractant.* Physical Chemistry Chemical Physics, 2003. **5**(4): p. 726-733.
236. Alyapyshev, M.Y., et al., *Extraction of americium and europium from perchloric acid solutions with N,N'-dialkyl-and N,N,N',N'-tetraalkylpyridine-2,6-*

dicarboxamides. Russian Journal of Applied Chemistry, 2006. **79**(11): p. 1808-1815.
237. Alyapyshev, M.Y., et al., *Dependence of extraction properties of 2,6-dicarboxypyridine diamides on extractant structure.* Solvent Extraction and Ion Exchange, 2011. **29**(4): p. 619-636.
238. Horwltz, E.P., et al., *EXTRACTION OF Am FROM NITRIC ACID BY CARBAMOYL-PHOSPHORYL EXTRACTANTS: THE INFLUENCE OF SUBSTITUENTS ON THE SELECTIVITY OF Am OVER Fe AND SELECTED FISSION PRODUCTS.* Solvent Extraction and Ion Exchange, 1986. **4**(3): p. 449-494.
239. Legin, A.V., et al., *Cross-sensitive rare-earth metal sensors based on bidentate neutral organophosphorus compounds and chlorinated cobalt dicarbollide.* Analytica Chimica Acta, 2006. **572**(2): p. 243-247.
240. Paulenova, A., et al., *Extraction of lanthanides with diamides of dipicolinic acid from nitric acid solutions. I.* Separation Science and Technology, 2008. **43**(9-10): p. 2606-2618.
241. Kirsanov, D.O., et al., *New polymeric chemical sensors for determination of lead ions.* Russian Journal of Applied Chemistry, 2009. **82**(2): p. 247-254.